NASA-AEC
Prog.-
Fall 1967
c.1



LOAN COPY: RETU
AFWL (WLIL-
KIRTLAND AFB, N

University of California

Ernest O. Lawrence Radiation Laboratory

JOINT NASA-AEC PROGRAM IN SPACE RADIATION BIOLOGY

PROGRESS REPORT • FALL 1967

Berkeley, California



0067263

UCRL-17751
UC-48 Biology and Medicine
TID-4500 (50th Ed.)

NASA Contract No. R-104, Task No 2
AEC Contract No. W-7405-eng-48

JOINT NASA-AEC PROGRAM
in
SPACE RADIATION BIOLOGY

PROGRESS REPORT-FALL 1967

Donner Laboratory and Donner Pavilion

LAWRENCE RADIATION LABORATORY
University of California, Berkeley, California

September 1967

Printed in the United States of America
Available from
Clearinghouse for Federal Scientific and Technical Information
National Bureau of Standards, U.S. Department of Commerce
Springfield, Virginia 22151
Price: Printed Copy $3.00, Microfiche $0.65

FOREWORD

The joint NASA–AEC program at the Donner Laboratory was established with the aim of better understanding the effects of space radiations and relating them to the special problems of NASA· to help insure the safety of astronauts during space flight, to understand possible interactions between radiation effects and other factors of space and planetary exploration, and to understand basic aspects of the relations of radiations to exobiology

Special facilities of the Laboratory include two cyclotrons, which allow studies with proton and helium-ion radiations, and a heavy-ion linear accelerator, which produces low-range accelerated ions up to argon.

Page intentionally left blank

Page intentionally left blank

Contents

Foreword iii

Molecular Studies

Introduction 1

Electron Spin Resonance Studies of H_2O Radiolysis and Linear Accelerator of Development Directed Toward Establishment of Pulse Radiolysis Facilities
T. E. Gunter 3

Production of Free Radicals and Radiation Damage in Trypsin by Irradiation with Electrons at 4.2 °K
W. B. G. Jones 9

Excited Electronic States in Nucleic Acid Components and Their Relation to Radiation Damage
M. D. Shetlar 19

Effects of Homogeneous Magnetic Fields Upon Biological Systems
N. M. Amer 25

Cellular Studies

Introduction 27

The Effect of Various LET Radiations on "Stem Cells" as Measured by the Spleen Colony-Forming Technique
J. M. Feola and J. C. Schooley 29

Synergistic Action of x Rays and Ultrasonic Waves on Mammalian Cells Cultured *in vitro*
B. I. Martins 37

Radiation Effects in Space Flight

Introduction 41

Effect of Radiation on the Developing Flour Beetle, *Tribolium confusum*
B. M. Buckhold and J. V. Slater 43

Radiological Physics

Introduction 53

Semiconductor Devices and Their Applications to Dosimetry of Heavy-Charged-Particle Beams
M. R. Raju 55

Energy-Loss Fluctuations
H. D. Maccabee 59

Simulated Solar-Flare Irradiation in the Laboratory
J. T. Lyman 63

Beam Scanning and Microbeam at the 88-Inch Cyclotron
G. P. Welch 77

Mammalian Radiobiology and Neuroradiobiology

Introduction 81

Space-Related Mammalian Radiobiology
H. Aceto 83

Vestibular Organs: The Structure and Function of the Vestibular Organs as They Relate to the Manned Exploration of Space
L. W. McDonald and R. G. Plantz 97

Vestibular Organs: Testing the Function of Vestibular Receptors
R. G. Plantz and L. W. McDonald 109

Vestibular Organs: Radiation Effects on Structure and Function
L. W. McDonald and R. G. Plantz 117

The Righting Reflex of the Frog as Influenced by Irradiation
C. T. Gaffey and V. S. Montoya 123

The Vestibular Apparatus as Influenced by Localized High-Energy Irradiation
C. T. Gaffey and V. S. Montoya 125

Brain Impedance Studies and Their Relation to Radiation Effects In Space Flight
R. L. Schoenbrun 127

Mathematical Modeling of Space Radiation Hazards
P. G. Steward and C. A. Tobias 137

Author Index 143

MOLECULAR STUDIES

Introduction

We hope to improve understanding of initial interactions between ionizing radiations and organic matter and the manner in which molecules are transformed to cause biological effects.

Special tools available include electron spin resonance equipment, spectroscopy, and special magnets. Exposures are carried out at a 5-MeV electron accelerator.

Earlier studies in the Laboratory have demonstrated free radicals induced by radiations in enzymes and in ice. It was also shown that even at liquid temperature these are secondary radicals. During the past year methods were developed to irradiate and measure molecular samples near liquid helium temperature. This may allow a quantitative accounting of all initial radical species in ice, in hydrated inorganic crystals, in enzymes, and in amino acids. LET dependence of various effects was also measured.

We have characterized inactivation of enzymes in the dry states, in water suspension as a function of pH, at various LET, at various temperatures, and in the presence of radiation modifiers.

The relationship between enzyme inactivation and free radicals induced remains one of the long-term goals.

Another long-term goal is to identify and understand the free radicals induced in dried and cooled cellular material (e.g., spores of B. megaterium) and the relationship of the free radicals to lethality and mutations in cells.

Another goal is to understand "annealing" of free radicals when molecules and cells are stored at low temperature, so that radiation damage disappears.

Triplet states induced in nucleic acids are of current interest.

The study of magnetic field effects has led to the initiation of research on liquid-crystal states of biologically important compounds.

Examples of Recent Publications

Thomas E Gunter, Paramagnetic Resonance of OH Radical in Solids and Proton Spin-Lattice Relaxation at High Fields and Low Temperature (Thesis), June 1966

Thomas E Gunter, Electron Paramagnetic Studies of the Radiolysis of H_2O in the Solid State, J. Chem. Phys. 46, 3818-3839 (1967).

Thormond Hendrikson, Production of Free Radicals in Solid Biological Substances by Heavy Ions, Radiation Res. 27, 676-693 (1966).

Tor Brustad, Effects of Accelerated Heavy Ions on Enzymes in the Dry State and in Aqueous Solutions, in Proceedings of the First International Symposium on the Biological Interpretation of Dose from Accelerator-Produced Radiation, Berkeley, California, March 13-16, 1967, Oak Ridge Report CONF-670305.

Nabil M. Amer, The Effects of Homogeneous Magnetic Fields, Ambient Gas Composition, and Temperature on Development of Tribolium confusum, UCRL-16854, Dec. 1965.

ELECTRON SPIN RESONANCE STUDIES OF H_2O RADIOLYSIS AND LINEAR ACCELERATOR DEVELOPMENT DIRECTED TOWARD ESTABLISHMENT OF PULSE RADIOLYSIS FACILITIES

Thomas E Gunter

Electron spin resonance (ESR) provides an excellent experimental tool to use in radical identification Since free radicals contain an unpaired orbital electron, they are invariably paramagnetic. ESR, which is sensitive only to paramagnetic species, and is almost unaffected by the nonmagnetic molecules in the sample, hence allows one to study free radicals even at low radical abundance

Identification of a free radical through ESR is usually made through a knowledge of the number and relative intensities of spectral lines predictable through a knowledge of the hyperfine interaction.

Regardless of whether or not the radical can be identified through its spectrum, its spin concentration may be determined by calculating the area under its absorption curve and comparing it to the corresponding area under the absorption curve of a standard whose spin concentration is known Hence such parameters as radiation yield and spin concentration at saturation of the crystal's available sites can be determined through ESR techniques

OH produced by radiolysis of H_2O has been investigated at this Laboratory, by use of the ESR technique, [1] in single crystals of ice, $CaSO_4$ $2H_2O$, and $Li_2SO_4 \cdot H_2O$. These studies were carried out at 77°K except for a few preliminary studies made at 4.2°K.

In these studies, the effective spin Hamiltonian was determined for OH, trapped in each of the above-mentioned crystal lattices For the ice, the experimentally determined spectroscopic splitting tensor was shown to be in agreement with a simple theory based on crystal field theory. The experimentally determined hyperfine splitting of the OH radical was shown to be in agreement with that predicted by an LCAO MO calculation (see Fig 1 and Table I).

In the irradiated sulfates, magnetic resonance spectra of OH, H atoms, and some form of trapped electron were observed.

Radiation yield measurements for OH in ice at 77°K are shown in Fig 2 over the dose range 10^4 to 10^9 rads.

The preliminary spectroscopic studies at 4 2°K have indicated interesting changes in the ESR spectrum of ice (irradiated at 77°K)

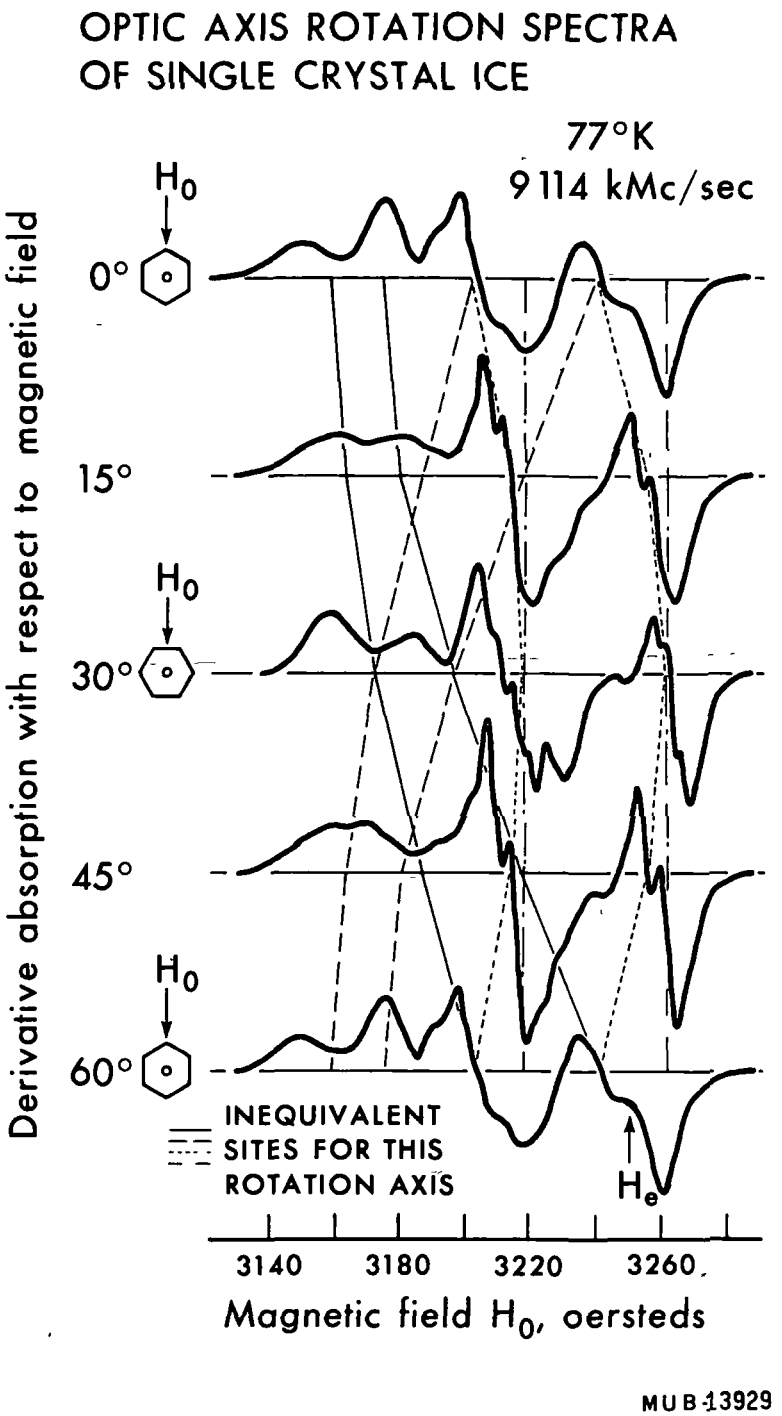


Fig 1. Derivative of resonance absorption vs field for a series of crystal orientations from OH in hexagonal, single-crystal ice. Rotation is about the crystal optic axis. The lines show absorption line positions predicted by the fitted effective spin Hamiltonian. The difference in the spectra shown at 15 and at 45 deg is believed to be due to errors in crystal orientation.

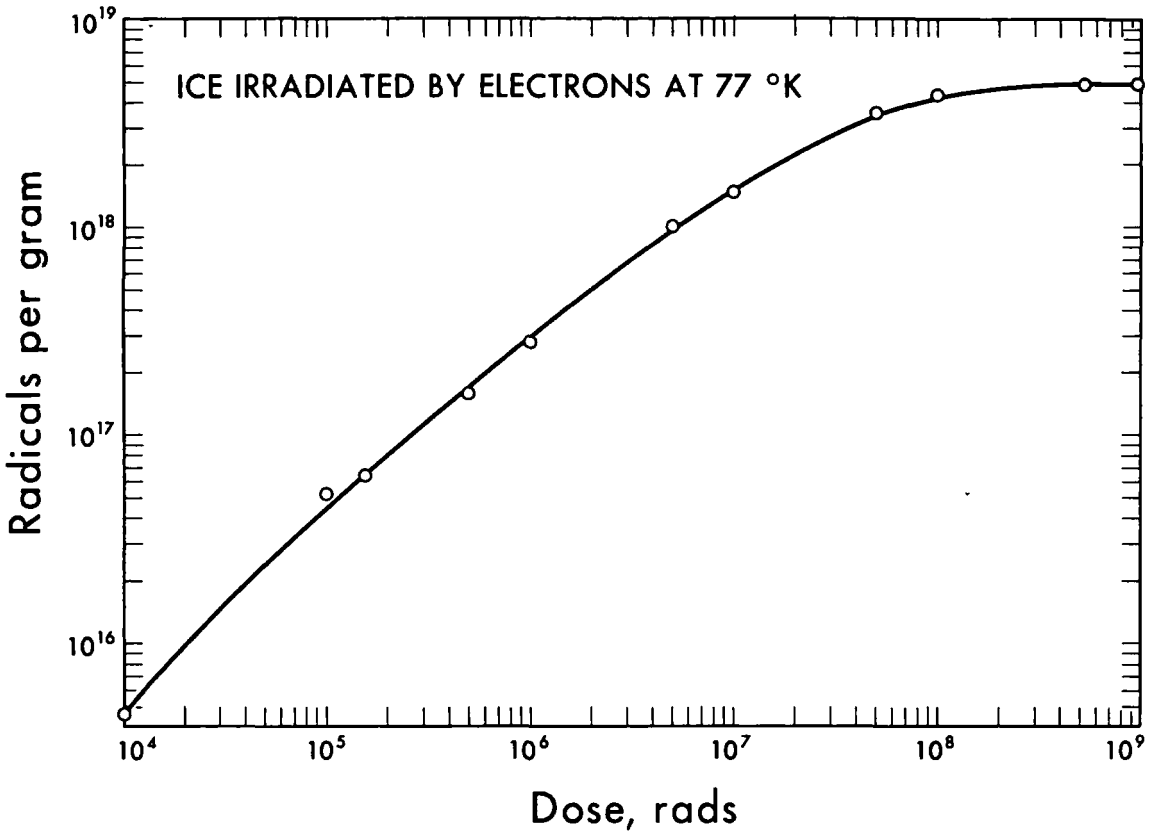


Fig. 2. Number of trapped OH radicals vs dose for irradiated H_2O at 77°K. The radiation yield determined from the low-dose end of this curve is G_{OH} = 0.8 radical/100 eV.

Table I. OH experimental and theoretical spin-Hamiltonian parameters.

Experimental values, OH in ice	Experimental values, OH in vapor	Predicted values
$g_{\|\|} = 2\ 0615 \pm 0.010$	- - -	2.0631
$g_{\perp} = 2\ 0095 \pm 0.005$	- - -	2.0077
$A_z = 7\ \text{Oe} \pm 5\ \text{Oe}$	$5\ \text{Oe} \pm 0.3\ \text{Oe}$ [a]	$5.019\ \text{Oe}$ [b]
$A_x = A_y = -43\ \text{Oe} \pm 5\ \text{Oe}$	$-42.6\ \text{Oe} \pm 0.3\ \text{Oe}$ [a]	$-38.87\ \text{Oe}$ [b]
$A_{\text{isotropic}} = -26\ 3\ \text{Oe} \pm 5\ \text{Oe}$	$-26.7\ \text{Oe} \pm 0.2\ \text{Oe}$ [a]	$-24.24\ \text{Oe}$ [b]

a. Ref. 2
b. Ref. 3

with temperature, in the range 77°K to 4.2°K. These observed line-shape changes cannot be completely explained on the basis of present data, but they may have to do with the presence of other paramagnetic species whose spectra are "washed out" because of large line widths at 77°K.

Improvements in the spectrometer system are necessary in order to complete this work. These improvements are currently being made.

The technique of low-temperature trapping of reactive species produced by radiolysis of biologically interesting materials is, of course, only one of the methods by which such species may be studied.

In collaboration with the radiation chemistry group here at Lawrence Radiation Laboratory, we are seeking to set up an optical pulse radiolysis system.

Our part of this work consists of improving the short pulse capability of our electron linear accelerator so that nanosecond or even subnanosecond rise and fall times of the beam are obtainable. Dose rates must also be increased, of course, to allow high doses to be delivered in the short pulses

The changes are planned to be carried out in three steps, each improving the electron linac and leaving it in operating condition so that loss of experiment time is minimized. The three steps might be described as

1. Design and construction of an electron gun and injection acceleration cavity.
2. Incorporation into the system of the Stanford Accelerating Guide.
3. Addition of an electron bunching system.

Step 1 will allow pulse lengths which are continuously variable from subnanoseconds to 7.5 microseconds. Beam intensity will be continuously variable from zero to the maximum allowed by the accelerating guide design (about 175 mA per pulse). Beam energy will be variable from 0.5 to 8 MeV.

Step 2 will extend the useful beam energy to from 0.5 to 25 MeV and will increase the beam intensity to the maximum allowed by the Stanford Accelerating Guide, which should be in excess of 300 mA per pulse.

Step 3 will further shorten the pulse length.

At present, step 1 has reached the test stand stage.

References

1. T. E. Gunter, J. Chem. Phys. 46, 3813 (1967).
2. H. E. Radford, Phys. Rev. 126, 1035 (1962).
3. K. Kayama, J. Chem. Phys. 39, 1507 (1963).

Page intentionally left blank

Page intentionally left blank

PRODUCTION OF FREE RADICALS AND RADIATION DAMAGE IN TRYPSIN BY IRRADIATION WITH ELECTRONS AT 4.2°K

W. Barrie Jones *

General Background

Although biophysicists and radiobiologists have sought for many years to elucidate the molecular mechanism(s) by which radiation inactivates molecules of biological significance, the question of the relative importance of ionizations versus excitations in this process remains unanswered.[1] With development of the technique of electron spin resonance (ESR) analysis, after the work of the Russian scientist, Zavoisky,[2] it became possible to study the free radicals produced by irradiation. (A free radical may be defined as a molecule or part of a molecule in which the normal chemical bonding has been modified so that an unpaired electron is left associated with the system. The uncompensated spin motion of this odd electron causes the free radical to exhibit a magnetic moment, ESR analysis is based upon the measurement of the energy associated with the spin and moment of the unpaired electron.) It is evident that appearance of free radicals produced by ionizing radiation can be used as an index of molecular damage. Furthermore, the irradiation-induced inactivation of enzymes can also be taken as evidence of damage to the enzyme molecule. The possible implication of the irradiation-produced free radical as the agent of molecular damage was suggested by recent studies,[3-5] which showed that there seem to be correlations between the yield of free radicals induced in dry enzymes by ionizing radiation and the corresponding inactivation of the enzyme. Thus Henriksen[3] has shown that the change in total yield of free radicals produced by irradiation of trypsin as a function of temperature exactly parallels the change in enzyme inactivation over the same temperature range. Similar parallel changes in radical yield and enzyme inactivation were observed[4] when the stopping power of the radiation was varied over the range from 2 to 2×10^4 MeV $g^{-1}cm^2$. In a study of the inactivation of RNase by ^{60}Co γ rays, Hunt and Williams[5] found a good correlation between inactivation of the enzyme and the yield of the "doublet" type of radical, and, using this correlation, were able to make accurate predictions for the effect of postirradiation exposure to O_2 on the radiosensitivity of the enzyme. However, Brustad and co-workers[6] did not find the same correlation between inactivation of trypsin and the yield of uv-induced free radicals. In considering this conflict, it should be borne in mind that free radicals are very reactive chemical species, that the radicals studied in the works outlined above are NOT the initial spin centers, but are the relatively more stable "secondary" radicals which may well be among the last steps in the chain of reactions leading from the primary

*USAEC Postdoctoral Fellow

absorption events, and that the injury which leads to inactivation of the enzyme molecule may be related to one of the earlier events in the reaction chain. Thus the question of whether free radicals produced in the enzyme molecule cause enzyme inactivation or merely serve to indicate damage already done cannot be decided until the first free radicals (initial spin centers) have been characterized and their yields checked for correlation against enzyme inactivation. It was realization of this problem that led to the research described in this brief paper. Because of the great reactivity of the initial spin centers, it is necessary to go to extremely low temperatures in order to stabilize the radical for a sufficient time to allow ESR spectral and yield measurements to be made.

Long-Range Goals

Although results presented here are quite preliminary, it would be well to briefly outline the form of the entire project:
(a) Check correlation between yield of initial spin centers and inactivation of enzyme.
(b) Determine if the radiosensitivity at liquid helium temperature (4.2°K) is the same as at liquid nitrogen temperature (77°K). If the sensitivities are not the same, then different mechanisms of damage production are operative at the two different temperatures and the conclusions drawn from the studies at liquid helium temperature would not be valid for explaining radiation effects at higher temperatures.
(c) Characterize the ESR spectrum of the enzyme radical (s), i.e., determine the number of lines, the line width, the spectroscopic g value for each line, etc.
(d) Try to pinpoint the location of the radical(s) in the enzyme molecule by irradiating component amino acids and peptides and examining their ESR spectra to determine if the spectrum of the enzyme can be ascribed to any of its component parts.
(e) If (d) is successful, try to grow single crystals of the amino acid(s) or peptide(s) exhibiting the same ESR spectrum as the enzyme. Then

(i) obtain crystallographic parameters from the literature, if available, or try to determine these parameters by use of x-ray diffraction or small-angle electron scattering in an electron microscope (see Ref. 7), depending on the size of the single crystal available.
(ii) Once the crystallography is known, irradiate the single-crystal form of the amino acid or peptide and study the ESR spectrum as a function of crystal orientation. From these results, determine the radical structure.

(f) Qualitatively characterize the reaction pathway(s) from the initial centers to the stable secondary radicals by irradiating at 4.2°K and measuring the yield of centers in the enzyme, warming slightly and again measuring the yield and noting any change in the spectrum, warming again, etc.

These goals may seem ambitious, but their achievement requires only a great deal of time and effort. The requisite techniques for their accomplishment are all available.

Preliminary Results for Trypsin

Dry, powdered trypsin, twice crystallized, obtained from Sigma Chemical Co., St. Louis, Mo., stored in a desiccator over silica gel at -20°C, was placed in a glass sample tube which was evacuated with a mercury diffusion pump to a pressure of 1 to 3×10^{-5} mm Hg, the tube was then sealed with a torch. The sample tube is of a special design (see Fig. 1) which allows the sample to be irradiated through the irradiation port of the irradiation cryostat (Fig. 2), after which the "gate" inside the sample tube is actuated and the sample then falls to the bottom of the tube, which is centered inside the ESR resonance cavity. In this manner it is possible to both irradiate the sample and measure its ESR spectrum while keeping the sample always at 4.2°K; and, since the irradiated portion of the glass sample tube is kept outside the ESR cavity, the F centers formed in the glass by the irradiation do not interfere with the measurement of the spins produced in the sample. The "gate" inside the sample tube is a brass disk upon which the sample rests; after irradiation, a sharp blow on the sample support rod causes the disk to rotate and drop the sample. The cryostat shown in Fig. 2 holds helium for about 4 hr if low doses have been delivered, and it has now been modified with an additional transfer opening on the top to allow liquid helium to be added while the sample is in place.

Using the above equipment and irradiating with 6.5-MeV electrons from the Berkeley Linac to give doses of 1 to 20 Mrad at a dose rate of approximately 1 Mrad/min, I found that trypsin displayed the same radiosensitivity at liquid helium temperature as at liquid nitrogen temperature. The ESR spectrum of trypsin irradiated at 4.2°K is seen in Fig. 3; it consists of an unresolved doublet with a line width (both lines) of 24.85 Oe, with spectroscopic g values g_D (both lines) = 2.0021 and $g_{\text{lesser line}}$ = 2.0010. Although one of the simplest processes by which the normal chemical binding could be altered to produce a free radical would be the removal of a hydrogen atom, no hydrogen atoms were seen. (This may be a problem of sensitivity, and modifications of the spectrometer to vastly increase its sensitivity are now in progress.)

The amino acid sequence in the region of the active site has been determined for trypsin (for a review, see Ref. 8) by use of the competitive inhibitor, diisopropylphosphofluorodate (DFP), which reacts with the active site of trypsin to give trypsin-DIP. Hydrolysis of this reaction product yields fragments of various lengths with the DIP attached. From the analysis of these fragments, a sequence of fifteen amino acids has been determined in the region of the active site, as shown in Fig. 4. In addition, it is felt that the active site probably has histidine in close proximity to the serine, with the histidine brought from elsewhere in the protein by secondary and tertiary folding. Now

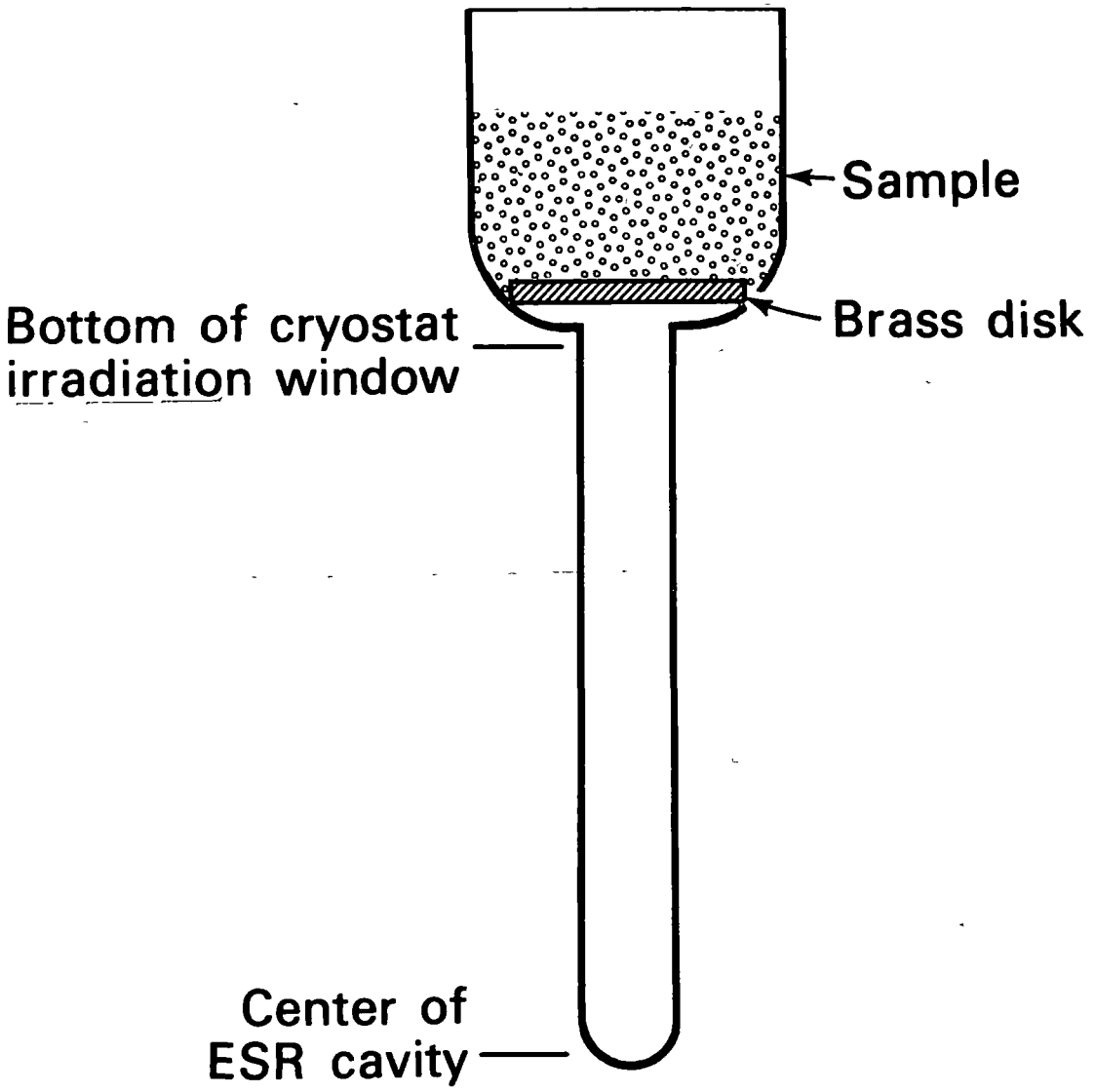


Fig. 1. Schematic of sample tube. The dimensions are such that the correct positioning of the sample for irradiation automatically places the inside bottom of the tube at the center of the ESR cavity.

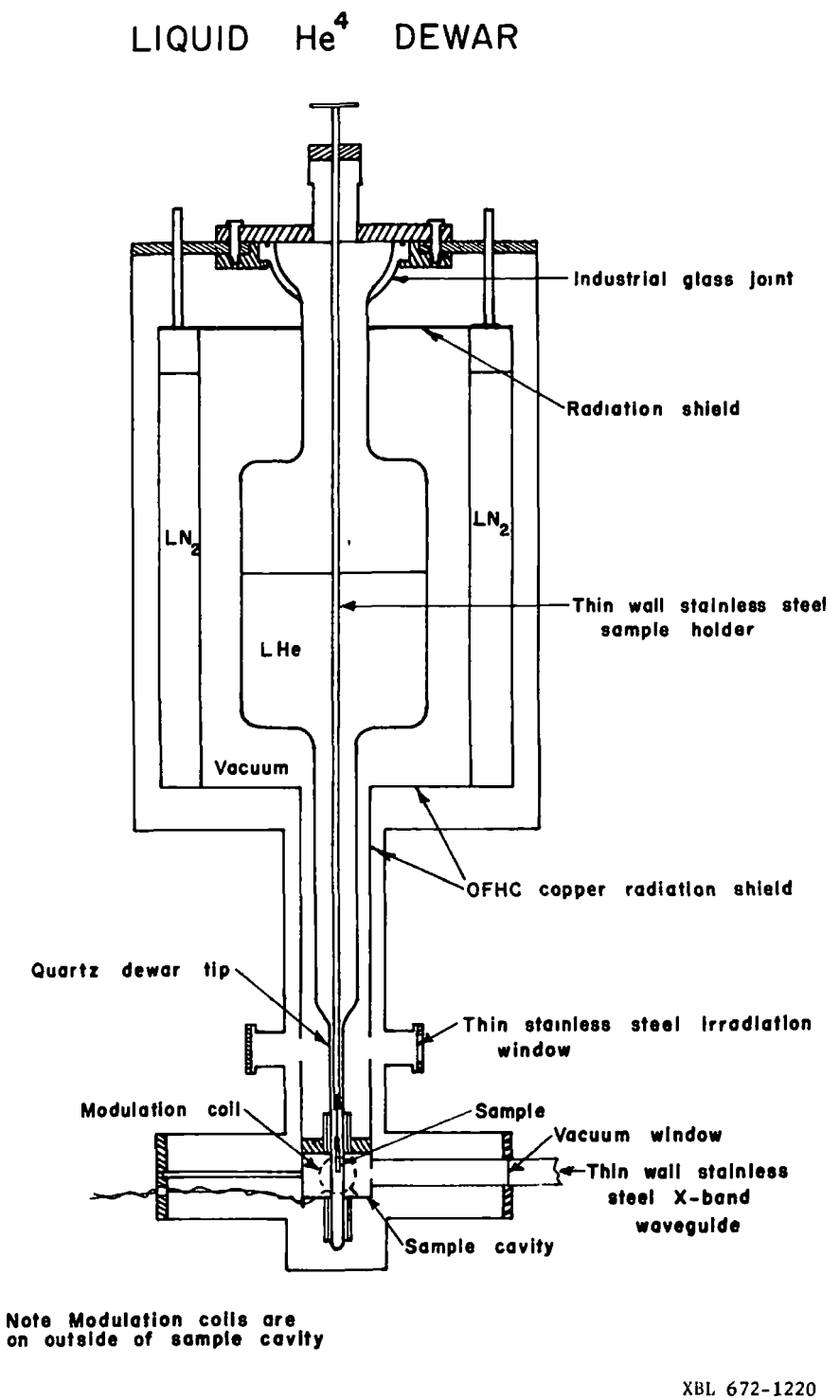
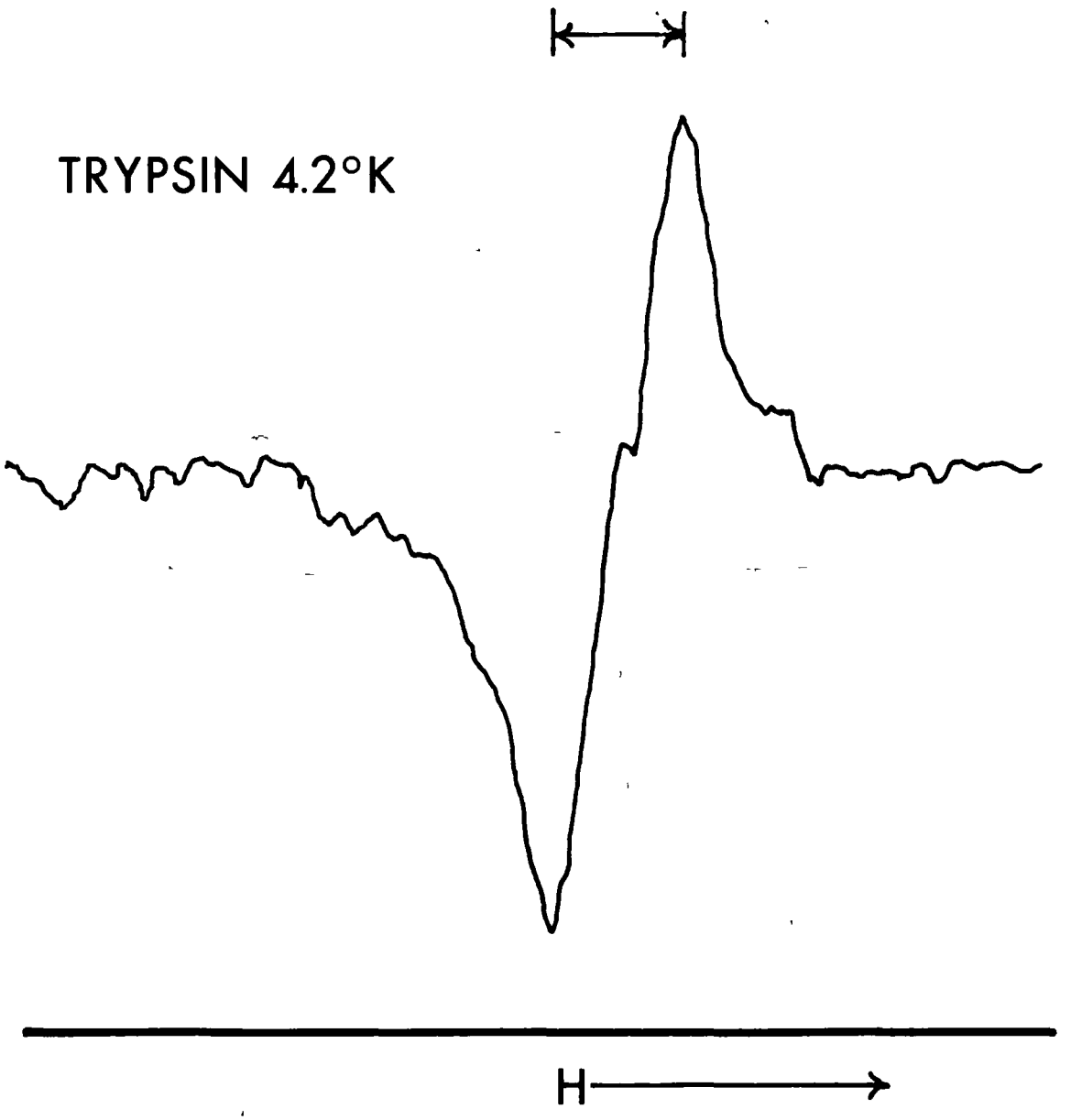
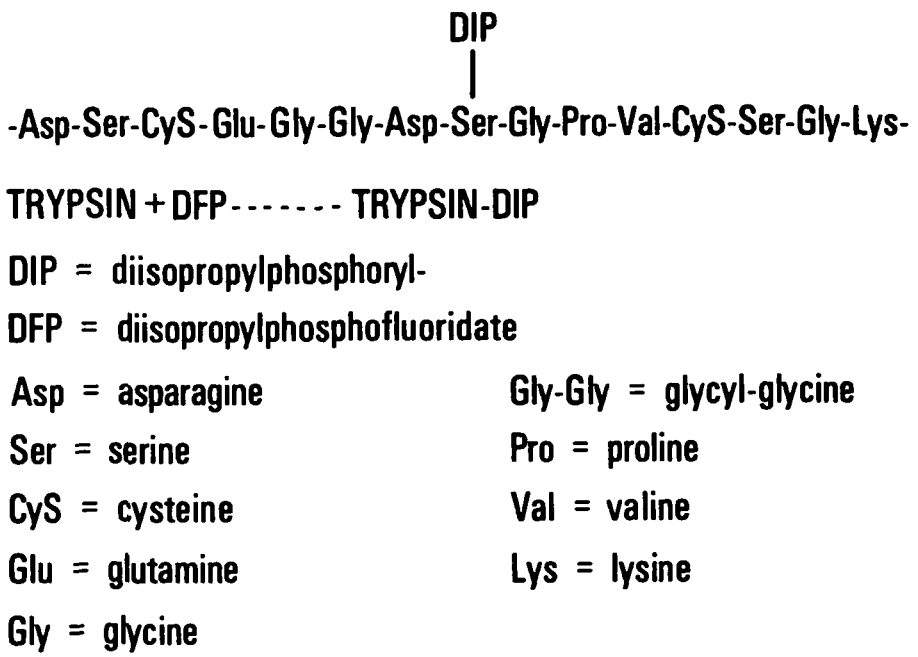


Fig. 2. Cryostat for irradiation at liquid helium temperature. This view shows a single crystal and crystal holder used in place of the glass sample tube.



XBL 673-1262

Fig. 3. ESR spectrum of trypsin irradiated and measured at 4.2°K.



DBL 678-1737

Fig. 4. Amino acid sequence in the region of the trypsin active site.

since I am ultimately concerned with the relation of the initial spin centers to enzyme inactivation, it seemed very desirable to irradiate the amino acids in the region of the active site to see if any would give the same (or similar) ESR spectra as observed for trypsin. Consequently histidine, the dipeptide glycyl-glycine, and all the amino acids of Fig. 4 except glutamine have been irradiated at 4.2°K, and their ESR spectra have been determined. Absolute yield measurements have not been possible, due to marked instability in our integrator; however, relative yield measurements were made upon the derivative spectra by comparing amplitudes after taking into account differences in line width. The results of these measurements may be briefly summarized as follows: except for glycine, glycyl-glycine, and serine, all the amino acids had yields of initial spins at least one order of magnitude less than the yield in trypsin, while the yields in glycine, glycyl-glycine, and serine were of the same order of magnitude as the yields in trypsin. Since serine is the only member of this trio which is clearly involved in the active site, the serine ESR spectrum was of prime interest. However, it can be seen (Fig. 5) that the serine spectrum bears no resemblance to the trypsin spectrum; the total line width of this spectrum is approximately 62 Oe. These factors make it unlikely that serine contributes significantly to the ESR spectrum seen for trypsin.

Glycine and glycyl-glycine give ESR spectra which appear to be identical to the trypsin spectrum of Fig. 3, the spectroscopic g values are the same within the accuracy of the measurement. However, the line width for glycine is approximately 42 Oe, compared with 25 Oe for trypsin. When two glycine moieties are combined in glycyl-glycine, the line width falls to approximately 28 Oe; it would be most interesting to see if the addition of a glu- or -asp to a gly-gly unit brought the total line width still closer to the 25 Oe observed for trypsin.

On the basis of these results, it is tempting to conclude that the initial spin centers in trypsin are formed in the gly-gly units or perhaps in a dipeptide unit composed of glycine and one other amino acid. Further studies are being undertaken with gly-ser, gly-asp, gly-pro, gly-glu, and ser-gly (see Fig. 4) to evaluate the latter possibility, and glutamine itself will be carefully checked. Growth of single crystals of glycine, glycyl-glycine, and the other relevant dipeptides has been started, and the identification of the radical structure should be in full swing by late fall or early winter. The truly interesting part of this project has just begun; positive identification of the initial centers of radiation damage in trypsin should be possible within the next year.

In addition to the obvious need to search out "knowledge for knowledge's sake," there is a practical benefit to be derived from the basic research described in this paper. Intelligent prophylaxis of radiation lesions at the molecular level can be done more readily

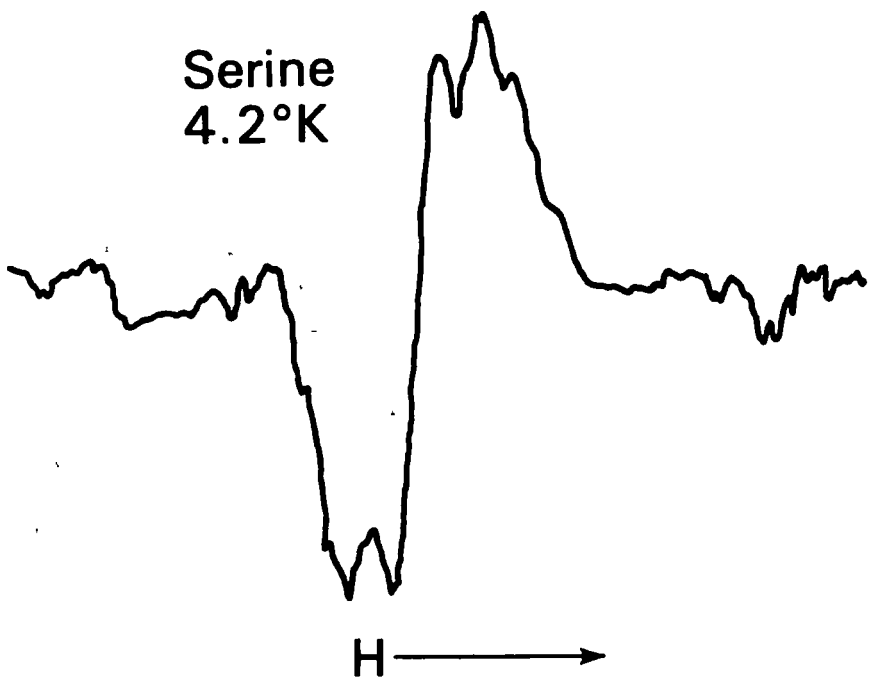


Fig. 5. ESR spectrum of serine irradiated and measured at 4.2°K.

when the initial centers of damage have been identified. Thus work carrying the unlikely title displayed on the first page of this paper may eventually provide direct benefit to an astronaut exposed to the radiation hazards of space travel.

References

1. L. G. Augenstein, T. Brustad, and R. Mason, The Relative Roles of Ionization and Excitation Processes in the Radiation Inactivation of Enzymes, Advan. Rad. Biol. 1, 227-266 (1964).
2. E. J. Zavoisky, Phys. (USSR) 9, 211, 245, 447 (1945).
3. T. Henriksen, Effect of the Irradiation Temperature on the Production of Free Radicals in Solid Biological Compounds Exposed to Various Ionizing Radiations, Radiation Res. 27, 694-709 (1966).
4. T. Henriksen, Production of Free Radicals in Solid Biological Substances by Heavy Ions, Radiation Res. 27, 676-693 (1966).
5. J. W. Hunt and J. F. Williams, Radiation Damage in Dry Ribonuclease: Yields of Free Radicals and Other Chemical Lesions Compared With Inactivation Efficiency, Radiation Res. 23, 26-52 (1964).
6. T. Brustad, H. B. Steen, and J. Dryset, Inactivation and Induction of Free Radicals in Dried Trypsin, Radiation Res. 27, 217-228 (1966).
7. R. Glaeser (Donner Laboratory), personal communication.
8. Biochemists' Handbook, Ed. by C. Long (D. Van Nostrand, Princeton, 1961).

EXCITED ELECTRONIC STATES IN NUCLEIC ACID COMPONENTS AND THEIR RELATION TO RADIATION DAMAGE

Martin D. Shetlar

In the past decade or so, much information has been brought forth concerning the identity of the final reaction products and of reactive chemical intermediates involved in pathways leading to radiation damage. In many cases, non-free-radical species in excited states are thought to be intermediates. However, relatively little definite information has been forthcoming on questions such as (a) are singlet or triplet states (or both) involved in the production of damage products, or (b) are excited singlet or triplet states immediate precursors of observed free radicals? An understanding of the processes occurring at the excited-state level is vital for eventual delineation of the complete reaction pathway leading to radiation damage.

Of the excited states which may be involved in radiation damage processes, those most likely to participate in pathways leading to damage are the lowest singlet and triplet states of the original molecule or of chemical intermediates. This is because of the very fast rate processes leading to deactivation of higher electronic states, in contrast to considerably slower rates for chemical reaction with other chemical species (dissociation processes, of course, can take place during the time required for a molecular vibration). In nondissociative processes, it should be sufficient to study the reactive properties of the lowest triplet and singlet excited states in the reactions of interest.

The specific goals of the present research are:

1. To find which radiation damage processes are attributable to processes leading through the lowest triplet states and which must be assigned to singlet-state reactions.
2. To try to find, on the basis of the results of the above research, an experimental understanding of the sensitization of nucleic acids to radiation damage by substitution of halogenated base analogs.

Two approaches are being used to help solve these problems:

A. The use of triplet-triplet (T-T) absorption to help probe the energy-level manifold of nucleic acid components.

B. The use of triplet quenchers to help determine the relative importance of the triplet state and singlet states in processes leading to reactive damage.

A. Triplet-Triplet Absorption

To understand the rationale behind the use of T-T absorption as a tool for the achievement of the above goals, consider Fig. 1. In this

figure: Case A and Case B represent the energy-level structure of two pyrimidine bases. In Case A, an excited molecule decays in approximately 10^{-12} second to the lowest excited singlet state. There, within 10^{-8} sec it will either return to the ground state or cross over into the triplet manifold or react with an available chemical species. A similar situation holds in Case B except that intersystem crossing is much enhanced because

$$\text{rate}\,[{}^1S(n^2\pi\pi^*) \rightarrow {}^3T_1(n^2\pi\pi^*)]$$

$$<< \text{rate}\,[{}^1S^*(n^2\pi\pi^*) \rightarrow {}^3T_1(n\pi^2\pi^*)]$$

Since an excited nonbonding electron is involved in the second excited triplet state of the molecules in Fig. 1, environmental conditions have a large effect on the energy of this level. Similarly halogenation may shift this level from Case A to Case B. If the triplet state is a reactive intermediate in radiation damage, any effect which shifts a pyrimidine base from Case A to Case B will enhance its sensitivity to radiation damage. Indeed, in uracil the radiation sensitivity to ultraviolet radiation has been observed to vary as a function of pH and of solvent.

By examining the T-T absorption spectrum of the various nucleotides, nucleosides, and bases, especially as a function of pH, and likewise investigating the spectra of the halogenated analogs, one may gain insight into the reasons for the varied radiation-damage behavior of the nucleic acid components.

Results

A Dewar and light source have been constructed which allow steady-state illumination at 2536 Å of the sample in a long optical pathway at liquid nitrogen temperatures. The molecules under study are placed in solvents which form noncracking glasses at liquid nitrogen temperatures. The apparatus was tested by observing the previously reported T-T spectra of naphthalene, anthracene, and bromonaphthalene. The apparatus was also found suitable for phosphorescence and fluorescence studies.

Preliminary studies on thymine and uracil were carried out and the results of the phosphorescence and fluorescence studies of previous workers were confirmed. Faint absorption regions in the near-infrared region were observed, but the regions were not of sufficient intensity to allow definite conclusions to be drawn.

A high-intensity dc ultraviolet source has been acquired which will allow much higher concentrations of triplet-state molecules to be produced. This in turn will produce higher absorption intensities. A Dewar has been constructed for use with the Cary 14 Spectrophotometer that will allow greater sensitivity in scanning the infrared region for these transitions.

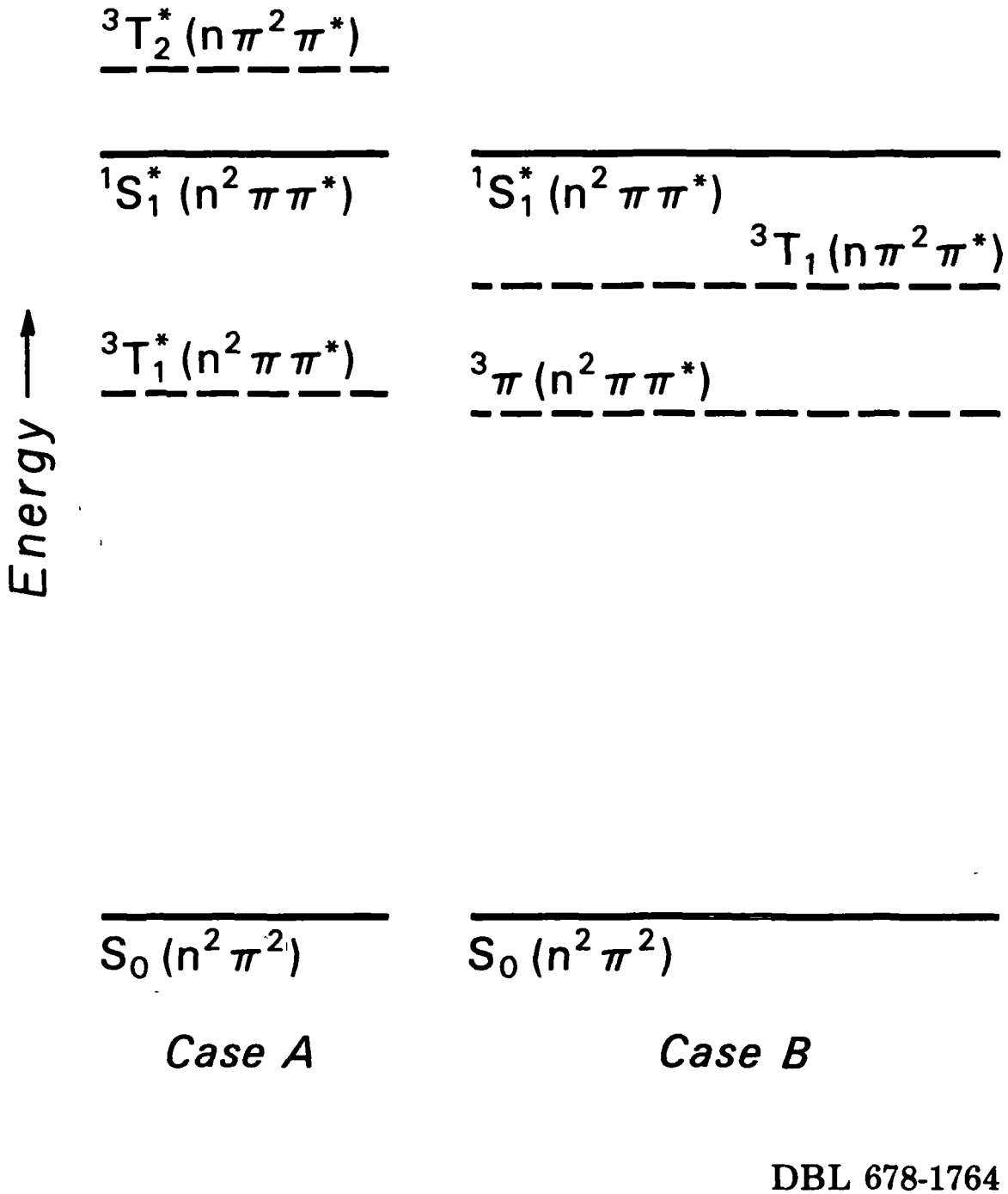


Fig. 1. Effect of environment on molecular energy levels. (See text.)

B. Triplet Quenching Studies

The use of triplet quenchers allows one to make detailed studies of the excited-state processes which occur during radiation-induced chemical damage.

By measurement of quantum yields of radiation-damage reaction product as a function of triplet quencher concentration, one can often derive such useful information as the lifetime of the triplet state under the environmental conditions of the reaction and the relative quantum yields of competing pathways passing through both the singlet state and the triplet state if such should exist.

A further use of triplet quenchers, in particular trans- and cis-piperylenes, is in the technique known as chemical spectroscopy. This technique allows one to determine the intersystem crossing quantum yields for an excited molecule in a given environment. Using this technique, one can gain information which is directly correlatable to the information gained through T-T absorption. In environments in which the previously described Case A holds, small intersystem crossing quantum yields should be observed. In Case B, larger intersystem crossing quantum yields should be observed. If one should find fortunate cases in which a change from Case A to Case B occurs as one changes the environment, one might be able to provide dramatic evidence of involvement of triplet states in reactions by measuring quantum yields of product as one moved from Case A to Case B.

Results

Thus far four reactions have been studied by use of triplet quenching methods.

1. Uracil in methanol: The photoreaction of uracil with methanol leads to the addition of methanol across the 5, 6 double bond as well as other reactions leading to unidentified products. It has been found that at least part of the damage occurs through triplet-state pathways. The lifetime of the uracil triplet state has been determined.
2. N, N-Dimenthyluracil in methanol: Triplet quenching studies of this system support the conclusion that all reaction proceeds through the lowest excited singlet state.
3. Uridylic acid in methanol: In this case, triplet quenching studies produced anomalous results. The quantum yield of photoproduct, instead of being decreased, was increased. A preliminary model explaining these results is being considered, but further experimental results are needed before definite conclusions can be drawn.
4. The interaction of uridine in ethanol has been studied in the greatest detail. It has been found that this molecule goes through both the triplet state and singlet state in the 5, 6 addition reaction of ethanol. A very large oxygen effect has been noted. The lifetime of the triplet state has been measured and assigned a value of 10^{-6} sec. The effects of oxygen on the singlet-triplet crossing rate are being studied.

It is planned to extend the above studies to

- Triplet quencher effects on reaction yields to cytidylic acid radiation-induced reactions.
- Dimerization reactions of thymidylic acid and orotic acid to determine excited-state pathways.
- Use of the method of chemical spectroscopy to determine intersystem crossing yields for important nucleic acid components and analogs and correlate these data in the manner mentioned above with T-T absorption data.

Page intentionally left blank

Page intentionally left blank

EFFECTS OF HOMOGENEOUS MAGNETIC FIELDS UPON BIOLOGICAL SYSTEMS

Nabil M. Amer

Amer[1] described the effects of homogeneous magnetic fields upon the development of Tribolium confusum incubated at constant ambient temperature as qualitatively equivalent to an "intrinsic cooling effect" of the order of 1°C/6000 gauss. One possible explanation for the relatively large magnetic field effect is the assumption that the field affects the structure and possibly the transport properties of biological membranes and macromolecules, altering their molecular arrangements and intermolecular forces.

We tested the "intrinsic cooling" hypothesis with substances with mesomorphic states which, when cooled, have the characteristic of changing their light-scattering properties as a function of temperature. The change is expressed in a shift in the wavelength of scattered light. When a mesomorphic state with a range of coloration between 34° and 37° was maintained at an ambient temperature of 37°C ± 0.1 and an external magnetic field of 6.3 kG was applied to the preparation, a gradual change in the wavelength of the scattered light was obtained (a shift from 4600 to 6200 Å).

Currently we are in the process of attempting to extend this analogy to hormones, particularly those governing the development of Tribolium.

1. Nabil M. Amer, Radiation Res. 19, 215, (1963) and Ph. D. Thesis, University of California, 1965.

Page intentionally left blank

Page intentionally left blank

CELLULAR STUDIES

Introduction

The effects of light and heavy accelerated nuclei on cell systems have been under study in the Laboratory for a number of years. Of current interest are:

- Kinetics of cell survival and relative biological effectiveness.
- Mutational and genetic effects and their molecular aspects.
- Environmental modification of radiation injury.
- Repair processes.
- Molecular mechanisms of hormonal effects in relation to cellular control processes.
- Search for synergistic effects (vibration, gravity, magnetic fields).
- Relationship of cellular injury to radiation syndrome in multicellular organisms. Because of the availability of extensive recent publications, this section of the report was kept brief.

Examples of Recent Publications

Paul W. Todd, Reversible and Irreversible Effects of Ionizing Radiations on the Reproductive Integrity of Mammalian Cells Cultured in vitro (Thesis), UCRL-11614, Aug. 1964.

John T. Lyman, Dark Recovery of Yeast Following Ionizing Radiations (Thesis), UCRL-16030, March 1965.

Edward Siegel, The Effects of Thyroid Hormones on Cultured Mammalian Cells, UCRL-16776, March 1966.

R. K. Mortimer, T. Brustad, and D. V Cormack, Influence of Linear Energy Transfer and Oxygen Tension on the Effectiveness of Ionizing Radiation for Induction of Mutations and Lethality in S cerevisiae, Radiation Res. 25, 465-482 (1965).

E. L. Powers, J. T. Lyman, and C. A. Tobias, Some Effects of Accelerated Charged Particles on Bacterial Spores, submitted to Intern. J. Radiation Biol.

E. Siegel and C. A. Tobias, End-Organ Effects of Thyroid Hormones: Subcellular Interactions in Cultured Cells, Science 153, 763-765 (1966).

E. Siegel and C. A. Tobias, Actions of Thyroid Hormones on Cultured Human Cells, Nature 212, 1318-1321 (1966).

C. A. Tobias and P. W. Todd, Heavy Charged Particles in Cancer Therapy, U. S. National Cancer Monograph No. 24, Radiobiology and Radiotherapy, National Cancer Institute, Bethesda, Maryland, pp. 1-21, 1967.

C. A. Tobias, N. M. Amer, J. K. Ashikawa, J. T. Lyman, L. W. McDonald, J. V. Slater, C. A. Sondhaus, and P. W. Todd, in Proceedings of Second International Symposium on Basic Environmental Problems of Man in Space, Paris 1965, (Springer-Verlag, 1967), pp. 141-159.

Collaborative studies are being carried out with workers in a number of other laboratories. Examples are F. de Serres, G. Stapleton, R. McGrath, and F. Oakberg, Oak Ridge National Laboratories; S. Nakai, Japan; D. V. Cormack and Roger Inch, Toronto; L. Powers, University of Texas; and Harold Smith, Brookhaven National Laboratory.

THE EFFECT OF VARIOUS LET RADIATIONS ON "STEM CELLS" AS MEASURED BY THE SPLEEN COLONY-FORMING TECHNIQUE

Jose M. Feola and John C. Schooley

The effects of heavy ions on mammalian cells have been determined with a high degree of precision by using the colony-forming ability as end point. [1, 2] Irradiation of monolayers of cells attached to the bottoms of plastic dishes allows accurate dosimetry, easy quantitation, and good control over environmental conditions for the study of the oxygen effect as well as other variables of interest for basic radiobiological research. [3, 4]

Results obtained with in vitro techniques are not directly applicable to radiotherapy unless the same effects can be demonstrated with in vivo techniques. It is also desirable to establish differential radiosensitivities of normal and tumor cells if possible.

The transplantation technique developed by Hewitt[5] and Hewitt and Wilson[6] has been used in this Laboratory[7, 8] to study the effects of heavy ions on tumor cells irradiated in vitro and grown in vivo. A number of technical problems, the main one being the impossibility of determining the distribution of the dose delivered to the cells, left these experiments in a qualitative stage.

The high degree of precision obtainable with the spleen colony-forming technique developed by Till and McCulloch[9] and McCulloch and Till, [10] and the possibility of irradiating cells in suspension in irradiation chambers of the type designed by Tor Brustad, [11] moved us to undertake a new series of experiments. These experiments were designed to yield information on the effects of heavy ions on normal and tumor cells, irradiated in vitro under normal, hypoxic, and hyperoxic conditions.

This first series of experiments deals with irradiations of bone marrow cells in suspension and assay in vivo by the spleen colony-forming method.

Materials and Methods

LAF_1 female mice were chosen for these experiments because of the possibility of further work with tumor cells which also produce spleen colonies in these animals. [12, 13] The $LD_{50/30}$ for ^{60}Co γ rays was determined to be 900 ± 50 rads.

The bone marrow of the mouse contains cells which, upon

transplantation into lethally irradiated hosts, settle down, proliferate, and form discrete nodules in the spleen which can be easily counted.

Mice were irradiated at 1.22 meters from a ^{60}Co source at a dose rate of 12.5 R/min in air. A dose of 1150 rads was given to all recipient mice. After irradiation, groups of five mice were housed in sterilized cages and allowed to drink chlorinated water containing 0.5 to 1% Terramycin. Control mice which received no bone marrow cells were included in all experiments, and the endogenous spleen colony level was less than 0.4 colony per spleen in most cases.

Bone marrow cells were obtained from the femurs and tibias of isologous donor mice and, after they had been counted with hemocytometers, a suspension containing 20×10^6 bone marrow cells per ml was prepared with minimum essential medium (MEM).

An irradiation chamber as shown in Fig. 1 was used. The beam entered the chamber through a 0.25-mil Mylar window over which area the particle fluence was constant. The thickness of the chamber is about 5.0 mm in the direction of the beam, so that the helium and carbon ions were stopped in the suspension in the chamber. The useful volume is 4.2 cc. No gas was flushed through the chamber in this series of experiments.

The suspension was stirred with a small magnet while it was irradiated, and the same was done with cell suspensions used for control groups. No differences in the spleen colony-forming ability were detected in control experiments done with suspensions stirred for up to 10 minutes and with suspensions not stirred.

Bone marrow cells (BMC) have been irradiated with x rays from a 250-kV x-ray machine (Philips) working at 230 kV (HVL = 1.6 mm Cu), TSD = 25 cm, and a dose rate of 110 R/min. Helium ions accelerated by the 88-inch synchrocyclotron have been used at two different LET's, namely, 175 and 555 MeV-cm^2/g (estimated track average LET); the energies before entering the chamber were 86 and 20 MeV, respectively. Finally, helium and carbon ions from the heavy-ion linear accelerator (Hilac) have been used to irradiate the cells at 330 and 3300 MeV-cm^2/g, respectively.

At full energy in vacuum the ions from the accelerator have an energy of 10.4 MeV/nucleon. This energy is slightly degraded before the beam enters the irradiation chamber. The energies at the entrance have been estimated to be 38.8 MeV for the ^4He ions and 99.6 MeV for the ^{12}C ions.

After the cell suspensions had been irradiated at different doses, two groups of 12 to 15 mice per dose were injected iv with two different concentrations of BMC (usually a factor of 2) in 0.5 ml of suspending medium. Two control groups (nonirradiated BMC) were injected

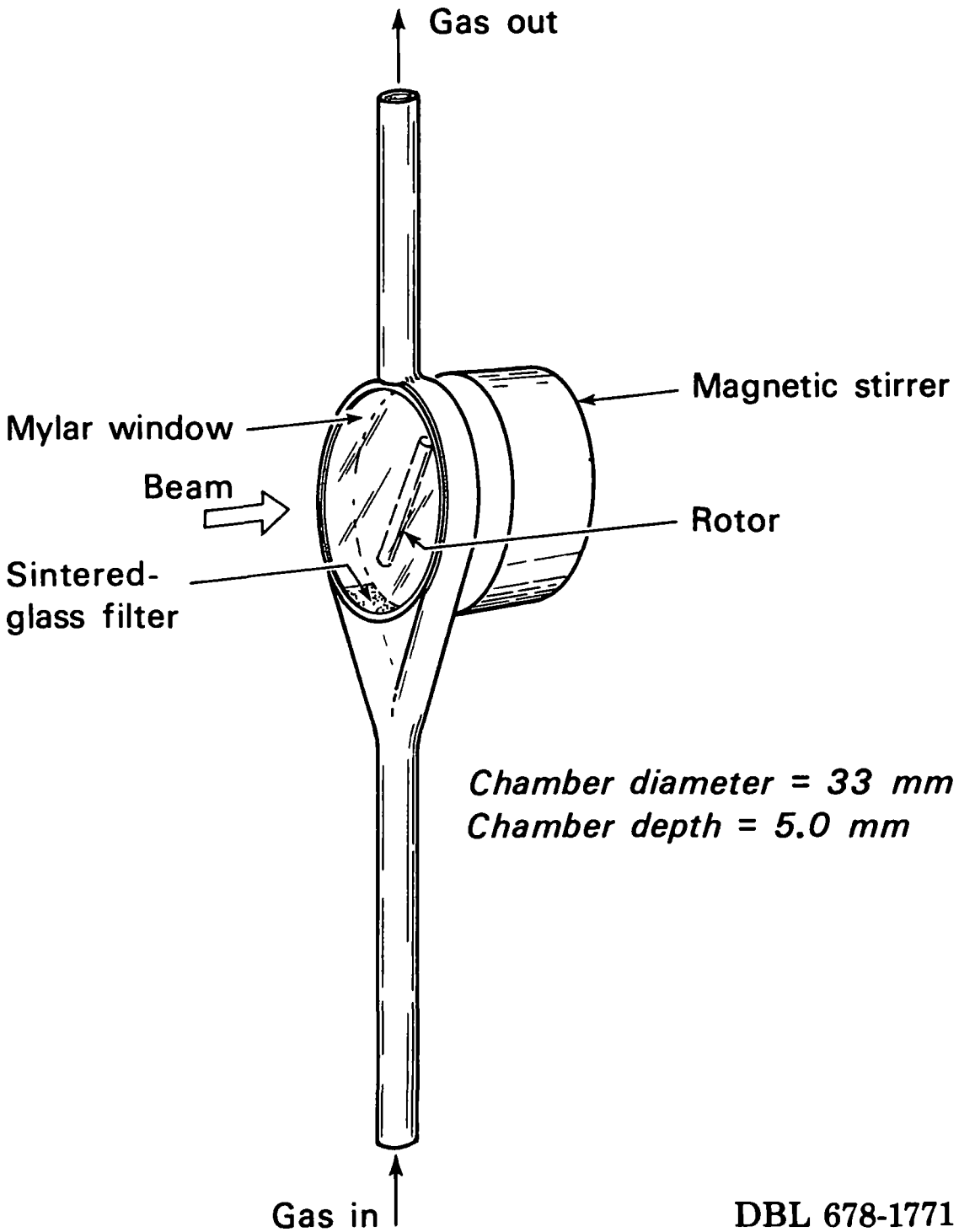


Fig. 1. Exposure chamber used for irradiation of BMC suspensions.

with 0.5 and 1.0×10^5 cells, respectively. Normally, 5×10^4 BMC produced 10 ± 2 colonies per spleen.

Mice were sacrificed after 10 days, and the spleens were removed and placed in vials containing Bouin's fixative. After 24 hours the number of colonies in each spleen was counted, and the averages and surviving fractions were calculated by comparison with control groups. Survival curves were obtained by visual fitting, and the mean lethal dose, D_0, was determined in each case.

Results

Table I. Preliminary results on the Effect of Various LET Radiations on "Stem Cells" as Measured by the Spleen Colony-Forming Technique

Radiation	LET_{av} MeV-cm^2/g	D_0 (rads)	Extrapolation number, n	RBE
x Rays, 230 kV	45	85 ± 5	2-3	1.000
^{4}He ions, 88-inch cyclotron	175	75 ± 10	2	1.1 ± 0.2
^{4}He ions, 88-inch cyclotron	555	90 ± 5	1	0.9 ± 0.1
^{4}He ions, Hilac	330	75 ± 15	1	1.1 ± 0.3
^{12}C ions, Hilac	3300	65 ± 15	1.8	1.3 ± 0.4

Table I summarizes preliminary results obtained. D_0 is the mean lethal dose. It is the dose required to reduce the proportion of surviving cells from 1 to 0.37 on the straight exponential part of the semilogarithmic cell-survival curve. The mean lethal dose has been used to estimate the relative biological effectiveness (RBE) of the heavy ions studied so far. The extrapolation number, n, is also shown. This is the intercept of the straight tail produced back to the zero-dose axis (see Fig. 2). Table II shows results of a typical experiment with x rays, and Fig. 2 shows the survival curve and extrapolation number obtained.

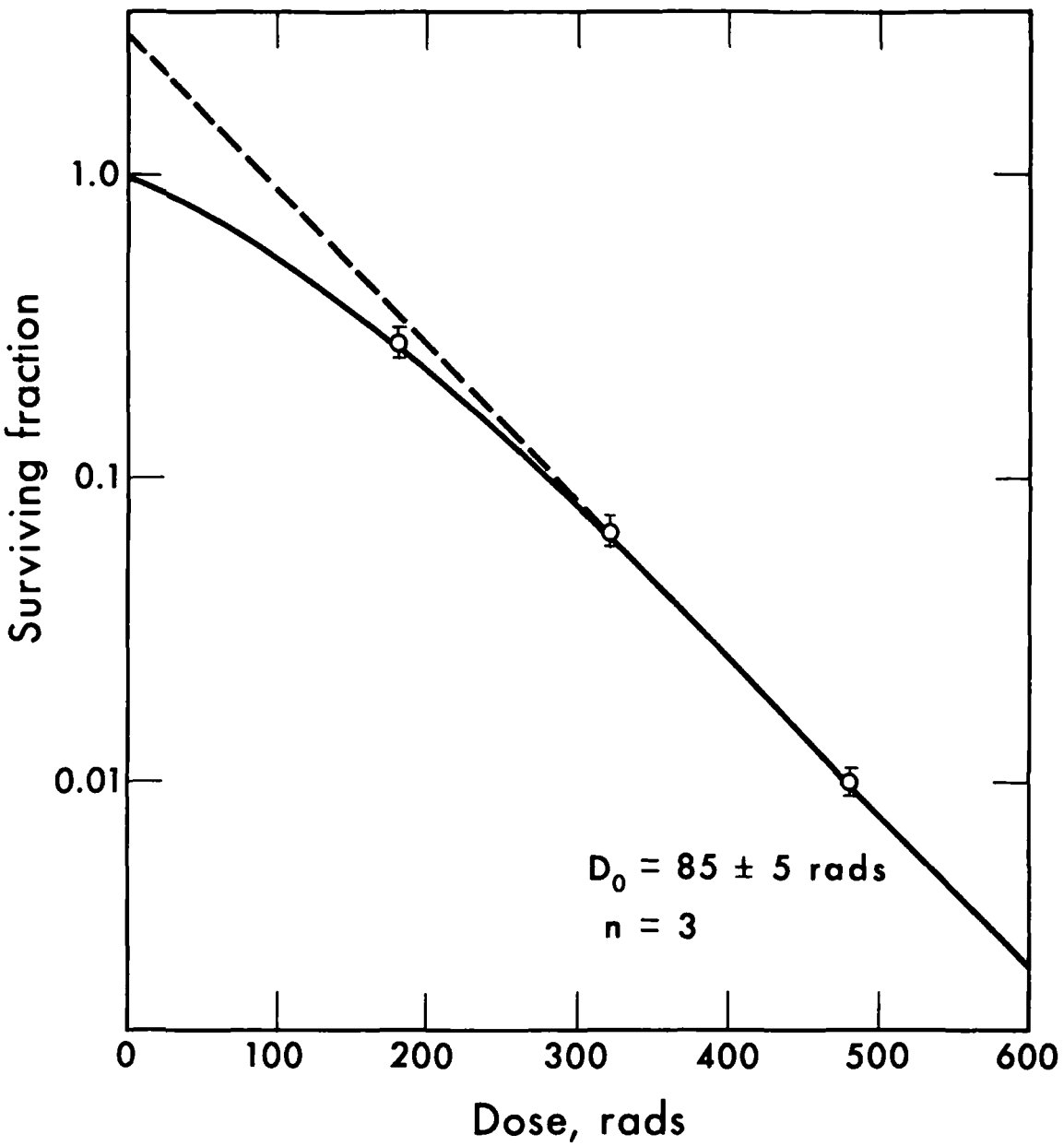


Fig. 2. Survival curve for bone marrow cells assayed by the spleen-colony technique.

Table II. Radiation Sensitivity of Colony-Forming Cells Irradiated In Vitro and Assayed in Heavily Irradiated Recipients

x-Ray doses (rads)	Cells injected	Average number of colonies per spleen	Standard deviation, S. D.	Standard error, S. E.	Surviving fraction ± S. E.
0	5×10^4	8.9	2.8	0.7	1.000
180	2×10^5	9.8	2.9	0.8	0.275 ± 0.050
320	1×10^6	12.3	2.6	0.7	0.069 ± 0.010
480	5×10^6	10.3	2.8	0.7	0.012 ± 0.002
0	1×10^5	12.9	2.1	0.5	1.000
180	4×10^5	14.6	2.1	0.6	0.283 ± 0.025
320	2×10^6	17.3	2.9	0.8	0.067 ± 0.006
480	1×10^7	13.2	2.4	0.7	0.010 ± 0.001

Discussion

Results reported here are from a series of preliminary experiments. Survival curves obtained by irradiation of the bone marrow cells with x rays are in good agreement with published reports.[14] Results obtained by irradiation with ^{4}He ions are in good agreement with our work with tumor cells.[15] The values reported for ^{12}C ions are a rough estimate made out of only one experiment. In two other experiments with these ions we have observed two slopes in the survival curves. The "resistant tail" with a higher D_0 than the initial portion of the curve is not due to a resistant component of the cell population. It is due to a deficient stirring of the cells while they are being irradiated. It shows up in the experiments with ^{12}C ions because of the shorter range of these ions in the cell suspension. It would be worse with heavier ions. We are in the process of solving this problem.

Flushing a gas through the chamber produces foaming even if the cells are washed three times. For this reason we have used only the magnetic stirrer in the experiments reported here. However, flushing is necessary if one wants to investigate the oxygen effect, and this problem, linking the concentration of cells and the pressure necessary to get the gas through the sintered glass filter, is now being worked out.

Future work will include the effects of heavier ions on normal as well as tumor cells,[16] the oxygen effect, and the effect of heavy ions on cells of different ploidy.

References

1. P. W. Todd, Reversible and Irreversible Effects of Ionizing Radiations on the Reproductive Integrity of Mammalian Cells Cultured in vitro (Ph. D. Thesis), Lawrence Radiation Laboratory Report UCRL-11614, Aug. 1964.
2. P. W. Todd, Reversible and Irreversible Effects of Densely Ionizing Radiations upon the Reproductive Capacity of Cultured Human Cells, Med. College of Virginia Quarterly 1· 2-14 (1966).
3. R. Tym and P. W. Todd, The Sensitization by Iododeoxyuridine of Cultured Human Cells to the Lethal Effect of X-Rays and Heavy Ions, Intern. J. Rad. Biol. 8, 589-603 (1964).
4. C. A. Tobias and P. W. Todd, Heavy Charged Particles in Cancer Therapy, National Cancer Institute Monograph No. 24, 1-21, 1965.
5. H. B. Hewitt, Studies of the Dissemination and Quantitative Transplantation of a Lymphocytic Leukemia of CBA Mice, Brit. J. Cancer 12, 378-401 (1958).
6. H. B. Hewitt and C. W. Wilson, A Survival Curve for Mammalian Leukaemia Cells Irradiated in vivo (implications for the treatment of mouse leukaemia by whole-body irradiation), Brit. J. Cancer 13, 69-75 (1959).
7. K. Sillesen, J. H. Lawrence, and J. T. Lyman, Heavy-Particle Ionization (He, Li, B, Ne) and the Proliferative Capacity of Neoplastic Cells "in vivo", Acta Isotopica 3, 107-126 (1963).
8. Y. Schmidlin, J. H. Lawrence, K. Sillesen, G. Welch, and J. Lyman, Effect of Heavy Particles on the Proliferative Capacity of Ascites Tumor Cells (Lumphoma) Grown in vivo, in Semiannual Report Biology and Medicine, Donner Laboratory, Lawrence Radiation Laboratory Report UCRL-11833, Dec. 1964, pages 80-94.
9. J. E. Till and E. A. McCulloch, A Direct Measurement of the Radiation Sensitivity of Normal Mouse Bone Marrow Cells, Radiation Res. 14, 213-222 (1961).
10. E. A. McCulloch and J. E. Till, The Sensitivity of Cells from Normal Mouse Bone Marrow to Gamma Radiation in vitro and in vivo, Radiation Res. 16, 822-832 (1962).
11. T. Brustad, Inactivation of Enzymes in Dilute Aqueous Solutions by X-Rays and Heavy Ions, in Biomedical Studies with Heavy-Ion Beams (Meeting of the Advisory Committee for Biology and Medicine, USAEC, March 9-11, 1967), Lawrence Radiation Laboratory Report UCRL-17357, March 1967, pages 68-78.
12. W. R. Bruce and B. E. Meeker, Dissemination and Growth of Transplanted Isologous Murine Lymphoma Cells, J. Natl. Cancer Inst. 32, 1145-1159 (1964).

13. W. R. Bruce, B. E. Meeker, and F. A. Valeriote, Comparison of the Sensitivity of Normal Hematopoietic and Transplanted Lymphoma Colony-Forming Cells to Chemotherapeutic Agents Administered in vivo, J. Natl. Cancer Inst. 37, 233-245 (1966).
14. L. Siminovitch, J. E. Till, and E. A. McCulloch, Radiation Responses of Hemopoietic Colony-Forming Cells Derived from Different Sources, Radiation Res. 24, 482-493, 1965.
15. J. M. Feola, Heavy Ion Effects on Ascites Tumor Cells, in Biomedical Studies with Heavy-Ion Beams (Meeting of the Advisory Committee for Biology and Medicine, USAEC, March 9-11, 1967), Lawrence Radiation Laboratory Report UCRL-17357, March 1967, pages 246-257.
16. R. S. Bush and W. R. Bruce, The Radiation Sensitivity of Transplanted Lymphoma Cells as Determined by the Spleen Colony Method, Radiation Res. 21, 612-621 (1964).

SYNERGISTIC ACTION OF X RAYS AND ULTRASONIC WAVES ON MAMMALIAN CELLS CULTURED IN VITRO

Bambino I. Martins

The action of radiations and of ultrasonic waves on living matter is complex and diverse It is the purpose of this study to elucidate the nature and mechanism of the action of ultrasound and the relationship of such action to that of ionizing radiations The work was done with mammalian cells from a Chinese hamster bone-marrow cell line (M3-1) cultured in vitro.

At the outset of the investigation, problems were encountered in the quantitative characterization of the physical parameters, especially frequency and intensity, of the ultrasonic waves. A commercially available 1-MHz quartz-crystal ultrasonic generator was used, but it was found that the instrument gave different energy outputs according to the setting of the frequency tuner Also there was no measurement of either the plate voltage or the plate current

The instrument was modified to provide independent control of the frequency and plate voltage. It is now possible to read the frequency on a digital frequency meter, as an experiment is going on, and also measure both the plate voltage and the plate current in order to obtain the power that drives the crystal, which is enclosed in a metallic casing. However, as neither the efficiency of the crystal nor the loss of energy due to coupling and other factors is known, the amount of ultrasonic energy absorbed in the medium in which the cells are cultured and sonicated is not known precisely. It is hoped to accomplish this in the near future by use of the thermocouple probe technique as described by Fry and Fry.

The experiments involve plating a known number of cells (10^2 to 10^5) into a petri dish and treating with ultrasound, using glycerine for coupling. After sonification the dishes are incubated at 36°C for a week and the number of colonies counted, after staining with methylene blue. From this the fraction of surviving cells as compared with controls is calculated.

Two series of experiments were done. The first series was concerned with the study of the relationship between lethality and sound intensity for different frequencies ranging from 0.92 to 1.05 MHz. The second series was designed to study the synergistic effect between ultrasound and x rays. For this purpose cells were sonicated at a given frequency and intensity, preceded or followed in 30 min by irradiation with 50-kVp x rays at 50, 200, 600, and 900 rads. For a given frequency the intensity of ultrasound was so chosen, on the basis of the results of the first series of experiments, as to have little effect by itself.

The experimental data lead to the following conclusions:

1. There is a threshold intensity of ultrasound which is required for cell death. Above this threshold intensity the number of surviving cells falls off very rapidly with increasing intensity. See Fig. 1.

2. The threshold intensity, as measured in terms of power input to the crystal, depends on the frequency. Measurements of the absorbed energy are in progress.

3. Even at intensities below threshold there is sublethal damage, as indicated by the observation that such cells are affected differently from nonsonicated cells when irradiated later with 50-kVp x rays.

4. A synergistic effect between ultrasound and x rays is demonstrated (Fig. 2). The degree of synergism depends on the intensity and frequency of ultrasound and the x ray dose. The synergistic effect is much more evident if the ultrasound follows rather than precedes x rays; in this case a subthreshold dose of ultrasound causes markedly more lethality than x rays alone.

The lethal effect observed in these experiments is apparently not due to the mechanical forces associated with the formation and collapse of cavitation bubbles, because the intensities used are far below the cavitation threshold potentials for the frequencies employed. A probable mechanism may lie in the displacement amplitude or oscillation of subcellular particles. This seems especially likely from the observation of the synergistic effect, particularly when ultrasound follows x rays, because this may occur in connection with the mechanism of chromosome breakage and rejoining.

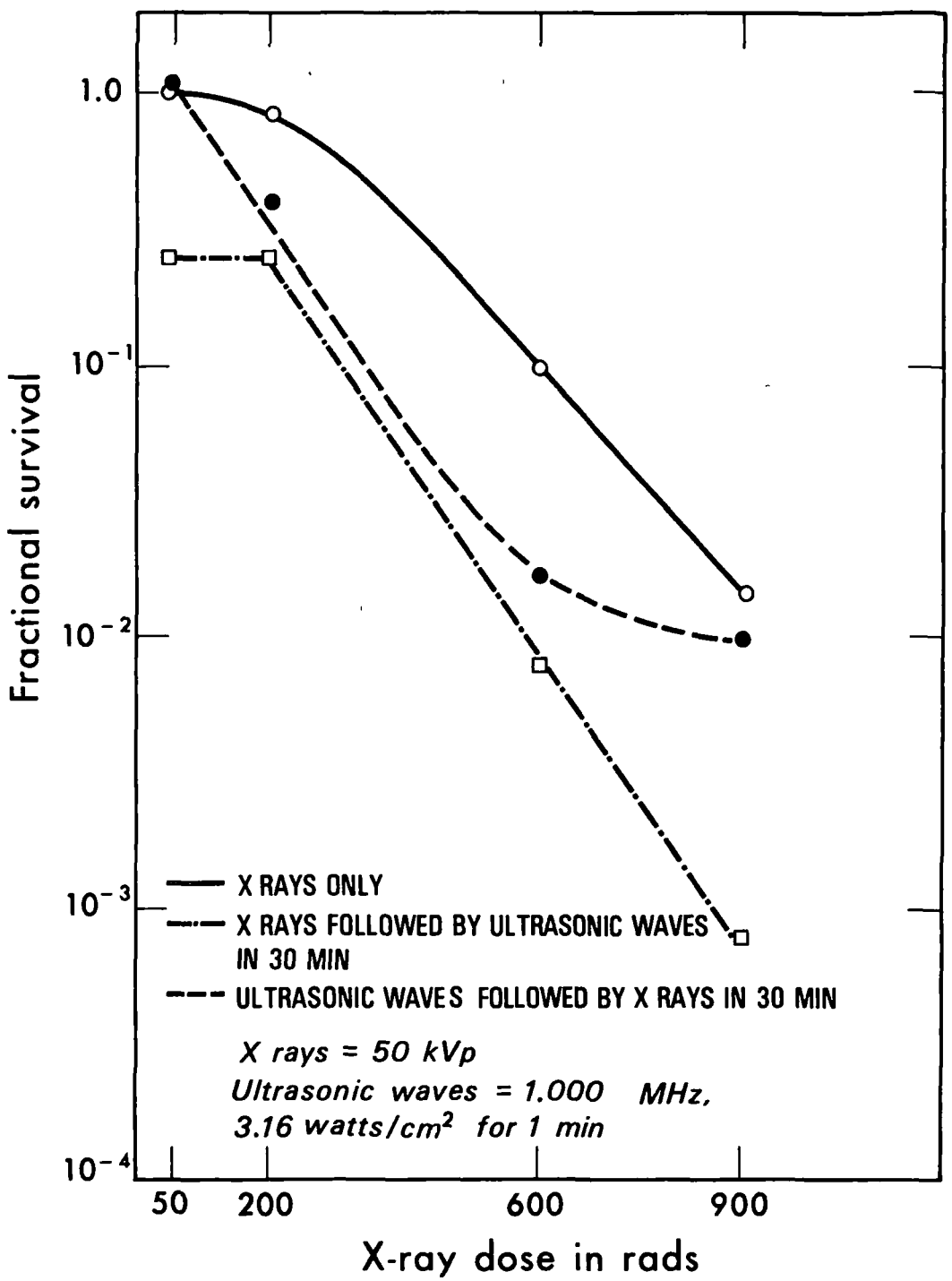


Fig. 1. Synergistic action of x rays and ultrasound at 1.000 Hz, 3.16 watts/cm^2.

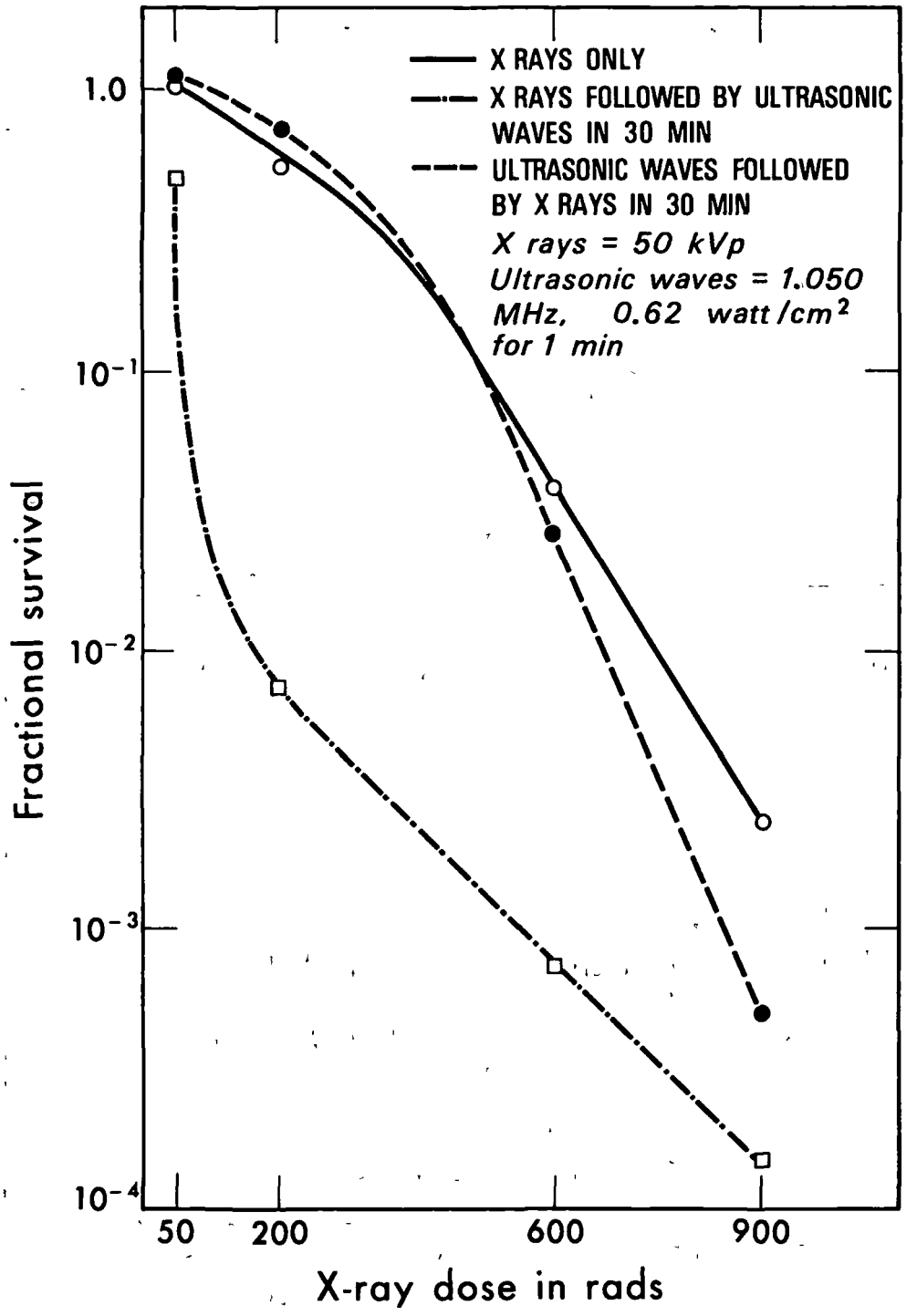


Fig. 2. Increased synergistic action of x rays and ultrasound at 1.050 Hz, 0.62 watt/cm^2.

RADIATION EFFECTS IN SPACE FLIGHT

Introduction

The pupal form of the flour beetle, Tribolium confusum, offers opportunity for convenient experiments--both in the laboratory, where expected flight conditions can be simulated, and on actual flights--on the effects of radiation.

Irradiation of pupae leads to wing abnormalities; the incidence of abnormality is affected by the age of irradiation and by such factors as temperature, oxygen tension, and magnetic field.

Studies of the interrelationship of various parameters is continuing.

Page intentionally left blank

Page intentionally left blank

EFFECT OF RADIATION ON THE DEVELOPING FLOUR BEETLE, TRIBOLIUM CONFUSUM

Brenda M. Buckhold and John V. Slater

For several years, an interesting developmental abnormality has been studied in the flour beetle, Tribolium confusum. When irradiated with 2000 R of x rays or γ rays, young pupae develop into adults having a wing abnormality which consists of a median elytral split, elytral blistering, and protrusion of the underlying membranous wings. One or more of these effects are observed with varying degrees of severity as the dose is lowered from this severe damage response level. For pupae between the ages of 16 and 24 hr, a dose-response curve to 180-keV x rays may be obtained which shows an extreme shoulder, a very sharp response above 1200 R, and an ED_{50} of 1430 R (Fig. 1).

Various physical and chemical parameters, such as temperature, O_2 tension, and magnetic fields, have been shown to alter this response to radiation. One of the parameters studied in detail has been temperature, with which a synergistic effect has been found in terms of percentage of wing abnormalities obtained with radiation.

Another point of interest is the variation in sensitivity to x rays (measured by percent wing abnormality) according to the age of the beetles. Larvae are somewhat sensitive to x rays as far back as 50 hr prepupation, but the sensitivity more than doubles at about 24 hr prepupation (Fig. 2). Pupae have two periods of maximum sensitivity at about 10 and 24 hr postpupation, and sensitivity drops to control values ($\approx$2%) at about 30 hr postpupation (Fig. 3).

In the same dose range, another effect has become apparent in pupae 1 to 24 hr old, i.e., a delay in eclosion, so that the pupal period is longer as a result of irradiation (Fig. 4). This delay averages 3.1 hr over the normal pupal period of 6.45 days. When the frequency distribution curves for the irradiated pupae are broken down into distribution curves for visibly normal and visibly abnormal adults (Fig. 5), it is seen that the visibly abnormal adults had an eclosion delay of 4.6 hr compared with only 2.2 hr for those which were visibly normal. It is seen from the distributions that the visibly abnormal adults were essentially all delayed, but that some of the visibly normal adults were delayed also. In other words, eclosion delay appears to be a necessary but not sufficient condition for a wing abnormality. Eclosion delay may thus be a more general phenomenon reflecting various kinds of metabolic damage which may or may not be involved in wing formation.

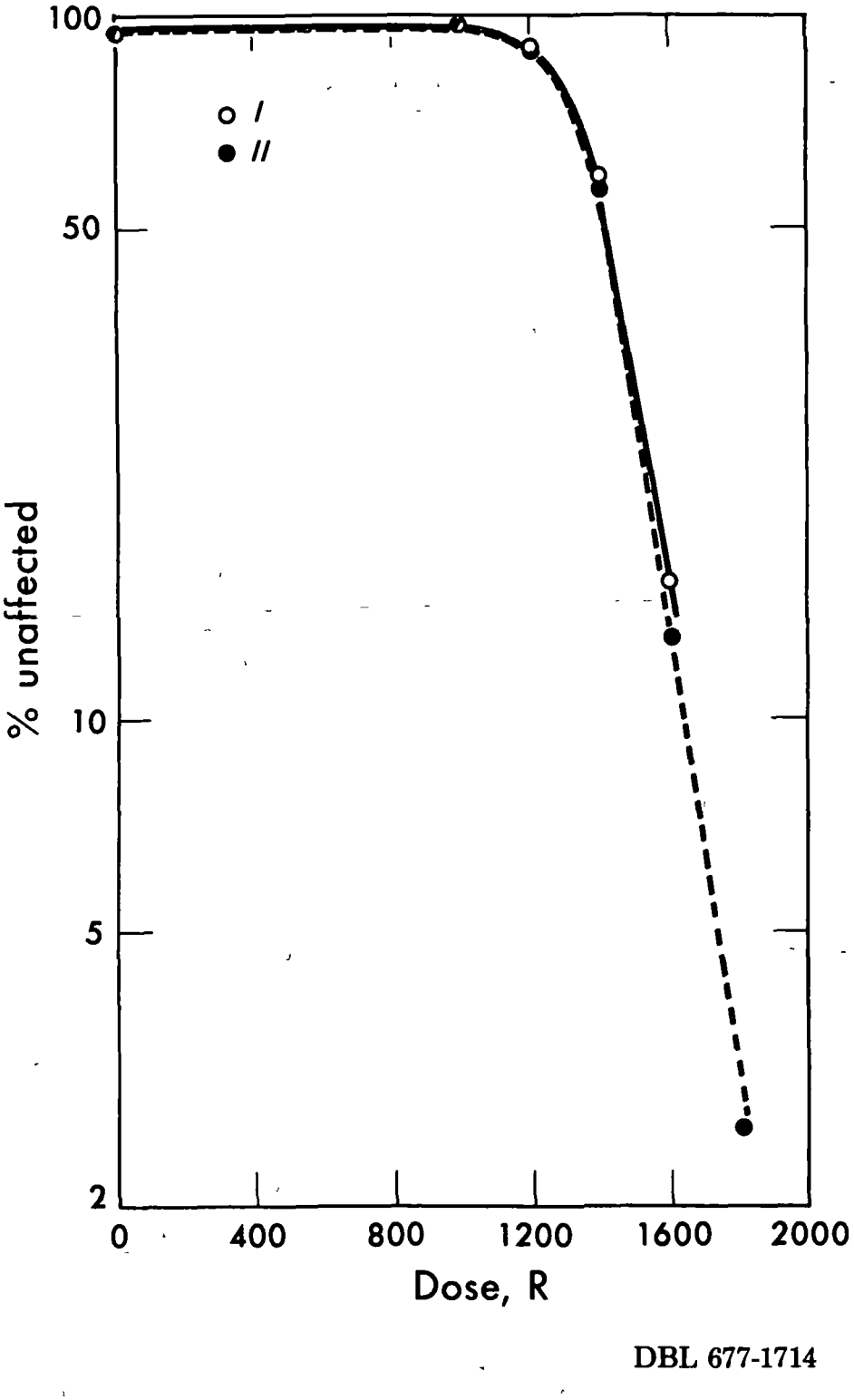
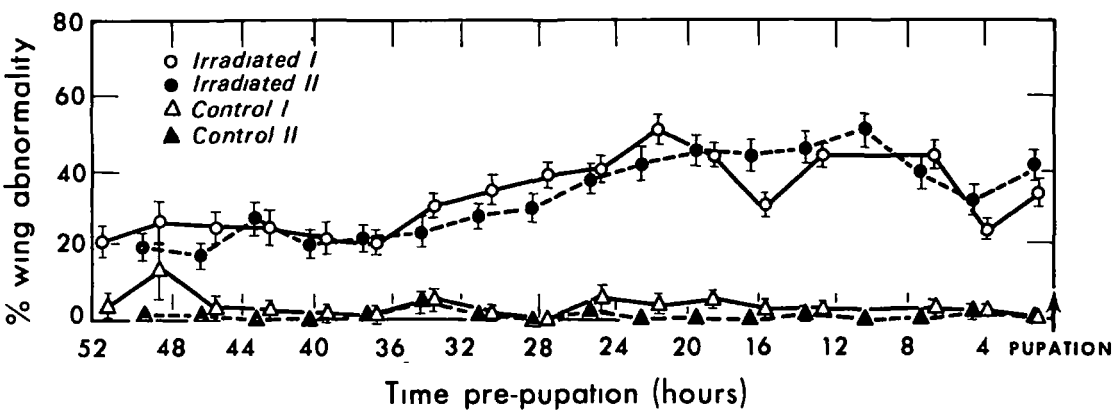


Fig. 1. Dose-response curve for Tribolium confusum pupae between 16 and 24 hr old exposed to 180-keV x rays.



DBL 677-1715

Fig. 2. Sensitivity of Tribolium confusum larvae to 1400 R of 180-keV x rays as a function of larval age when irradiated.

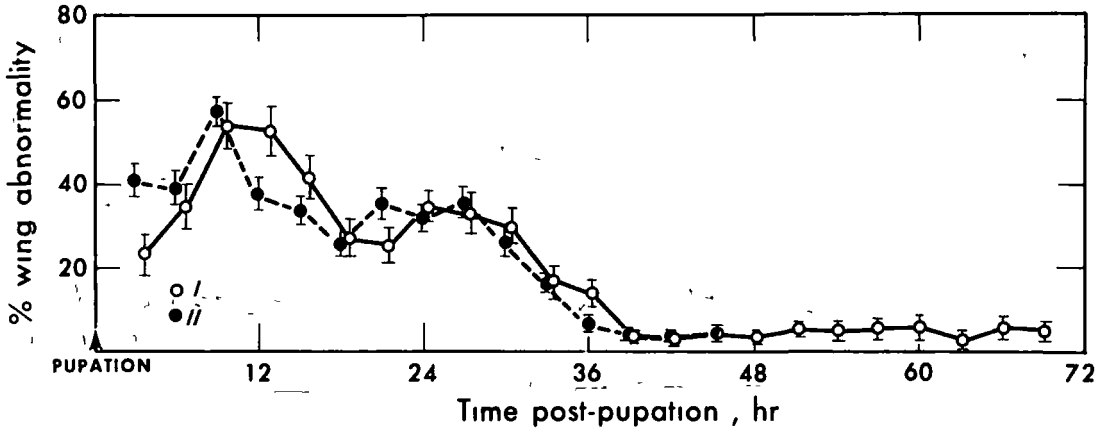


Fig. 3. Sensitivity of Tribolium confusum pupae to 1400 R of 180-keV x rays as a function of pupal age when irradiated.

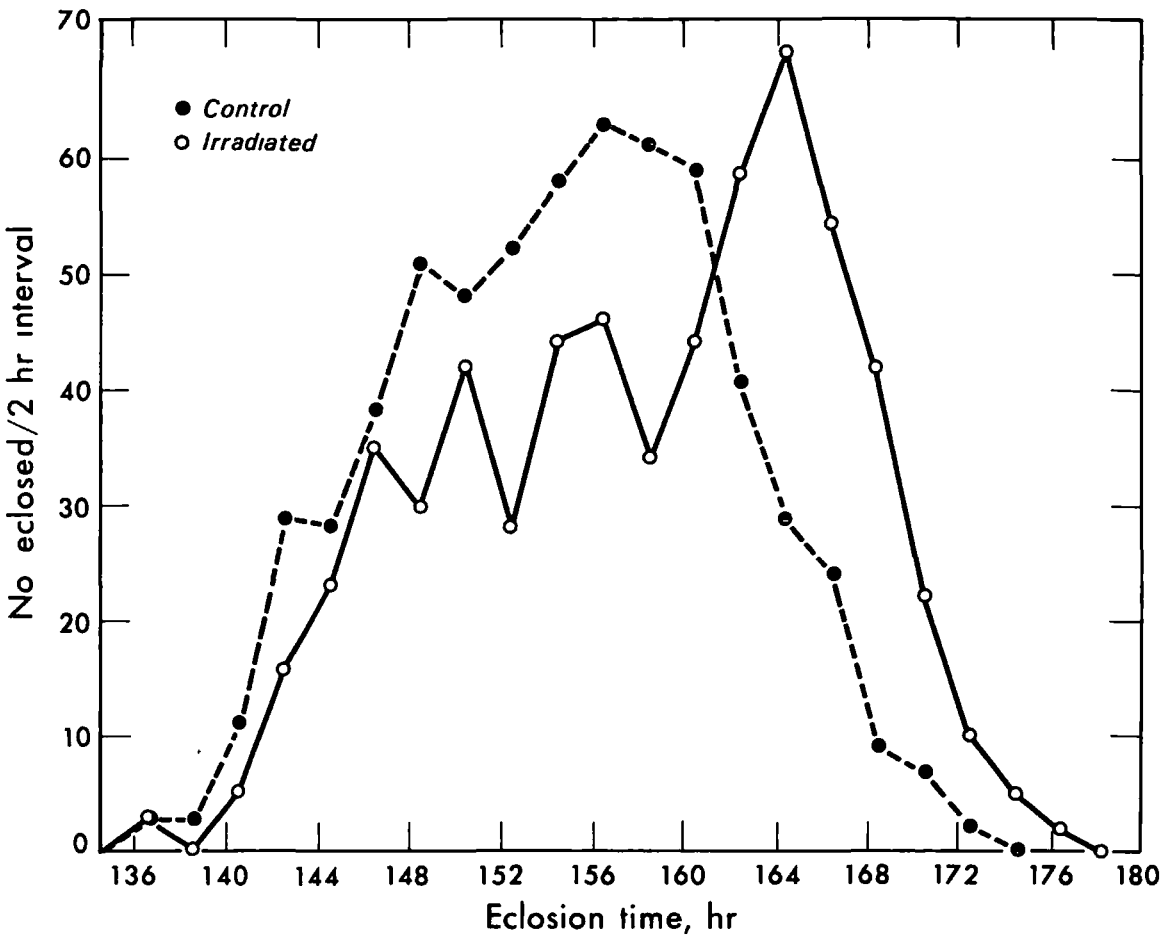


Fig. 4. Frequency distribution of the length of the Tribolium confusum pupal period for pupae exposed to 1400 R of 180-keV x rays compared with the distribution for unirradiated pupae.

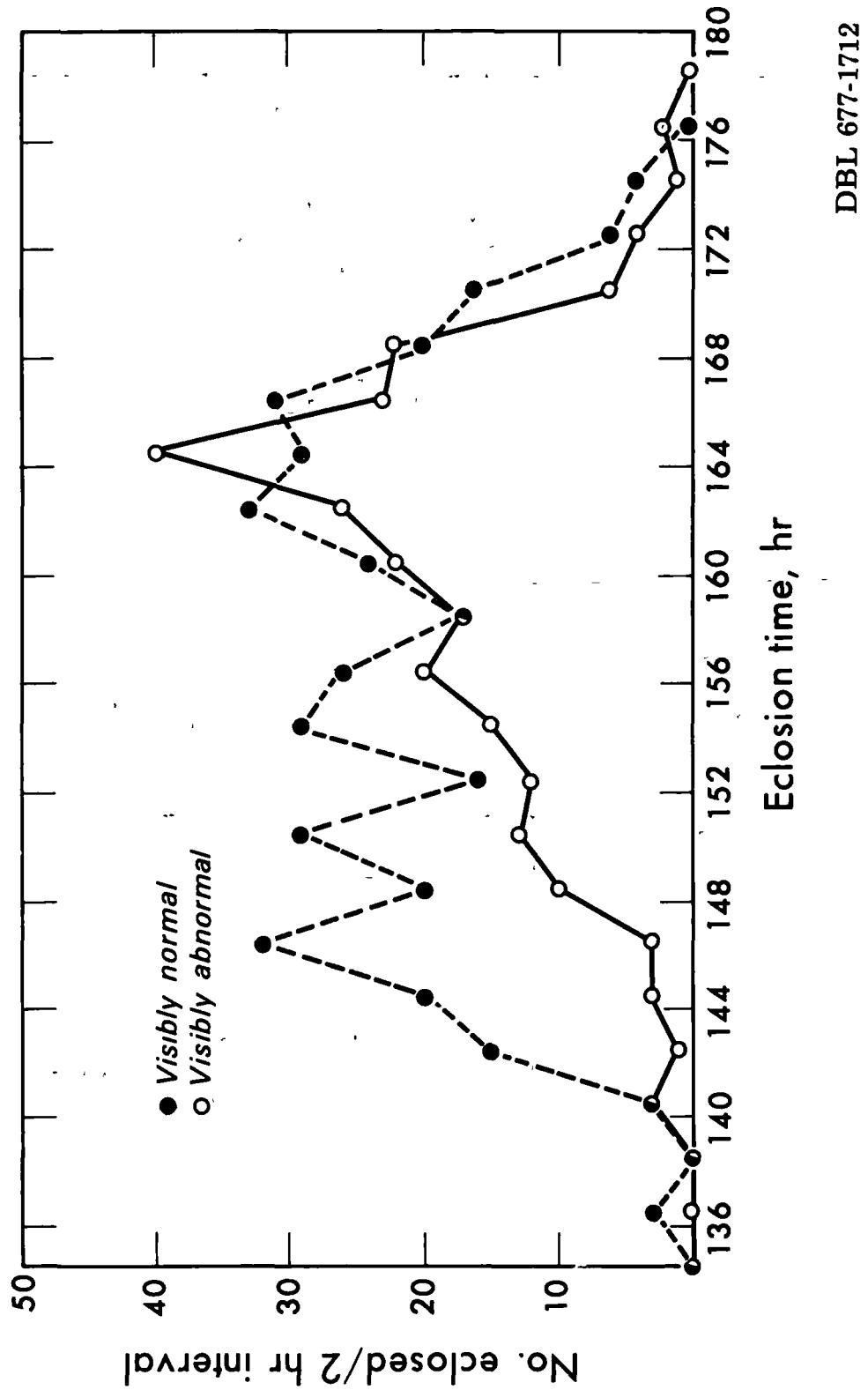


Fig. 5. Frequency distribution for Tribolium confusum pupae irradiated with 1400 R of 180-keV x rays. Those with visible wing abnormalities are compared with those which are visibly normal.

Gravity has been considered to play an integral part in the development of organisms. Thus, it would be of interest to study both the effect of weightlessness alone and the effect of combined weightlessness and radiation during the sensitive period of beetle development. Such an experiment can be done effectively in a space-flight environment, and several properties of Tribolium confusum make it ideally suited for such an investigation, viz: its ease of maintenance prior to flight, including nonsterile conditions, and the freedom from a nutritive medium requirement for pupae during flight.

In the laboratory, some studies have been done on the effect on developing pupae of increased gravity through centrifugation combined with radiation. Since there was visible vibration of the centrifuge, an additional control was provided by placing irradiated pupae on top of the centrifuge, so that they were vibrated, but not centrifuged. In comparison with this vibration control, there was a marked increase in response (wing abnormalities) in pupae centrifuged for 3 days post-irradiation in the 30° C incubator. On the assumption of a typical logarithmic "dose"-response curve for gravity superposed on irradiation, one can look at the response to increased gravitational acceleration following irradiation in terms of the difference between the logarithms of the percent unaffected for the centrifuged pupae, log C, and the vibration control pupae, log V, i.e.,

$$\text{Effect of centrifugation} = E = \log V/C, \quad (1)$$

or

$$E = \log V/C. \quad (2)$$

V/C plotted on a log scale against the acceleration due to gravity in g's (Fig. 6) shows that, although there is considerable scatter in the data, there is a definite increase in the response, which is considerably greater than the increase due to the centrifugation alone in unirradiated controls (a maximum of 8% wing abnormalities at 36 g's, compared with 1 to 3%-control values). There is some concern over whether this synergistic effect of increased gravitational acceleration might really be due to a temperature difference, since the inside of the centrifuge is about 1.3° warmer than the outside top of the centrifuge where the vibration controls were kept. This possibility is currently being tested.

The plan for the space-flight-radiation experiment is essentially to orbit for 3 days a large number (≈600) of 16- to 24-hr-old pupae, a portion of them in the presence of a γ-emitter, ^{85}Sr, and a portion shielded from the source. An identical ground control, including a matched radiation source, will be maintained. Due to the low source strength on board, the pupae are preirradiated with 1350 R of 180-keV x rays to bring them into their sensitive dose range so that the additional 100 R received during flight will contribute to the majority of the wing damage.

There has been one flight, which was launched Dec. 14, 1966. Since the capsule did not deorbit on schedule, all flight data were lost.

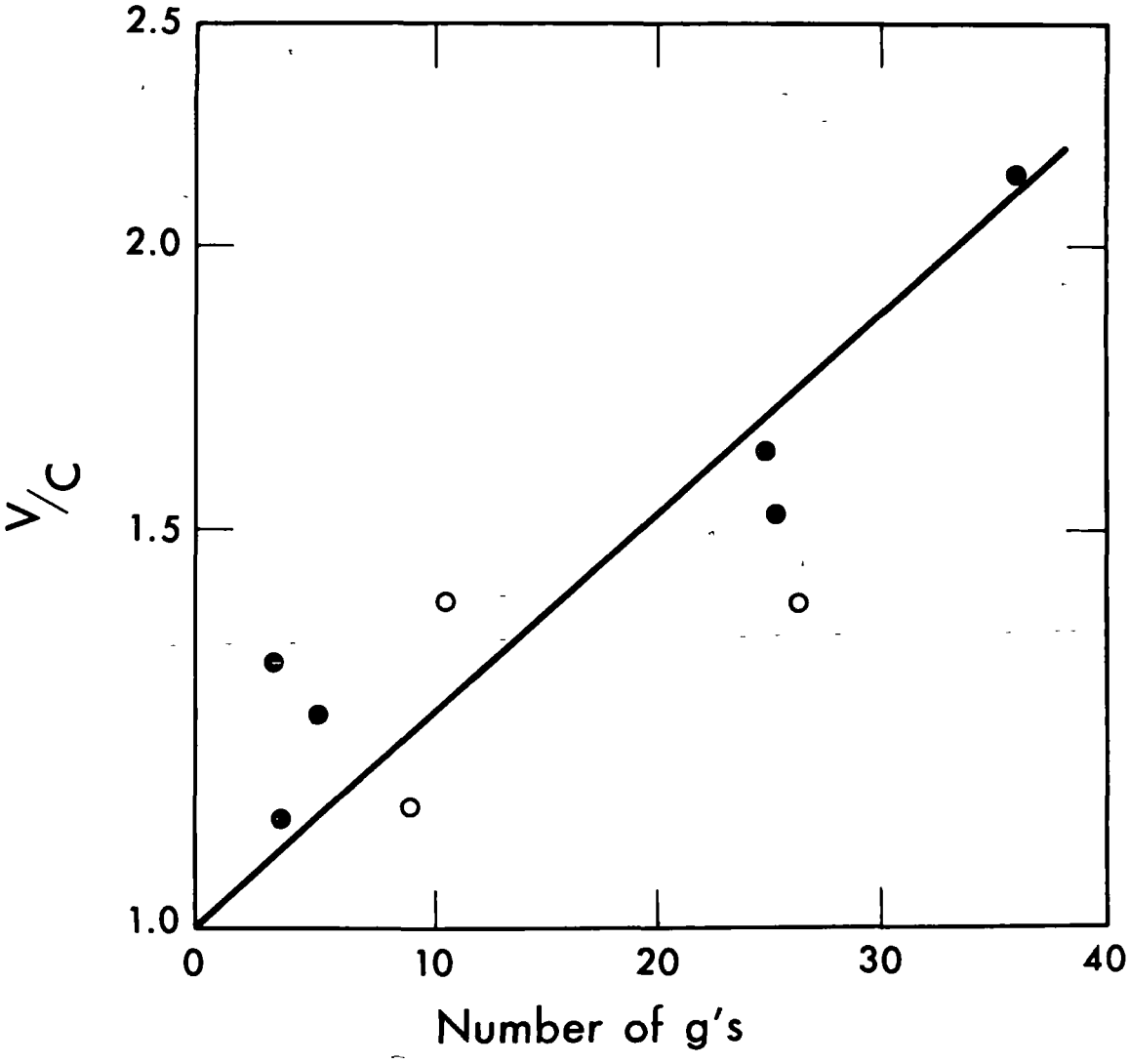


Fig. 6. The percentage of adults unaffected for Tribolium confusum pupae which had been both vibrated and irradiated divided by the percentage unaffected for those which had been centrifuged and irradiated, plotted logarithmically as a function of the gravitational acceleration. Open circles = actual vibration controls obtained. Solid circles = extrapolated and interpolated vibration controls.

Ground control data (Table I) showed that the preirradiation and capsule irradiation doses were as expected, according to the wing abnormality response. Measurements of the pupal period demonstrated also the expected eclosion delay due to irradiation, the unexpected delay in the preirradiated incubator control being due probably to a transfer of this control to an old module which had had an old culture growing in it. This was done to preserve the first module for the next flight. Thus, since conditions were not identical to the other controls, it is difficult to attribute this difference to any one parameter. No transfer need be done on the next flight, so this problem will be avoided. The next launch is scheduled for Aug. 23, 1967.

Table I. Ground control results.

Package	Percent wing abnormality	Calculated[a] dose delivered (R)	Apparent[b] dose delivered(R)	Pupal period (days)
Source+preirradiation	70.6	1640[c]	1500[c]	6.54
Source alone	9.7	230	1140[d]	6.42
Shielded+preirradiation	37.1	1410	1390	6.56
Shielded, no preirrad.	3.1	----	----	6.40
Incubator+preirradiation	39.4	1410	1400	6.71
Incubator, no preirrad.	6.3	----	----	6.47

a. Calculated from amount of dose delivered during sensitive portion of pupal period.
b. Interpolated from dose-response curve.
c. An additional 230 R was expected, but about 100 R was delivered in effect; consistent with previous ground controls for simulated flight.
d. Apparently spurious, not found on previous ground controls.

Page intentionally left blank

Page intentionally left blank

RADIOLOGICAL PHYSICS

Introduction

Recent developments in instrumentation, particularly the emergence of fast "solid state" counters, pulse-height analysis, and computation, allow new experimental approaches to a number of problems.

Exact measurements on the rate of energy transfer and its fluctuations were performed. Experimental approaches are being made to the problem of energy distribution of δ rays.

For the purpose of solar-flare simulation, methods were developed for automated isodose surface measurements For accurate area dose control in skin irradiation studies, a beam sweeper was designed and built at the 88-inch cyclotron

Collaborative studies were carried out with Nabuo Oda (Japan) on δ-ray studies; with Norman Baily, UCRL, on the use of proportional counters and tissue-equivalent chambers; and with the USNDRL San Francisco Laboratory on calorimetric dosimetry

Calculations carried out under the Omnitron study program on important beam parameters helped this program.

Further progress in radiological physics is essential for the success of the mammalian and cellular research programs.

Examples of Recent Publications

Howard D Maccabee, Fluctuations of Energy Loss by Heavy Charged Particles in Matter (Thesis), UCRL-16931, July 1965.

Palmer G. Steward and Roger Wallace, Calculation of Stopping Power and Range-Energy Values for Any Heavy Ion in Nongaseous Media, UCRL-17314, Dec. 1966

Gerald M Litton, Penetration of High Energy Heavy Ions, Including Multiple Scattering, Nuclear and Other Stochastic Effects, UCRL-17392, Aug. 1967.

Page intentionally left blank

Page intentionally left blank

SEMICONDUCTOR DEVICES AND THEIR APPLICATIONS TO DOSIMETRY OF HEAVY-CHARGED-PARTICLE BEAMS

Mudundi R. Raju

In biomedical studies using heavy-charged-particle beams, it is important to know the dose and also the distribution of linear energy transfer of the individual particles in the region of interest.

The semiconductor detectors have revolutionized radiation detection The use of solid as a detector is very attractive because of its high stopping power Another advantage is the low energy required to produce a hole-electron pair (3.6 eV for silicon) nearly ten times as much charge is liberated for a given energy loss in silicon as in gas, which leads to small statistical fluctuations in the number of charge pairs and to improved energy resolution over gas-filled counters. Another attractive feature of these detectors, besides their excellent energy resolution and fast response, is that their response is linear with energy deposited in the detector, regardless of the type of particle. This linear response is of paramount importance for their use with heavy ions [1]

The optimum performance of semiconductor detectors can be realized only if the detector and preamplifier and other associated electronics are designed to match one another In this respect, the semiconductor detector and associated electronics development group headed by Fred S. Goulding at the Lawrence Radiation Laboratory, Berkeley, has been of great help for our heavy-charged-particle measurements with semiconductor detectors. [2] In addition special detectors are being designed to suit various specific applications.

The most probable energy-loss measurements of protons of energies up to a maximum of 730 MeV and helium ions up to a maximum of 910 MeV, using lithium-drifted silicon detectors of different thicknesses up to 5 mm, agreed well with the values predicted by theory. [3] Theories of fluctuations of energy loss of high- and intermediate-energy protons and of helium ions have been thoroughly investigated by using semiconductor detector devices of various thicknesses, and the results are found to be in good agreement with theory. [4]

Depending on the energy of the particles and the thickness of the detector, a given detector may be used to measure either specific energy-loss distribution or energy distribution. If the detector is thin, so that the energy deposited by the particle in it is very small compared with the energy of the particles, the detector can be used to measure the specific energy-loss distribution. On the other hand, if the detector is thick enough to stop all the particles in the beam, then

it can be used to measure the energy distribution of the particles.

The Bragg peak of heavy charged particles is used for various radiobiological investigations. In order to evaluate the LET distribution of heavy charged particles at the Bragg peak position, the energy distribution of these particles was measured by use of lithium-drifted silicon detectors thick enough to stop the beam, and was found to be much higher than one would normally expect. From these measurements it seems that the modal energy of the heavy charged particles at the Bragg-peak position is roughly 10% of the primary beam energy [3]

Semiconductor detectors are being used at the heavy-ion linear accelerator (Hilac) routinely by the Biomedical group to measure the energy of the heavy-ion beam

Semiconductor detectors have been extremely useful for energy and energy-loss measurements of heavy-charged-particle beams. The use of these detectors to measure doses of intense beams is rather limited due to radiation damage in them.

However, some of the commercial signal silicon diodes made for general circuit applications can profitably be used for measuring doses of intense heavy-charged-particle beams. The radiation damage need not be a limiting factor for their use as radiation dosemeters. [5] If the diode is preexposed to radiation doses of the order of 10^6 rads, the sensitivity of the diode is reduced by a factor of the order of 3, but the sensitivity does not change significantly thereafter with further radiation exposures involved in dose measurement. The short-circuit current of such a preexposed diode is found to be proportional to the dose for dose rates from 25 rad/min to 5000 rad/min, and has been used successfully at the Bragg peaks of 50-MeV protons and 910-MeV helium ion beams.[6] Because of their small physical size (of the order of a cubic millimeter), these diodes are found to be very useful for dose measurements and for measuring beam profiles of small collimated beams, and these diodes are being routinely used at the biomedical facilities of the cyclotrons here.

The techniques of heavy-charged-particle measurements are extensively discussed elsewhere by Raju et al. [7]

References

1. John T. Lyman, Dark Recovery of Yeast Following Ionizing Radiation, (Ph. D. Thesis), Lawrence Radiation Laboratory Report UCRL-16030, March 1965.
2. F. S. Goulding, Nucl. Instr. Methods 43, 1 (1966).
3. Mudundi R. Raju, Heavy-Particle Studies with Silicon Detectors, Lawrence Radiation Laboratory Report UCRL-16354, Aug. 1965, also in Proceedings of the Workshop Conference on Space Radiation Biology, Berkeley, California, Sept. 1965 (to be published in Radiation Research).
4. Howard D. Maccabee, Fluctuations of Energy Loss by Heavy Charged Particles in Matter, (Ph. D. Thesis), Lawrence Radiation Laboratory Report UCRL-16931, July 1966.
5. M. A. Koehler, in Proceedings of the Workshop Conference on Space Radiation Biology, Berkeley, California, Sept. 1965 (to be published in Radiation Research).
6. M. R. Raju, Phys. Med. Biol. 11, 371-376 (1966).
7. M. R. Raju, J. T. Lyman, T. Brustad, and C. A. Tobias (1967), Heavy Charged Particle Beams, chapter in Radiation Dosimetry, Eds. Attix and Tochilin (to be published).

Page intentionally left blank

Page intentionally left blank

ENERGY-LOSS FLUCTUATIONS

Howard D. Maccabee

When man ventures into the space environment, he exposes himself to a veritable "bath" of charged particulate radiation, including solar and galactic cosmic-ray protons, mesons, electrons, and heavy ions. The biological effects of this radiation depend on the quantity and quality of ionization energy deposited in strategic molecules, cells, tissues, and organs. The laws which determine the average amount of energy lost by particles in a given thickness of material are, in general, well known and verified.

The ionizing collision process is a random statistical process, however, and therefore we expect large variations of energy loss (from the average) to occur in traversals by different particles through an absorber.

We have been investigating the phenomenon of energy-loss fluctuations (often called energy-loss straggling) from several different viewpoints, including experimental, theoretical, and possible radiobiological applications.

A body of theory predicts the energy-loss probability distribution, depending on the number of collisions in the highest (and therefore, least frequent) collision energy group. The parameter κ is a measure of the number of high-energy collisions, and we can write

$$\kappa = 0.150\ s\ Z\ z^2\ (1-\beta^2)/A\beta^4,$$

where s = absorber "thickness" in g/cm^2,
Z = absorber atomic number,
z = particle charge number,
β = particle velocity/speed of light,
A = absorber atomic weight.

The theory has been verified conclusively only at its end points, however--i.e., for large κ (slower particles in thicker absorbers) and for small κ (faster particles in thinner absorbers). When $\kappa \gg 1$, Bohr's theory is valid, and the energy-loss distribution is a narrow symmetric Gaussian, with the most probable energy loss equal to the average.[1] When $\kappa \lesssim 0.01$, Landau's theory is valid, yielding a broad asymmetric distribution with a peak around the most probable energy loss (which is significantly less than the average) and a long high-energy-loss "tail".[2]

In the important intermediate region of $0.01 \lesssim \kappa \lesssim 1$, Vavilov's theory is believed valid, but the experimental evidence has been sparse.[3] We have measured the energy-loss distributions for cases of κ from 0.003 to 2.23, using 45-MeV and 730-MeV protons, 370-MeV π mesons,

and 910-MeV He^{+2} ions in silicon semiconductor detectors of various thicknesses. We have found very good agreement with the Vavilov theoretical distributions, and good agreement on the values of the most probable energy loss, and have published our results.[4]

These theories, however, may break down under certain extreme conditions, namely when resonance collisions with atomic electrons distort the assumed collision spectrum and when the total number of collisions is too small for application of continuum statistics, i.e., in the limit of absorber thinness. Another investigator has raised the question of possible deviations at ultrahigh particle velocities, i.e., when the kinetic energy is much greater than the particle rest energy. The question has also been raised of the disparity between energy loss and energy deposition in the absorber, owing to escape of the most energetic δ rays (secondary electrons) from the absorber. We are continuing our experimental investigation of these effects, using the semiconductor detector system and gas proportional counters, and using computers for a theoretical study, including Monte Carlo and stochastic calculations.

Rossi has shown that the spectrum of local energy density in small volumes (e.g., that of a cell) is an important factor influencing radiobiological effects, and has developed the art of microdosimetry.[5] It is clear that fluctuations of energy loss in cell-like thicknesses will affect the local energy deposition. Indeed, Kellerer has recently pointed out that in many cases, energy-loss straggling is the dominant factor determining the variance of the spectrum of local energy density, especially for sparsely ionizing radiation and small volumes.[6] We are currently considering the radiobiological implications of these effects.

References

1. N. Bohr, Phil. Mag. 30, 581 (1915).
2. L. Landau, J. Phys. USSR 8, 201 (1955).
3. P. V. Vavilov, Soviet Phys. JETP 5, 749 (1957).
4. H. D. Maccabee and M. R. Raju, Nucl. Instr. Methods 37, 176 (1965).

H. D. Maccabee, M. R. Raju, and C. A. Tobias, IEEE Trans. Nucl. Sci. NS-13[3], 176 (1966);

Howard D. Maccabee, Fluctuations of Energy Loss by Heavy Charged Particles in Matter (Ph. D. Thesis), Lawrence Radiation Laboratory Report UCRL-16931, July 1966;

H. D. Maccabee and M. R. Raju, Ionization Fluctuations in Cells and Thin Dosimeters, to be published in Proceedings of the First International Symposium on Biological Interpretation of Dose, Berkeley, March 1967.
5. H. H. Rossi, Radiation Res. 10, 522 (1959), Radiation Res. Suppl. 2, 290 (1960);

H. H. Rossi, M. H. Biavati, and W. Gross, Radiation Res. 15, 431 (1961).
6. A. M. Kellerer, Microdosimetry and the Theory of Straggling, in Panel on Biophysical Aspects of Radiation Quality, IAEA, Vienna, March 1967.

Page intentionally left blank

Page intentionally left blank

SIMULATED SOLAR-FLARE IRRADIATION IN THE LABORATORY

John T Lyman

Perhaps the major radiation hazard on a lunar mission is presented by the large solar flares that eject high fluxes of protons and helium ions capable of penetrating the walls of a lightly shielded space vehicle or space suit [1, 2] In order to assess the effects of this type of irradiation so that reasonable tolerance levels may be set, it would be desirable to in some manner simulate the solar flare radiation in the laboratory.

Modisette and co-workers[3] have carried out a statistical analysis of solar proton events for the purpose of making dose estimations. They have represented the time-integrated omnidirectional integral proton spectrum as

$$J_p(>E) = J_0 \exp[-P(E)/P_0],$$

where $J_p(>E)$ = fluence of protons having kinetic energy greater than E,
$P(E)$ = rigidity = pc/Ze,
p = particle momentum,
c = velocity of light,
Ze = charge of particle,
J_0, P_0 = parameters characterizing a particular flare, they find that P_0 varies between 50 and 200 MV

Scott[4] has calculated the dose per incident particle greater than 30 MeV behind varying thicknesses of shields for protons normally incident on slabs of shielding material. The incident spectra were within the range of given by Modisette.

The ratio of the dose at 10 g/cm^2 depth to the dose at the surface varied from about 0 0005 to 0 1, depending primarily upon the P_0 value chosen and slightly upon the shielding material.

We have chosen to use the 910-MeV helium ion beam from the 184-inch synchrocyclotron for this study In order to produce a total-body irradiation of the experimental test animal it is necessary to either enlarge the beam by magnetic scanning or by scattering, so that the beam diameter is greater than the major dimensions of the animal, or to mechanically scan the animal across a small beam Mechanical difficulties and stress to the animal make this latter procedure impractical.

Because of the relative simplicity of the method, scattering the beam to obtain the required diameter was chosen The primary

absorber for this scattering is 3.82 cm of copper located about 1 m downstream from the vacuum window and about 7 3 m upstream from the chosen irradiation area. This absorber also reduces the beam energy to about 400 MeV, this degraded beam has a residual range of about 9 cm of water. The next problem is to transform the depth-dose distribution of the monoenergetic heavy-charged-particle beam, which is characterized by a Bragg peak, into an exponentially decreasing depth-dose distribution. This can be accomplished by appropriately modulating the energy of the residual beam by further degrading the beam through use of a variable-thickness absorber. The addition of this variable absorber also reduces the beam intensity due to inelastic nuclear collisions. The additional absorber also increases the rms scattering angle, resulting in a broader beam diameter, and also the profile of the beam is flatter for the lower-energy beam than for the higher-energy beam. These changes reduce the height of the Bragg peak in addition to shifting the peak to a shallower depth within an absorber.

The resulting depth-dose distributions in a water tank for beams of five different residual energies were determined. These data were obtained with an ionization-chamber probe which was submerged in the water tank. The probe could be remotely positioned within the tank. All measurements were made relative to the particle fluence entering the cave. With the use of these five curves as input to a computer program, an attempt was made to obtain an exponential depth-dose distribution by appropriately weighting the individual curves. It was found that the desired conditions (a factor-of-100 decrease in dose within 9 cm of water) the resultant distribution was not sufficiently smooth, so the input data were augmented by the use of five more curves, which were derived from the original data by interpolation or extrapolation; see Fig. 1. With the use of ten residual energy beams the computer program calculated the relative fluence incident upon each of the 10 different absorbers, so that when the resulting ionization was summed, the depth-dose distribution closely approximated the desired distribution (Fig. 2).

For experimental verification of the resultant distribution, and for irradiation of animals, it would be more desirable to perform only one irradiation instead of 10 separate irradiations. This can be accomplished by the use of a composite absorber, called a "ridge filter."[5] This filter is composed of a number of repeating units which are placed side by side so as to form a large absorber through which the whole beam must pass. Each unit is essentially a step-wise variable-thickness copper absorber. The width of the individual step determines the relative intensity, and the total thickness of the step determines the residual energy (Fig. 3). The entire filter is oscillated on a line perpendicular both to the beam axis and to the length of the individual units of the ridge filter

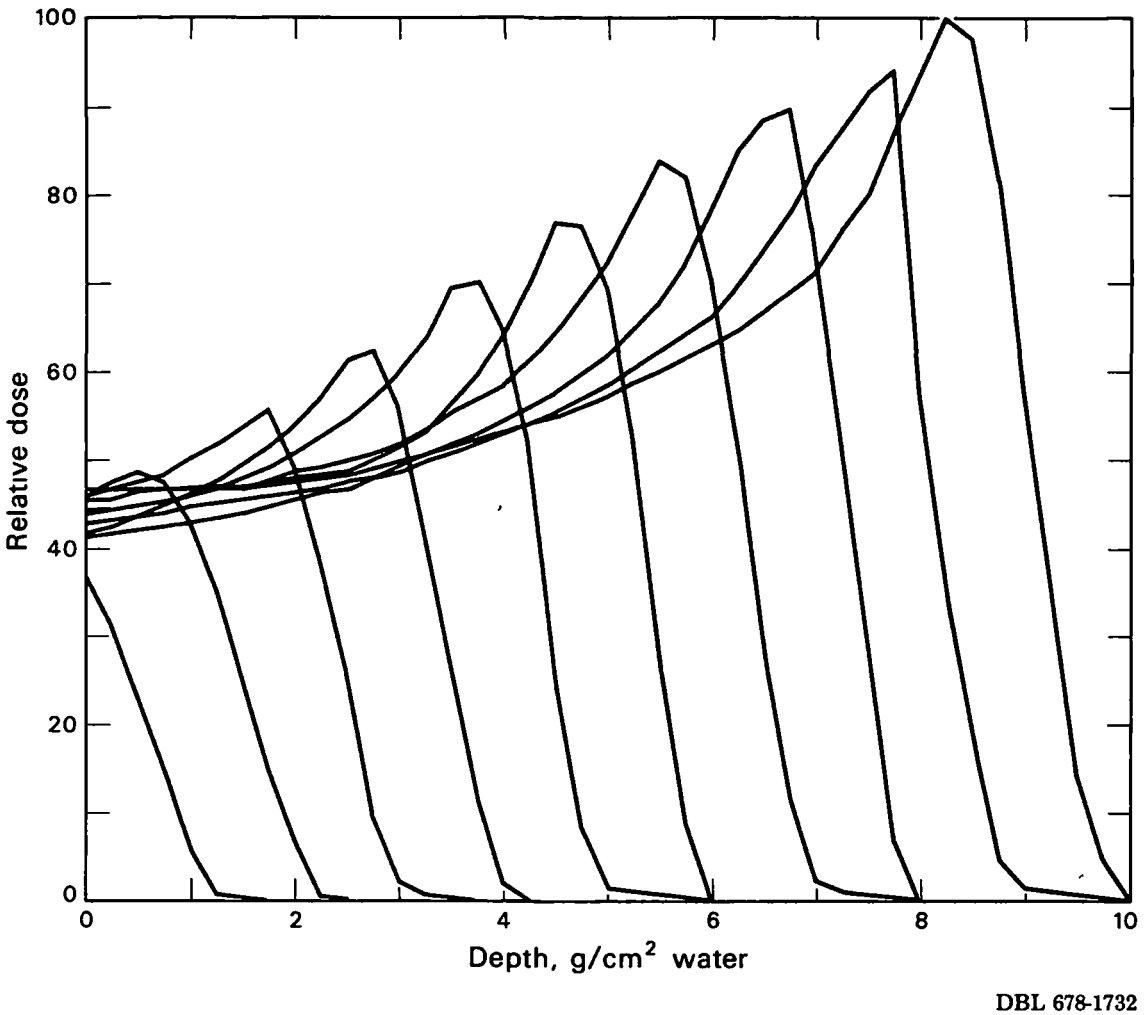


Fig. 1. Bragg curves of the 10 helium-ion beams of different energies used as input to the computer program.

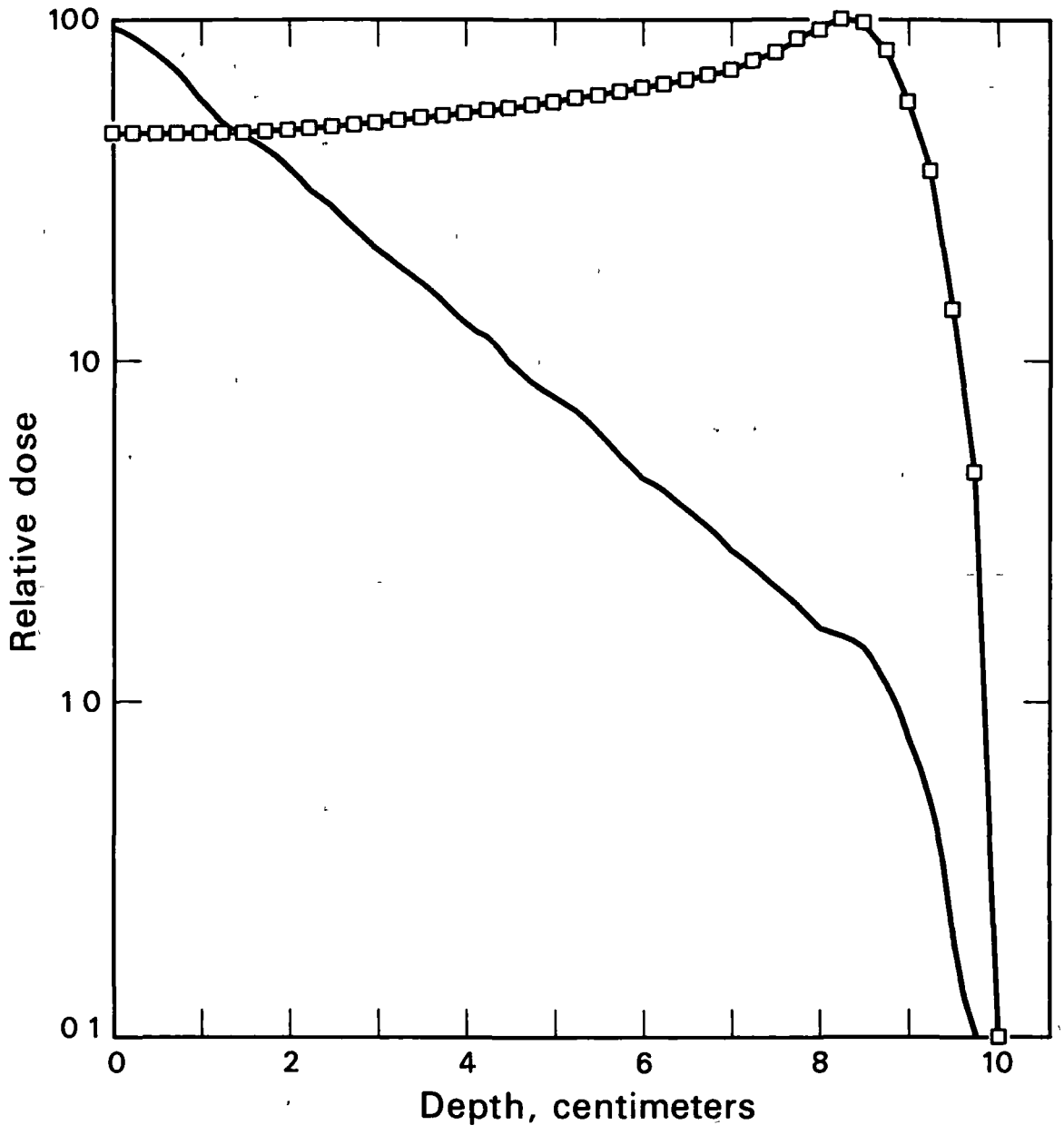


Fig. 2. Calculated depth-dose distribution produced by properly weighting the 10 Bragg curves in order to approximate an exponentially decreasing depth-dose distribution. The highest-energy Bragg peak is also shown for comparison.

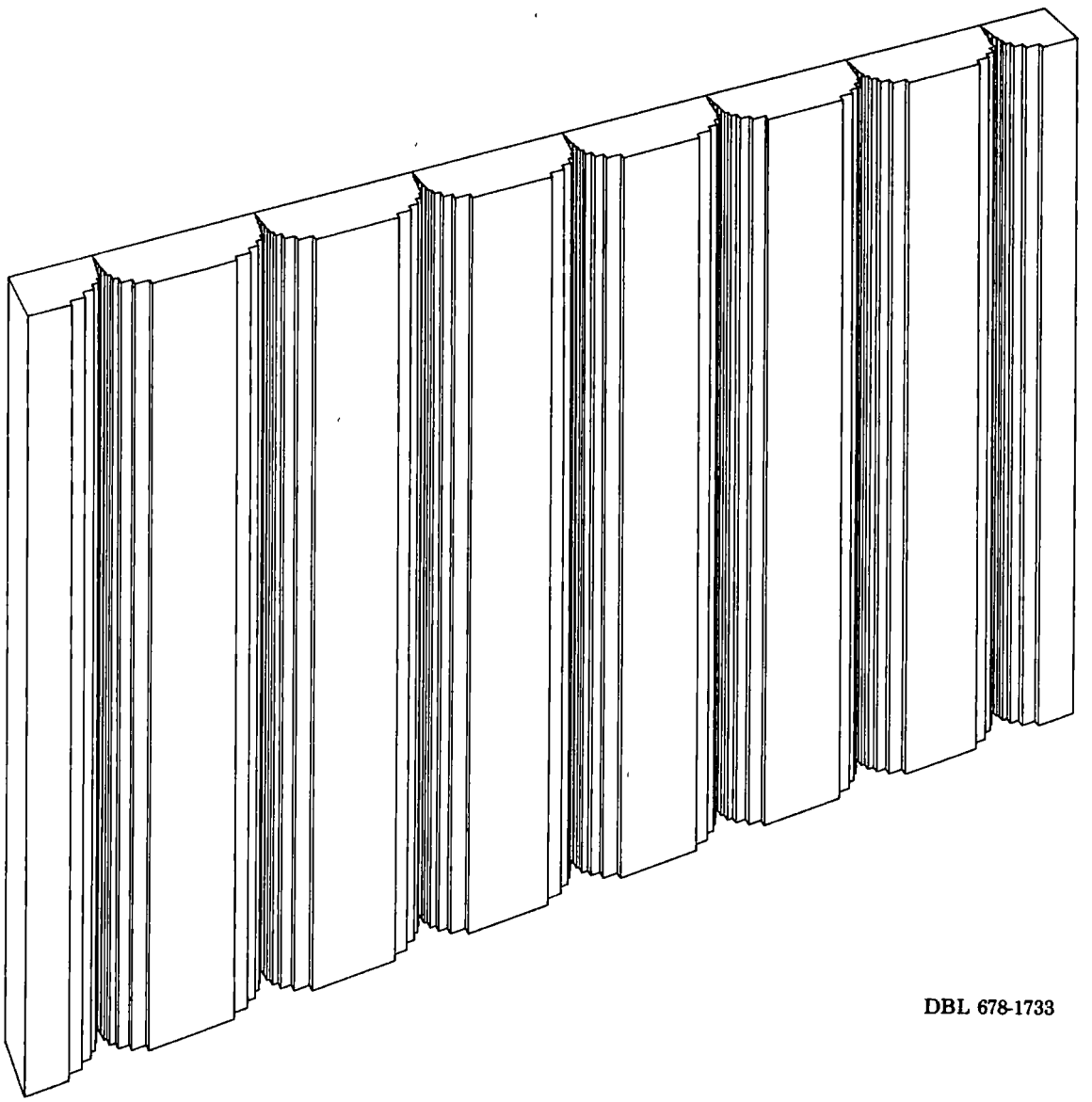


Fig. 3. Perspective view of the ridge filter.

Measurements of the depth-dose distribution resulting from the use of a ridge filter were made by use of an ionization chamber mounted on a two-dimensional scanning platform, and a water tank. Figure 4 shows the transformed depth-dose distribution as well as the distribution that is characteristic of the beam that has not passed through the ridge filter. Figure 5 shows the experimental isodose distribution within the water tank for the transformed beam

The exponentially decreasing depth-dose curve has two components; the first is due to the degraded helium ions, the second--which is evident beyond the maximum range of the helium ions (about 9 cm)--is due to the production of secondary particles, primarily in the copper scattering absorber and the ridge filter but also in the water tank. Placing the initial copper absorber before a steering magnet so that the degraded helium ions are deflected away from the secondary particles generated in the 3.82 cm of copper reduces the intensity of this second component. This is illustrated in Fig. 6. This figure is of integral-range curves of the beam with the copper absorber in the two different locations. These data were obtained with two plastic scintillators connected in coincidence to monitor the beam. A third plastic scintillator measures the beam after the particles pass through a variable absorber. Coincident pulses from the first two scintillators (AB) were interpreted to indicate that a particle was incident upon the surface of the absorber. A pulse from the third scintillator that was also coincident with pulses from the first two scintillators (ABC) was interpreted to indicate that the particle had passed through the absorber. The integral-range curve is a plot of the ratio of ABC coincidences to the AB coincidences as a function of the absorber thickness. It can also be seen in this figure that the particle fluence falls off in essentially the same manner as does the dose. This indicates that the average LET along the depth-dose curve is relatively constant. From a practical point of view, it is not possible to place the initial absorber before the steering magnet because of the large reduction in beam intensity due to the poor efficiency of the beam transport system for such a scattered beam, collimation by the beam transport pipes prevents the beam from being sufficiently enlarged in diameter.

The energy-loss distribution was measured by use of a thin silicon semiconductor detector.[6] Pulse-height distributions were obtained at various depths within the water tank. These are shown in Fig. 7. These curves show that there is a broad LET distribution. The relative importance of the different groups of helium ions depends upon their relative abundance. The most abundant group is that with the lowest residual energy remaining at that thickness, the group with the next lowest residual energy is the next most abundant, and so on. The major peak in the energy-loss distribution seems to be mainly the result of the two lowest-energy groups. There is a portion of the distribution to the left of this major peak which increases in height relative to the helium ion peak with increasing absorber thickness, and also shifts toward higher energy losses. At the position near the maximum range of the helium

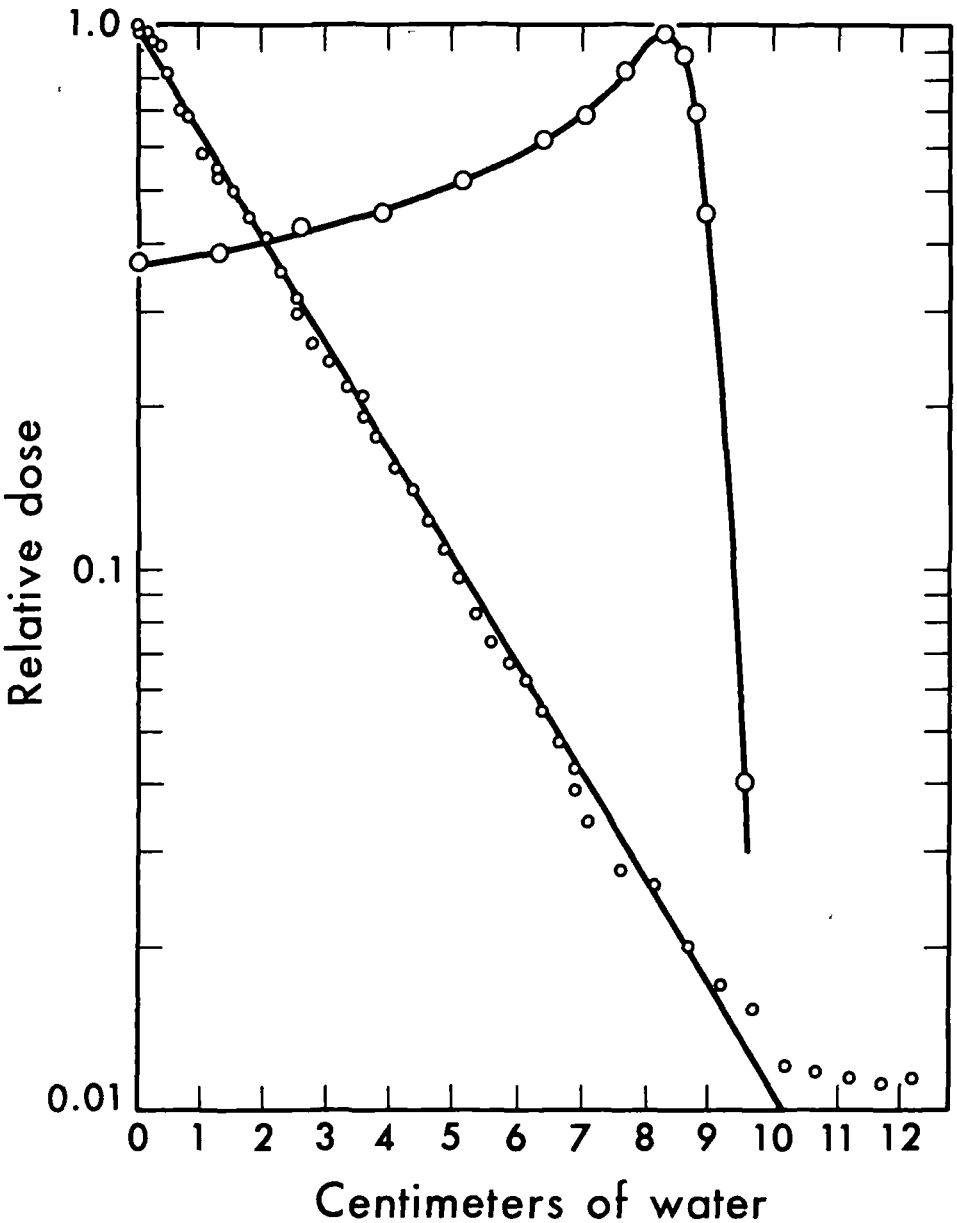


Fig. 4. Experimental depth-dose distribution of the helium ion beam with and without use of the ridge filter.

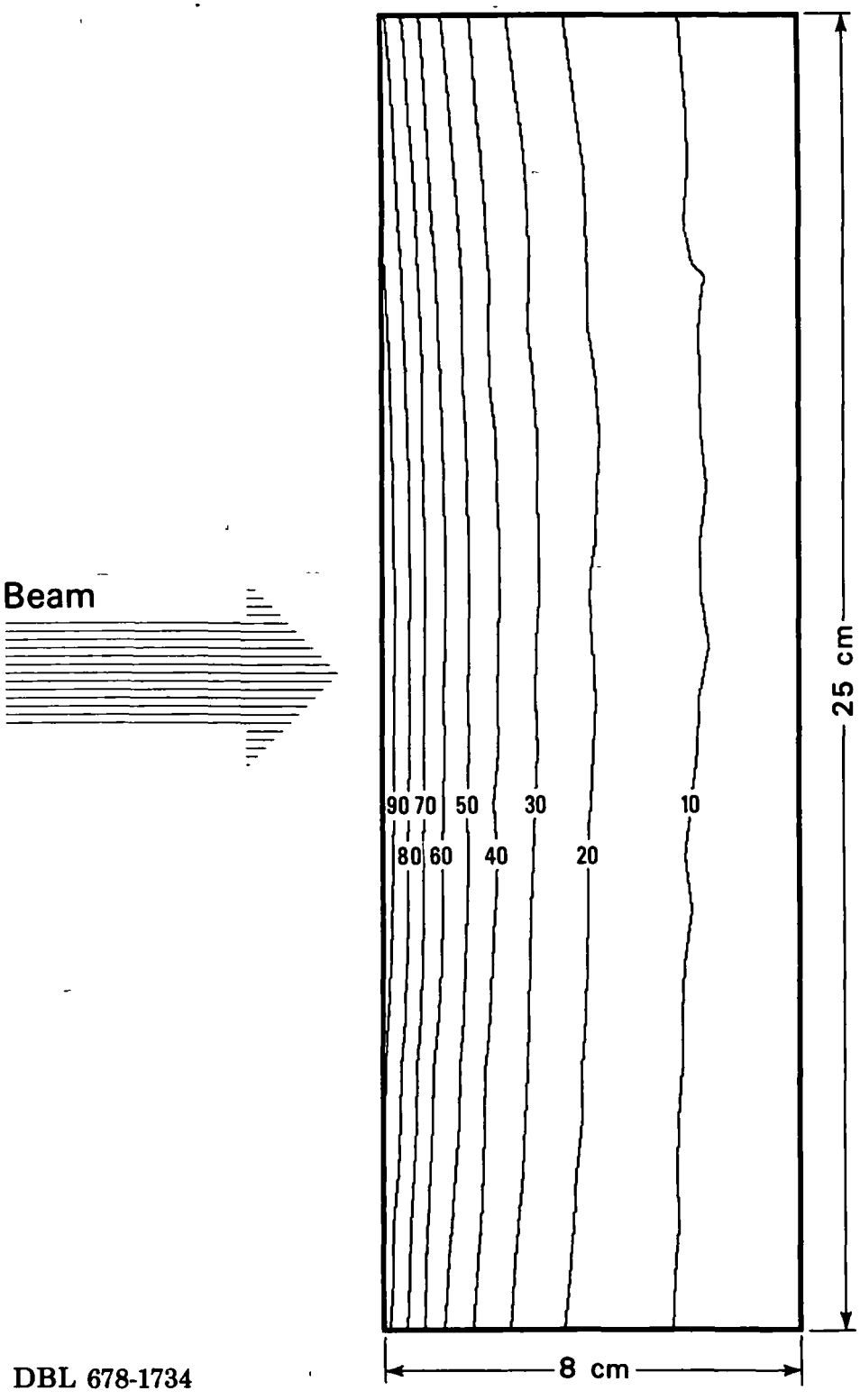


Fig. 5. Isodose distribution within a unilaterally irradiated rectangular water tank.

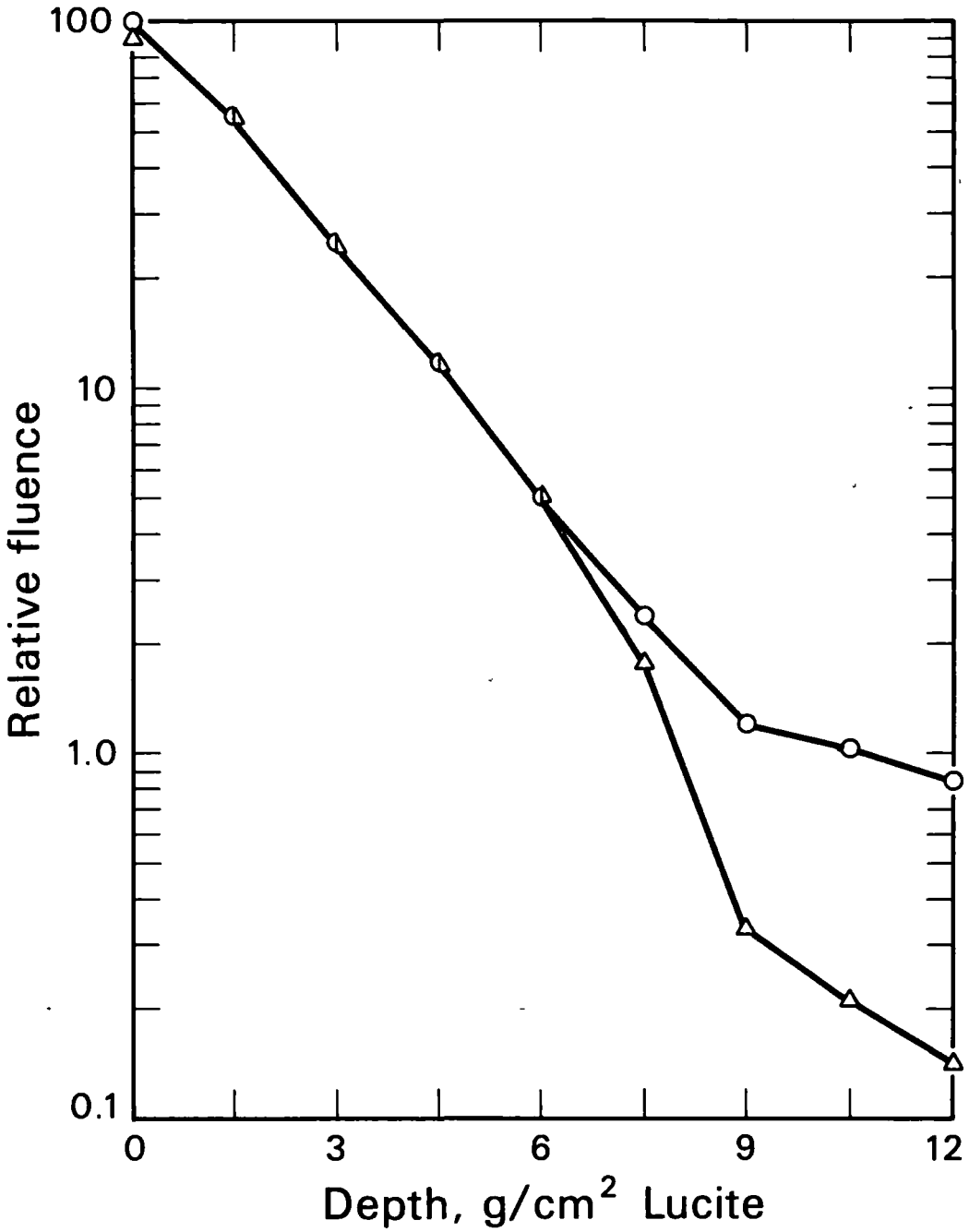


Fig. 6. Integral-range curves obtained with Lucite absorbers. A reduction in background was accomplished by momentum-analyzing the beam after the initial energy degradation.

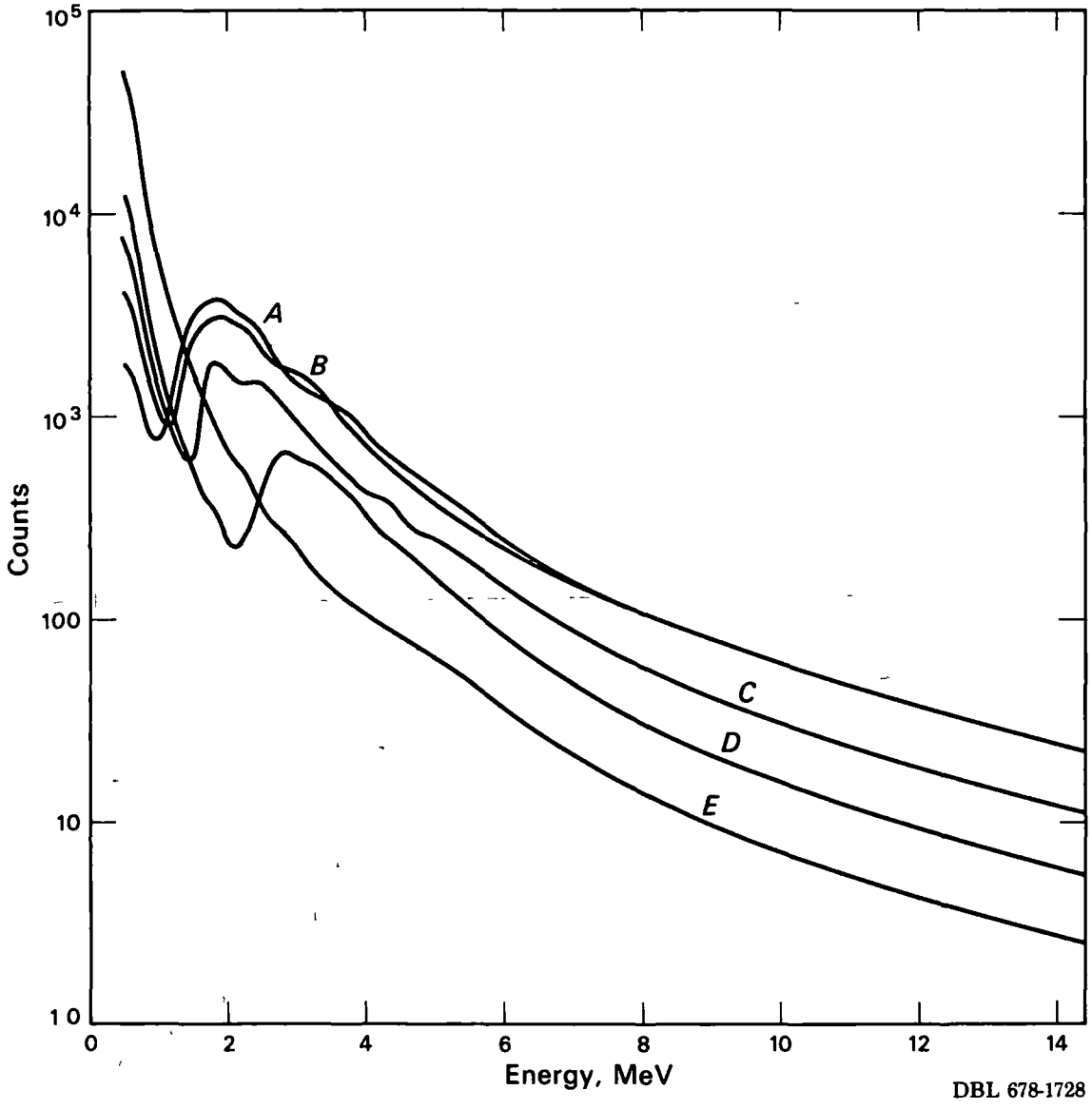


Fig. 7. Energy-loss distribution for the ridge-filter-transformed beam at various depths within the water tank: (a) 0 cm; (b) 2.5 cm; (c) 5.1 cm; (d) 7.6 cm; (e) 10.2 cm.

ions (Fig. 7d) the peak of the energy-loss distributions is shifted to a higher energy, since there is no longer a more penetrating helium ion component with a lower LET. Therefore the peak due to the helium ions is not augmented by a smaller component of a lower-LET helium ion beam.

In order to more completely simulate a solar flare irradiation, the test object must be rotated during exposure. A simple omnilateral irradiation (rotation about a major axis of the object which is at a right angle to the beam) may be sufficient for most purposes. The depth dose distribution that results from the omnilateral irradiation of a right circular cylinder is shown in Fig. 8 for cylinders of different radii as a function of the distance from the surface. At the center of a cylinder the dose essentially is that which would be found at an equivalent depth in a monodirectionally irradiated slab. The dose at the surface is given relative to that of a cylinder with a vanishingly small radius. For cylinders with increasingly larger radii the relative surface dose approaches 50%.

The simulation of an omnidirectional irradiation results in a more rapid falloff in dose as a function of distance from the surface in the transverse planes away from the ends of the cylinder, Fig. 9. The maximum dose occurs at the maximum radius at the ends of the cylinder, the points with the least self-shielding.

As can be seen from Fig. 8, the depth-dose distribution within an experimental animal which has been irradiated with this simulated solar flare depends strongly upon the dimensions of the animal. Large animals have a lower ratio of the midline to the surface dose than smaller animals. This ratio in a man exposed to a solar flare similar to Bailey's "typical" solar flare[7] depends upon the amount of shielding surrounding the astronaut A thick shield will lower the surface dose but, when compared with a thinner shield, will increase the ratio of the midline dose to the surface dose.[8]

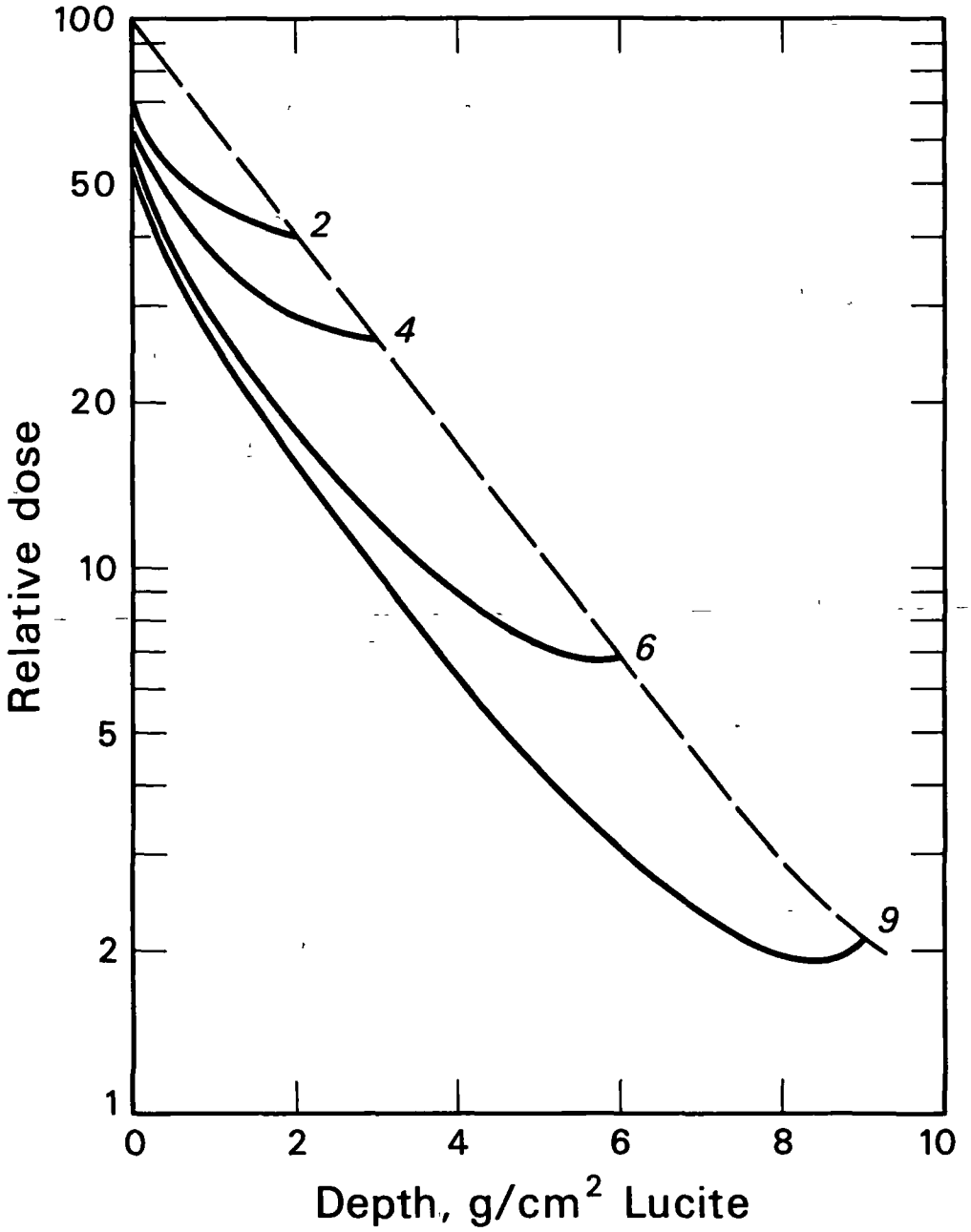
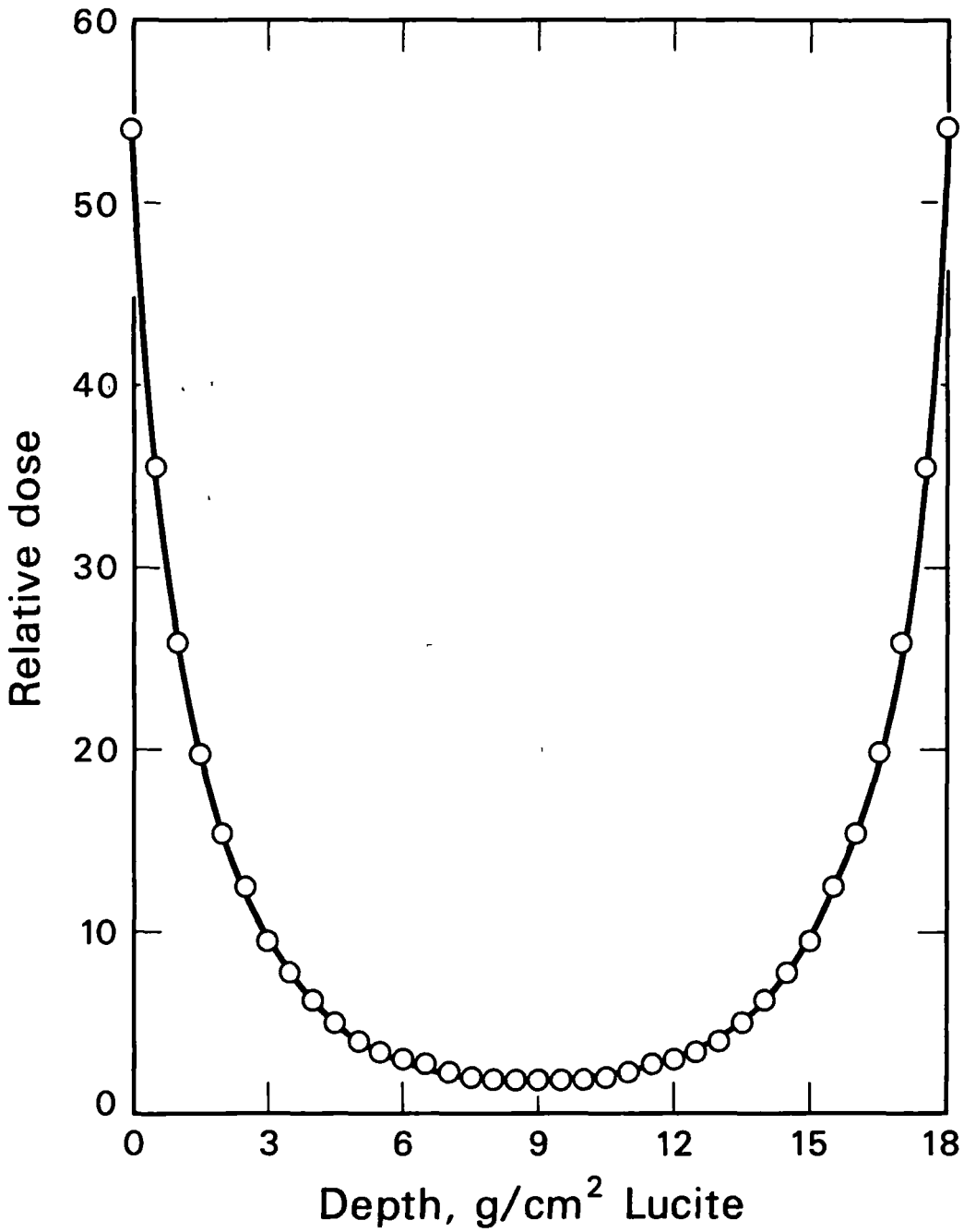


Fig. 8. Depth-dose distribution along a radius in right circular cylinders of various radii which have been omnilaterally irradiated, calculated by utilizing the experimentally obtained depth-dose distribution with the ridge filter (see Fig. 4).



DBL 678-1727

Fig. 9. Depth dose distribution along a diameter for an omnilaterally irradiated right circular cylinder. The diameter is in a plane away from the ends of the cylinder.

References

1. J A. Van Allen, Corpuscular Radiations in Space, Radiation Res. 14, 540 (1961)
2 W R Webber and P S Freier, An Evaluation of the Radiation Hazard Due to Solar Cosmic Rays, in Proceedings of Symposium on the Protection Against Radiation Hazards in Space, in Gatlinburg, Tenn., Nov. 5-7, 1962, pp. 12-32.
3. J Modisette, T. M. Vinson, and A. C. Hardy, Model Solar Proton Environments for Manned Spacecraft Design, National Aeronautics and Space Administration Report NASA-TN-D-2746, 1965.
4. W W. Scott, Estimates of Primary and Secondary Particle Doses Behind Aluminum and Polyethylene Slabs Due to Incident Solar Flare and Van Allen Belt Protons, Oak Ridge National Laboratory Report, ORNL-RSIC-18, 1967
5 B G. Karlson, Methoden zur Berechnung and Erzielung einiger für die Tiefentherapie mit hochenergetischen Protonen gunstiger Dosisverteilungen, Strahlentherapie 124, 481 (1964).
6. H. D. Maccabee, M. R. Raju, and C. A Tobias, Fluctuations of Energy Loss in Semiconductor Detectors, IEEE Trans Nucl. Sci. NS-13, 176-178 (1966).
7. D. K. Bailey, Time Variations of the Energy Spectrum of Solar Cosmic Rays in Relation to the Radiation Hazard in Space, J. Geophys. 67, 391-396 (1962).
8 D. L. Dye, Space Proton Doses at Points within the Human Body, in Proceedings of the Symposium on the Protection Against Radiation Hazards in Space, in Gatlinburg, Tennessee, Nov. 5-7, 1962, pp. 633-661.

BEAM SCANNING AND MICROBEAM AT THE 88-INCH CYCLOTRON

Graeme P. Welch

Scanning

The α-particle beam of maximum energy 120 MeV and proton beam of maximum energy 55 MeV from the 88-inch sector-focused cyclotron covers approximately 0 5 cm diameter at the target position but is quite inhomogeneous in intensity over its cross section For small targets, scattering by a thin aluminum or graphite foil has been used to obtain approximate uniformity and to increase the area covered, but the useful field is limited, a great deal of intensity is lost, the background is increased, and the energy spread and rate of energy loss spread are increased

For whole-skin irradiation of animals, scattering to increase beam size is impractical; a practical experimental technique is repetitive deflection of the beam in two perpendicular directions at different frequencies to cover a large surface (up to 12 inches square in our design) together with a slow rotation of the animal about a longitudinal axis. Once this scanning system is available, it is useful for small-animal irradiations, too, and the limitations of the scattering method are removed

The scanning equipment consists of two C-shaped hypersil electromagnets with 4-in gap and 4×6-in. pole faces surrounding a Pyrex beam tube 34 ft upstream from the target position. This is shown in Fig. 1, the arrangement of equipment in the biomedical cave at the 88-inch cyclotron, where the beam enters at the right and passes successively:

a quadrupole focusing magnet, marked 1 on the drawing,
- the beam scanner, 2,
- a 10-deg deflecting magnet, 3,
- 30 ft of vacuum pipe which increases in diameter from 4 to 16 in., 4,

and emerges through an aluminum foil window,
the irradiation bench, 5, on the bench are
- a monitor ionization chamber, 6 ,

an absorber wheel, 7,
- a quadrant ionization chamber, 8,

a remote-controlled mouse positioner, 9, and
a Faraday cup dosimeter, 10.

Provisionally the scanning magnets are supplied with dc limited to a maximum of 64 A at 44 V, and the switching is done with silicon-controlled rectifiers. The intention is to supply square waves of

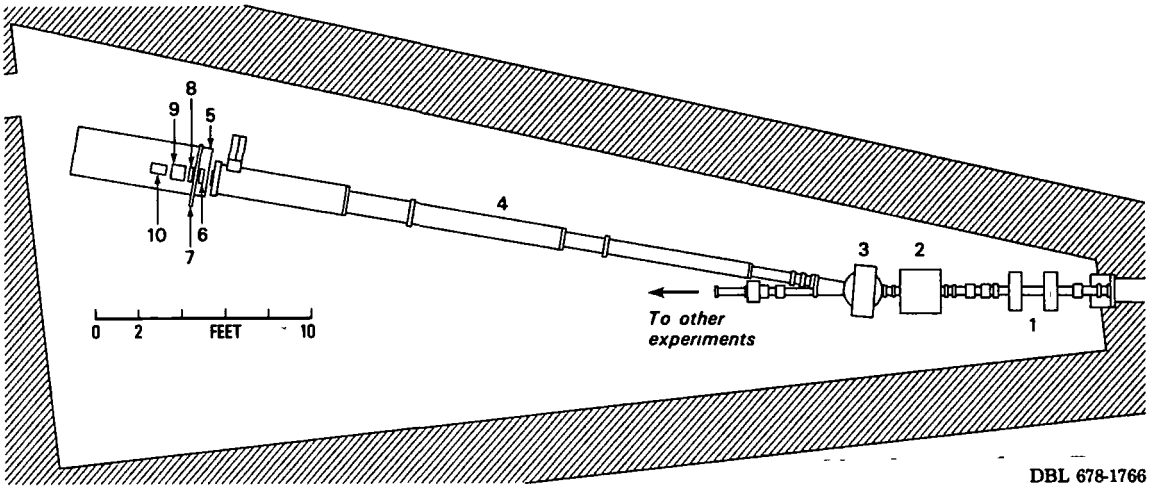


Fig. 1. Arrangement of equipment in the biomedical cave at the 88-inch cyclotron. (Numbers explained in text.)

voltage to the magnets, which will respond with triangular waves of current and magnetic flux, and thus sweep the beam linearly with time. Due to physical limitations of real magnets, the triangular current wave is rounded so that the beam spends more time at the periphery of the field. As a result only the approximately central 60% of the field is uniform within 5%, and the remainder must be discarded. Figure 2 shows a profile of a scanned 110-MeV alpha beam after the peripheral radiation had been dumped on a 2.5-in. -diameter graphite aperture just inside the end of the vacuum pipe, about 2.25 in. diameter is usable. To overcome this limitation and realize the full potential of the magnets a transistor feedback circuit has been designed which takes a signal from a pickup loop in the magnetic field and compares it with a triangular wave from a signal generator. The transistor amplifier driving the magnet then supplies a modified square wave such that the magnetic flux wave is as triangular as that of the signal generator. A small model of this circuit was assembled, but proved inadequate for complete evaluation, a larger model is being built.

As currently used the field is scanned two times per second, and no nonuniformity of the field due to overlapping or gaps between successive sweeps of the beam has been observed. With larger fields, however, nonuniformity may be a problem, and the solution may lie in increasing the time for a complete scan so that successive sweeps will merge, or, by introducing a thin scattering foil upstream from the scanner, to broaden the beam.

Development of the scanned beam is a part of a continuing study of skin effects of space irradiation. With the scanned α-particle beam 50 mice have been irradiated with the Bragg peak 0.25 and 0.5 mm beneath the skin surface (see the contribution of H. Aceto).

Microbeam

Critical alignment has become important in collimation of the beam to microdimensions, of the order of 25 microns diameter, for rat and mouse brain irradiations. Normally the beam has small random fluctuations about its central position. This is not a criticism of the 88-inch cyclotron but an acknowledgement of physical limitations probably present in all accelerator sources. Compensation for position fluctuation is not possible with the steering magnet because of its inertia. The relatively small beam sweeping magnet, however, is ideally suited, and when supplied by the small model feedback transistor circuit described above gave excellent control. In this case a feedback control signal was obtained from two electrodes of a quadrant ionization chamber and a differential amplifier. Whatever beam movement remained was undetectable. In the first run of this system on 26 July, 92 shots of 80-MeV α particles through a 25-μ platinum aperture were given on a 1/3-mm grid to a rat brain.

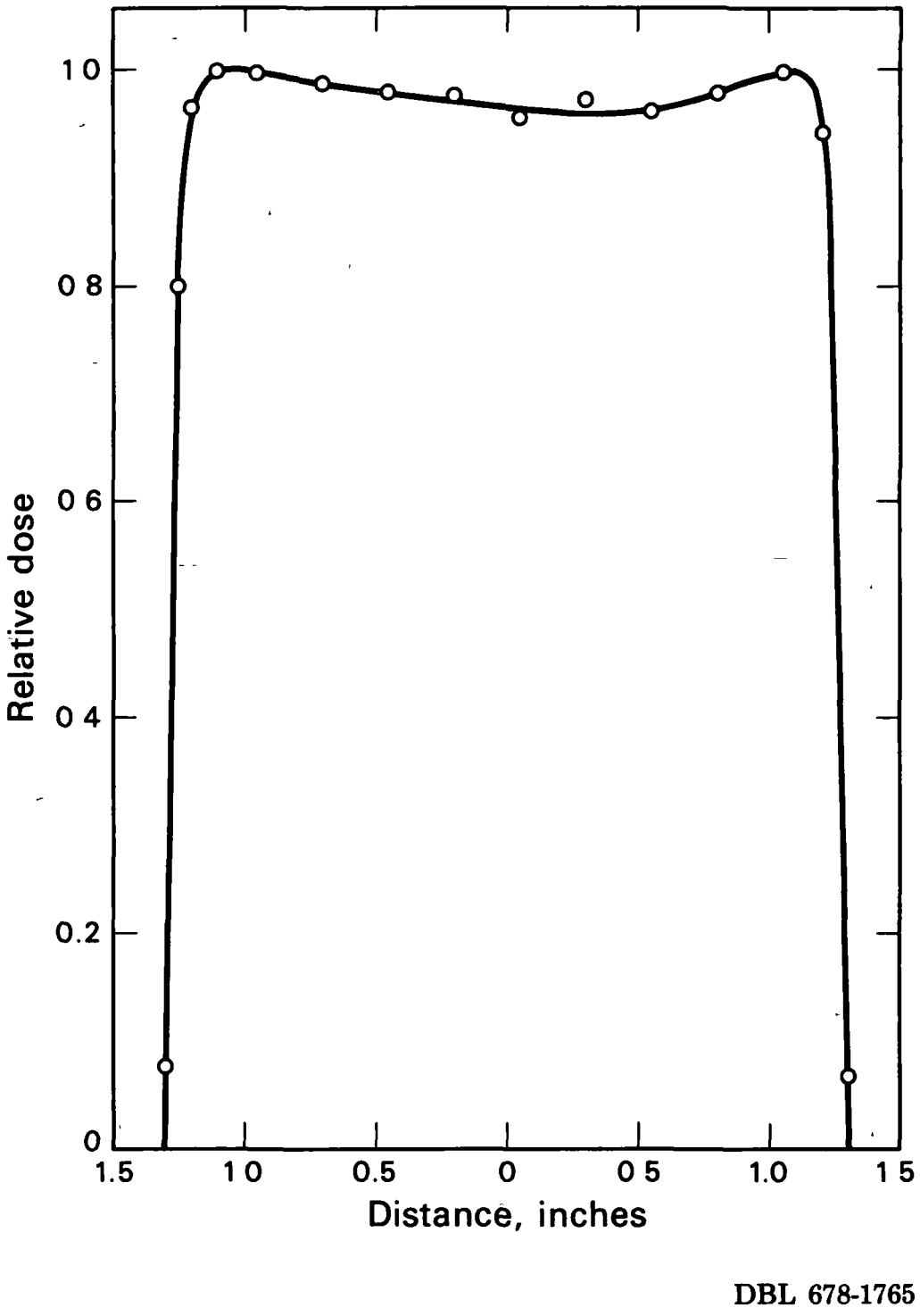


Fig. 2. Profile of scanned 110-MeV α-particle beam.

MAMMALIAN RADIOBIOLOGY AND NEURORADIOBIOLOGY

Introduction

At the beginning of development of interest in space flight it appeared that all one needs is a figure for "relative biological effectiveness" of space radiations and that this could be obtained by doing some acute lethality studies on large mammals.

Such studies were performed in detail on mice in this Laboratory with 730-MeV protons and 900-MeV helium ions, lethality on primates was also studied first in cooperation with Brooks Air Force Base and later with Ames Laboratory. Extensive proton data are available on large mammals from later work done by the Air Force at various laboratories and from the USSR. The LD_{50} is about the same, within 15%, as in a comparable exposure to γ rays. However, it is now realized that we must have more knowledge, for the following reasons:

1. The development of the lethality syndrome after protons is different from that after γ rays.
2. Solar flares produce peculiar distributions of depth dose and LET. High-LET radiation is a result of stopping low-energy protons and helium ions.
3. Astronauts must be protected from lethal doses by shielding, important questions remaining are: What symptoms will sublethal flare doses cause in space-flight environment? Could these impair the astronaut's efficiency as a pilot and observer? What delayed deleterious effects may be caused by medium-level doses in space flight?
4. Astronauts are also subjected to additional environmental stresses during space flight. Is there a synergism between these and radiation effects?
5. Later space flights are designed to be of several months' or years' duration; some solar flare radiation is unavoidable. What is the rate of recovery from the effects of space radiation and how can one predict and control astronaut exposures and keep these at safe levels?
6. A small part of cosmic rays consists of penetrating heavy nuclei. What are the effects of accumulating injury due to such particles?
7. Under certain conditions--for example, during egress from the space capsules and in the lunar excursion "module" (LEM)--high-intensity radiation may penetrate to the skin. What are the hazards of such exposures?

The solution of all the above problems would clearly require research efforts of major scope. It is also clear that simulation of space conditions for prolonged periods would not only prove very expensive and time-consuming, but might not furnish adequate answers soon enough.

The Laboratory has selected a few fields that appear to be of special interest and is proceeding on studies concerning these. The emphasis is on the understanding of cellular and molecular mechanisms, since this may allow intelligent estimates for "permissible levels" and for chemical or biological methods of protection.

Current emphasis is on:

. Understanding of the acute intestinal syndrome, since animals exhibit more of this when they are exposed to protons than following γ-ray exposure. This problem is being approached with germ-free mice.

. Relationship of injury to stem cells to hematological effects.

. Synergism of radiation effects and anoxia.

. Effects of radiation on the labyrinth and on systems responsible for orientation and equilibrium. These are essential to the astronaut, and are sometimes severely stressed in space flight.

. Effects of radiation on the central nervous system. Because of the apparent lack of recovery of the nervous system from radiation effects, and because of the relatively high sensitivity to certain psychological effects of radiation, injury to the nervous system could be of serious impact in long-term flights.

. Skin effects. Late development of neoplasm is of particular interest, since high-LET radiation is known to be of high carcinogenic potency.

. Mathematical models. There appears to be a need for better correlation and evaluation of diverse radiobiological data to provide reliable extrapolations for health protection purposes. A model is being developed in the Laboratory that can use dose distribution and timing data as input. It is hoped that the program, by the use of known radiobiological principles and quantities, will provide predictions for the magnitude of radiation injury sustained.

SPACE-RELATED MAMMALIAN RADIOBIOLOGY

Henry Aceto

Space radiation represents perhaps one of the more significant potential hazards of long-term space flight. On the basis of current radiation environment data it appears that a wide range of radiation exposure conditions is possible from chronic low-level (galactic cosmic rays) to acute lethal (solar-flare radiation) doses. A comprehensive radiobiologic evaluation of this potential hazard should encompass the biologic effects under space-simulating conditions over this entire range. Unfortunately, presently available data are mainly limited to a small portion of this range under conditions whose direct relevance to the anticipated space environment is questionable.

Information relating the biological effects of tens of rads or less per hour, which is the domain most relevant to the projected radiation environment, is indeed meagre compared with the copious acute exposure data available. It can of course be argued that since the major fraction of the radiation damage (if we exclude that portion resulting from heavy cosmic rays) can be recovered from, application of the relatively high dose-rate data to an assessment of the hazard involved provides a convenient safety factor. Moreover, since there is such a wide variety of equally valid time patterns of dose delivery, no one of these is of substantial value to the exclusion of all others, and the most limiting case is therefore acceptable. With this presupposition in mind let us examine the applicability of the available radiobiologic data to the space-radiation problem.

In the main, the data relate the effect of radiations of different type and quality (as a single stress factor) on various biologic parameters. However, the space environment is not characterized by the existence of radiation as a single stress factor. The astronaut will be subjected during space flight to an entire range of associated factors (vibration, acceleration, weightlessness, changes in gas composition and barometric pressure, numerous emotional psychic effects, etc) which will act on him in a variety of combinations and sequences. Therefore, for our data to have their most reliable application to future long-term manned space flights, they must relate the radiobiologic response of living systems to the multiple physical and environmental stress factors associated with such flights. Selye's concept of the General Adaptation Syndrome is useful in this connection, indicating that whereas the body is capable of mobilizing effective defense against any single stressor which is not immediately lethal, it cannot so readily do so in the face of two simultaneously or sequentially applied dissimilar stressors Because multiple stressors are to be anticipated in

space, although they may not necessarily be combined simultaneously, adaptability is likely to be reduced.[1] It is apparent, then, that any attempt to accurately determine a practical level of "acceptable radiation stress" (or tolerable dose) for space flight must include multiple stress studies.

This is not to say that studies involving radiation as a simple stressor are of no value to the problem. Indeed, the data that have been accumulated so far should be very useful in interpreting the mechanisms involved in combined-stress investigations. Moreover, further selected studies may be useful in elucidation of certain hitherto unexplained mechanisms of radiobiological action.

The mammalian radiobiology studies at this Laboratory have been designed on the basis of the foregoing discussion. A part of this program is represented by three relatively diverse studies:

(a) combined effect of proton irradiation and hypoxia on beagles,
(b) heavy-ion whole-body skin irradiation of mice,
(c) germ-free research in mice.

It is conceivable that radiation hypoxia could represent a real and serious problem to a long-term space flight. Because of the velocities reached, a meteor weighing several hundred grams could penetrate the aluminum hull of the spaceship or some component of equipment controlling the environment. Data from the micrometeorite experiment gathered by Explorer I indicate that particles of 10^{-9} g mass and larger would collide with a spaceship at the rate of 6/min, which increases 100-fold during a shower. From this Newell estimates that a spherical ship of 3 meters diameter might be punctured once a year.[2] Still other possible accidental causes of spaceship decompression that must be considered include loss of atmospheric pressure through equipment malfunction or cabin leakage due to hull imperfections. An entire space mission may be jeopardized if this contingency is realized in combination with a solar event; or, in the case of translunar flights, combined with the chronic galactic radiation hazards in space.

Konecci has demonstrated a decreased tolerance to hypoxic stress imposed during the postirradiation period in guinea pigs. The time of useful consciousness 24 hr after irradiation decreased significantly in animals exposed to 500 roentgens and then subjected to a simulated altitude of 30 000 ft.[3] Lethality studies indicate a decrease in the LD_{50}^{30} from approximately 600 to 500 R. For rats maintained at a simulated altitude of 15 000 ft during the postirradiation period the hematologic time pattern at this altitude following 450 R--as revealed by red blood cell volume, hemoglobin, hematocrit, and red blood cell counts--suggests that the increased mortality is due to an inadequate erythropoietic response.[4] The radiation-induced impairment of the hemopoietic system was sufficient to preclude an adaptive response to the hypoxic stress. Indeed, the additional stress served to aggravate the radiation-induced physiologic stress. The hypoxic animal, because

of its lower-than-normal partial pressure of alveolar oxygen, exhibits a decreased efficiency of hemoglobin-oxygen association. The oxygen capacity deficiency resulting from the radiation-caused cellular hypoplasia was thus compounded by that from hypoxia, and increased mortality ensued.

However, suppose the animal was subjected to hypoxia before radiation exposure? In this case would an adaptation to hypoxic stress in the absence of radiation modify the subsequent response to radiation? Konecci has shown, using radiation response as an indicator, that 6-month-acclimatized rats (2 months at 16 000 ft and 4 months at 18 000 ft) irradiated at ground level and immediately returned to 18 000 ft are in a distinctly superior physiologic state compared with controls. At thirty days 94% of the acclimatized animals survived an 800-R x-ray dose, compared with 12% of the ground-level controls.[5] It seems reasonable to assume that the vastly improved adaptive response to radiation in the polycythemic altitude-acclimatized animals may be in part attributed to a considerable alleviation of the radiation-induced tissue hypoxia. Others have shown that hyperplasia of bone marrow produced by exposure to low oxygen tension enhanced the resistance of erythroid elements of animals subsequently exposed to high levels of x irradiation.[6, 7] In contrast, Smith et al.[8] have reported that erythroid hyperplasia at the time of x irradiation is associated with a decreased tolerance to radiation stress. Absence of anemia was of no apparent value to the irradiated rats.

Perhaps at this point the role of tissue hypoxia and its modification of tissue respiratory process should be considered further. Several authors have shown that the rate of respiration (or oxygen consumption) progressively decreases after radiation.[9-11] Other investigators indicate an increased oxygen consumption,[12] while some conclude there is no change.[13] According to Manoilov, during irradiation of a biologic system, a state of tissue hypoxia results from a specific suppression of the aerobic phase of tissue respiration that takes place due to damage of iron-containing enzyme systems which participate in electron transfer from hydrogen to oxygen.[14] A concomitant effect of this suppression is blockage of the oxidative phosphorylative step of the tricarboxylic acid cycle in the system. Creasey and Stocken found that oxidative phosphorylation in nuclei isolated from spleen, thymus, bone marrow, and lymph nodes of irradiated rats exhibited considerable depression by doses as small as 25 R.[15]

Oxidation of organic substances may then proceed by a different pathway (oxidation by direct combination with oxygen from the air), which is not accompanied by the processes of phosphorylation and is energetically relatively inefficient. Oxygen consumption may even increase under these conditions. However, this apparent increased oxygen consumption may be misleading, since in reality the physiologic state of the biologic system is highly abnormal and is functionally hypoxic.

In the event of an accidental hypoxic episode in space accompanied by radiation exposure, the astronaut will not likely have had sufficient time to develop acclimatization to the hypoxic stress. The resultant dual stress will of course be accompanied by the other space flight stress factors. These factors have already been shown to produce an "adaptive" red cell volume loss of 20% in one of the astronauts of the Gemini V mission.

Still another factor that might contribute to the tissue respiratory deficiency is represented by the increased capillary fragility and resultant hemorrhage following radiation damage.[16] This factor may have particular significance to space flight, since the hemorrhagic response of primates to proton irradiation has been observed to be more pronounced than to ^{60}Co γ radiation or 2-MeV x rays.[17] The mechanism for this effect is not yet clear.

When one considers all these factors, it becomes apparent that there is a need for further evaluation of the homeostatic defect induced by different levels of proton radiation in the biologic response to hypoxic stress.

Female beagle dogs received a 270-MeV whole-body proton exposure of 200 rad and were then subjected to a prolonged altitude exposure at 18 000 ft during the postirradiation period. A part of the iron kinetics studies performed on these animals includes serial measurements of radioiron content in the plasma after intravenous injection of transferrin-bound tracer ^{59}Fe. Figure 1 illustrates a portion of these results as expressed by the plasma clearance rate (PCR). The base-line data for each animal were averaged and the results subsequent to the base-line period were normalized to this average value. Since the total plasma iron content appeared to stay relatively constant in any given animal before and after radiation, we may assume that the PCR is a reasonable indicator of erythropoiesis in the same animal, assuming no significant changes in pool kinetics. Examination of the external counting rates over the sacrum and liver seems to justify this last assumption.

The clearance rate of the irradiated control animals appears to reach its nadir at about 4 days (± a few days) postirradiation. It rises again to approach its preirradiation base-line value at about 23 days, followed by an overshoot, and returns to base line at 74 days. The nadir value appears to be compatible with the transit time of the surviving nucleated erythrocytic precursor pool in the marrow, assuming interruption of the stem cell input to this pool at the time of radiation.

This "overshoot" may be due to the response of returning erythropoiesis to increased erythropoietic stimulation seen following radiation (e.g., increased erythropoietin titre following radiation).

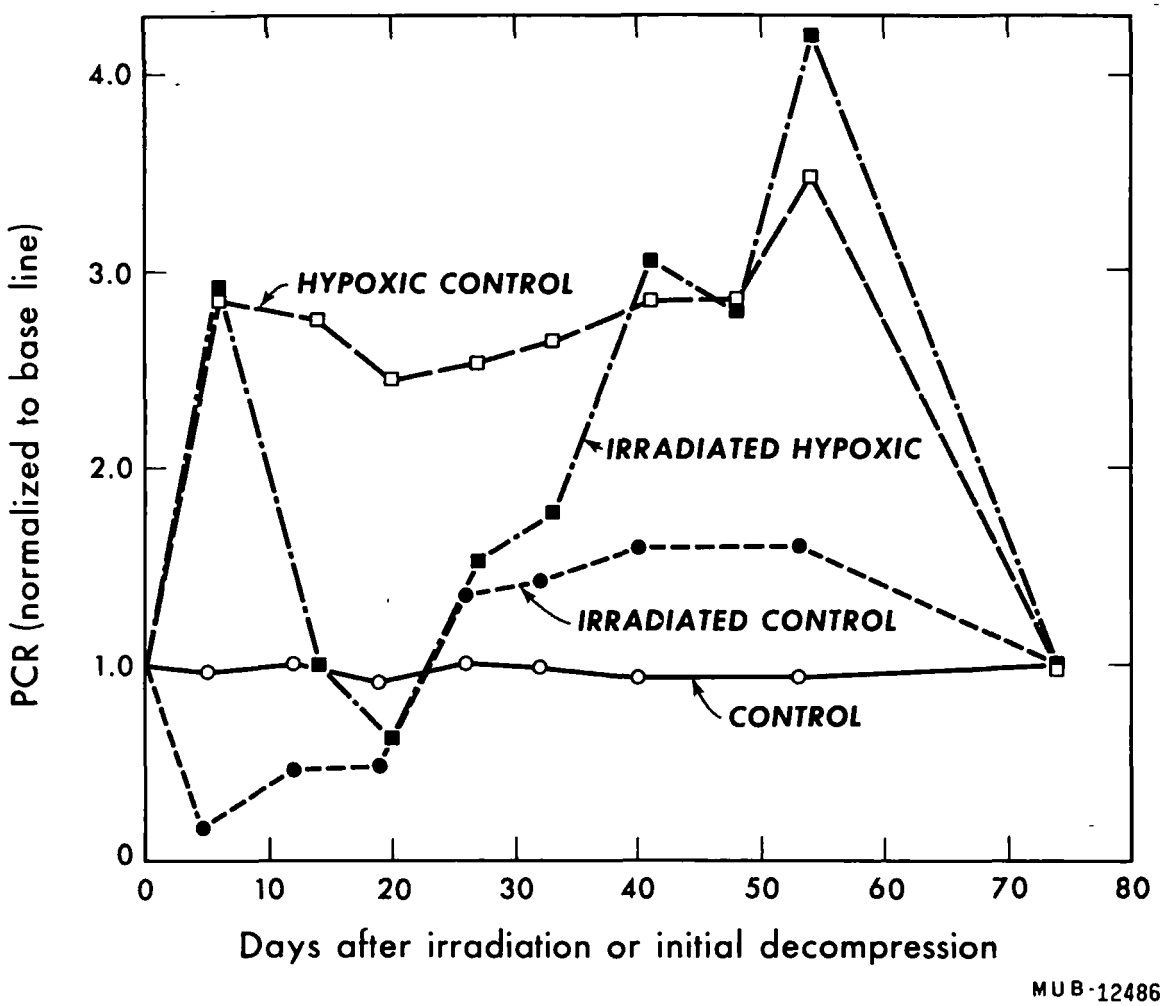


Fig. 1. Plasma clearance rate of beagles following radiation (200-rad) or hypoxia (18 000-ft altitude simulation) or both.

The hypoxic-control animals exhibit an increase in plasma radioiron clearance rate to almost three times its base-line values by the sixth day (± a few days) after entering the chamber, at which time the PCR appears to approach a plateau which it maintains until permanent recompression at 56 days. The cellular kinetics of the bone marrow suggest that this behavior may be explained by assuming hypoxic stimulation of the stem-cell pool. This stimulation and resultant proliferation results in a rapid rise to a maximum at approximately 6 days, which agrees well with the transit time of erythrocytic precursors originating in the stem-cell pool.

The irradiated-hypoxic animals exhibit the same initial response as the hypoxic-control animals. However, in this case, the rapid rise of the plasma radioiron clearance rate to almost three times the base-line value at 6 days is followed by a rapid decrease to a nadir at about 20 days. The recovery phase then follows, and the clearance rate reaches that of the hypoxic-control animal by 40 days. It is interesting to note that in the recovery phase the hypoxic-irradiated animal appears to reach values greater than those of the hypoxic-control animal, which may be due in part to the "overshoot" phenomenon observed in the irradiated-control animals. The response pattern of the irradiated-hypoxic animals suggests that despite severe damage, the stem cells and perhaps some of the very early pronormoblasts could still be stimulated by the hypoxia. However, after exhaustion of cells capable of hypoxic stimulation despite radiation damage, the proliferation of red cell precursors rapidly decreased until after recovery from radiation damage.

Another interesting observation is that the nadir of the irradiated-control curve is considerably lower than that of the irradiated-hypoxic curve. This result suggests that at no time is the response of the irradiated-hypoxic animal so severe as that of the hypoxic-control animals.

Hemoglobin content was determined by the cyanomethamoglobin method. The results of this test as indicated in Fig. 2 reveal a response similar to that of the clearance rate. The irradiated control animal exhibited a gradual decline in its hemoglobin content at a rate characteristic of the red cell lifetime. This behavior suggests complete cessation of input from the precursor stem cell pool.

The hypoxic-control and irradiated-hypoxic animals show an early rise in hemoglobin content. However, at about 8 to 10 days the irradiated hypoxic animal appears to exhaust its ability to be stimulated by the hypoxia, and the radiation damage begins to be expressed as the hemoglobin content follows a roughly linear rate of fall again characteristic of the red cell lifetime. A cursory examination of supplementary data suggests that this result is not attributable to either hemoconcentration or hemodilution.

Additional information that tends to give credence to the abortive rise and subsequent fall of erythropoiesis in the irradiated hypoxic

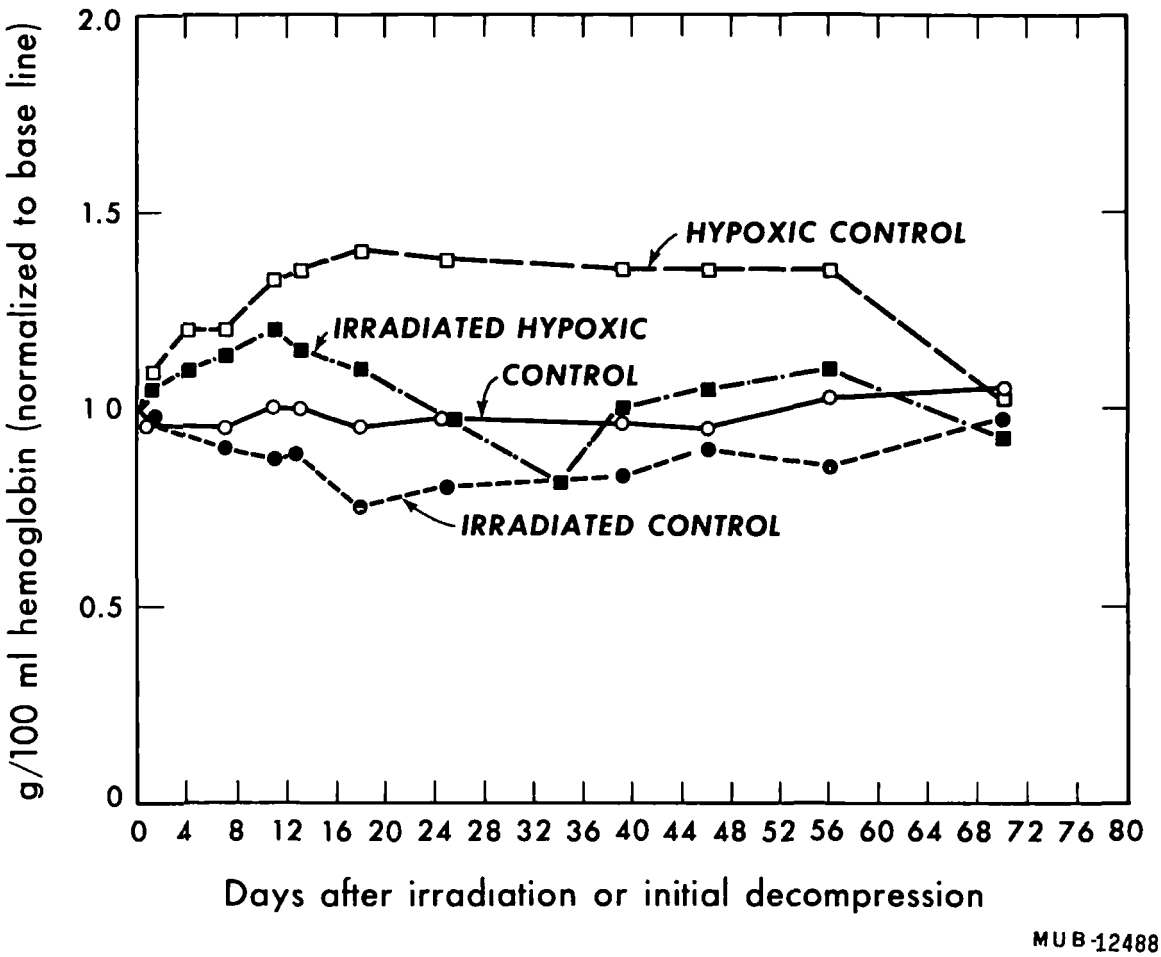


Fig. 2. Hemoglobin response of beagles following radiation (200 rad) or hypoxia (18 000-ft altitude simulation) or both.

animals is represented by the radioiron appearance curve in the peripheral erythrocytes (Fig. 3). The control curve represents the average of several determinations of the erythrocyte uptake and includes the 68% confidence limits of these results. A qualitative examination of the appearance curve taken at 7 days postirradiation suggests that there is indeed an elevation in the erythropoietic activity of the irradiated hypoxic animals comparable to that observed in the hypoxic controls.

The work of Newsom and Kimeldorf suggested that the blood picture of the irradiated rat during the first 20 days at altitude (15 000 ft) more closely resembled irradiated animals maintained at sea level than the altitude controls.[4] Our results do not support this conclusion, but suggest that during the first week postirradiation the animal at altitude has behavior more like that of the altitude controls than the irradiated control. It would then appear that the mechanism of homeostasis is functional and useful during this time. At times greater than 1 week a homeostatic defect is operative and the cellular respiratory processes are diminished until recovery occurs.

Our discussion thus far has mainly limited the stress response to that resulting from "systemic stressors" only. However, the observed physiological sequelae may also be the result of "neurotropic stressors" that affect primarily the central nervous system, such as fear, anxiety, apprehension, frustration, and irritation.[18] As a result of this neurogenic action there is an alteration in pituitary-adrenal function that may ultimately lead to increased levels of adrenal cortical activity and enhancement of cortical steroidogenesis. A similar enhancement of adrenocortical output has also been observed in skin injuries. Since corticosterone is an inhibitor of protein synthesis and mitotic activity there is a rationale for expecting the normal stress mechanism to enhance the effect of radiation damage to the skin, where both the major fraction of the solar flare radiation dose and the highest average LET will be delivered. A resultant metabolic deficiency and impairment of repair may partly explain Fox's findings, which indicate that thermal burns and skin disruptions push a dose of radiation that would normally cause a hemopoietic mode of injury into a gastrointestinal mode.[19]

The degree of effect on the skin is dependent on the depth-dose distribution in relation to the critical cells and structures comprising the organ. Radiations that do not penetrate the thickness of cornified layer of the skin would have no effect, regardless of the magnitude of the exposure dose. More energetic radiations penetrating through the epidermis would result in epidermal necrosis. Deeper penetration into the dermis would result in progressively severe effects, including damage to the dermal capillaries and other structures. In addition to the acute effects, late or delayed manifestations of somatic radiation damage may ultimately lead to the induction of skin tumors.

It is clear that a great deal of work remains to be done in this area with respect to both acute and chronic charged-particle irradiation

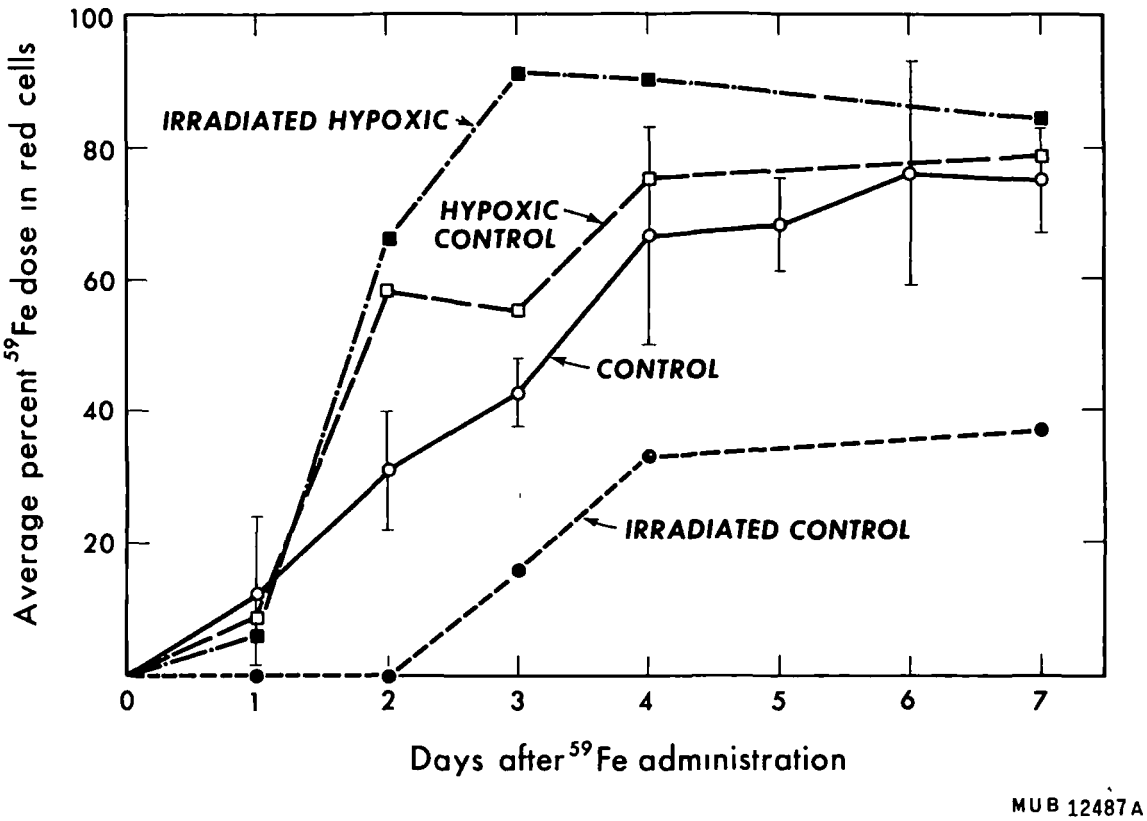


Fig. 3. Erythrocyte radioiron uptake response of beagles at 7 days postirradiation (200 rad).

of the skin.

Progress is being made in the development of a helium-ion beam whose physical characteristics are appropriate for skin irradiations. The variable-energy capability of the 88-inch cyclotron has been combined with energy degradation by aluminum foils to produce a beam of helium ions whose residual range corresponds to a specific depth in mouse skin. The depth of penetration is verified through histologic sections taken from irradiated animals. On the basis of these sections the entire integument of these animals is in the range 400 to 500 microns. A magnetic scanning device has been developed which will permit one to scan the beam of ions over a region corresponding to the geometrical dimensions of the animal (3 in.), thus providing a uniform distribution suitable for whole-body skin irradiation. Miniature semiconductor diode measurements of this distribution indicate a uniform beam intensity to within 10% over the entire distance corresponding to the longitudinal axis of the animal. Present efforts utilizing a silicon lithium-drifted detector are directed towards defining the LET distribution at various depths in the skin for the different mean residual ranges.

During the course of development of this beam and the verification of penetration depth for different foil thicknesses, an ancillary study was conducted that revealed a decrease in survival time with increasing depth of penetration in the skin of mice for graded peak doses ranging from 5000 to 30 000 rads.

Work is expected to commence soon relating the combined effect of various depths of penetration for helium-ion skin irradiations followed by a second-exposure installment from high-energy protons to the whole body. This study is designed primarily to verify the findings of Fox (discussed earlier) and to appraise the effects of heavy-ion irradiation on the skin. Included in this study will be observations of the carcinogenic properties of the helium ion beam.

Stressors, through their action on adrenal cortical activity, have also been implicated as a causative factor in decreased resistance to infections. Since an overdosage of ACTH and cortisone does in fact diminish resistance in experimental animals, this action may be partly explained by an increase in adrenocortical glucocorticoids (e.g., during stress), presumably chiefly by virtue of their antiinflammatory, lympholytic, and suppressive effects on antibody synthesis.

Radiation is a particularly potent stressor in this context. Not only does it make animals susceptible to infection by their own normally nonpathogenic intestinal flora, but it so lowers resistance that avirulent or even dead organisms may become lethal.[20] A frequent sequela of this impairment of the defense mechanism is widespread bacterial invasion of the blood stream (bacteremia). Bacteremia is commonly found in the heavily irradiated rodent.[21, 22] Eighty-five

percent of cultures from mice receiving 600 R were positive, and every animal showing bacteremia died. The organisms that were recovered were all members of the normal intestinal flora of mice.

A relevant study of the response of this mechanism to exogenous microorganisms was performed by Burke. Guinea pigs receiving 102-MeV proton exposures in the range of 22 to 170 rad over a 10-day period showed no difference from control in their ability to handle normal host flora. However, animals irradiated in the same way but challenged with nonresident bacteria revealed an increase in lesion size of 30 to 40% over those receiving no radiation.

It is evident from the foregoing discussion that radiation-induced infection and the role it plays in the radiation syndrome can be of significance,, particularly for long-term space flights. In order to more fully understand these processes a germ-free research program has been initiated. It is clear that germ-free and conventional animals exhibit anatomical, physiological, and immunological differences which may be used in the elucidation of fundamental mechanisms of action of ionizing radiation. Infection plays a major role in the gastrointestinal syndrome and the resulting mortality. The time of onset of the G. I. syndrome in axenic mice, as with conventional mice, is intimately connected to the time of mucosal denudation. The renewal rate of bowel epithelium in axenic mice is considerably lower than in the conventional mouse, indicating that bacteria, in some way, may normally contribute to the renewal of villus cells. Indeed, the time for loss of cells, and the time of denudation in axenic vs conventional mice, is twice as long in axenic (or germ-free) mice. In order to obtain a clearer understanding of this phenomenon, the influence of commensal bacteria as monocontaminants, and in combination, on the turnover rate of the intestinal epithelia will be one of the items investigated in the program.

Still another area in need of study is the mechanism of bile action with respect to the physiology of the intestinal epithelium in whole-body-irradiated animals. The absorption of bile salts by the small intestine following radiation decreases markedly and the salts are thus transported to the lower bowel, where they are converted to free acids by bacterial action. The bile acids exhibit a high degree of detergent activity in the bowel, resulting in diarrhea and excessive mucous secretion. Bile-duct cannulation has been shown to remove the diarrhea that is a characteristic part of the intestinal radiation syndrome. It seems reasonable to assume that the germ-free state would do the same.

Our initial application of this relatively new research technique is designed to elucidate the repeated observation indicating that proton-irradiated animals in the region of the LD_{50} show a tendency toward gastroenteric death even when the dose distribution in the body is relatively uniform. The more prominent gastrointestinal signs after

proton irradiation have been observed in both primates and rodents. On the basis of our previous discussion, it appears likely that infection should play a significant role in the observed difference. Proton irradiation of germ-free mice should then modify this difference of response and thereby serve as a useful tool in the elucidation of this phenomenon. Germ-free and conventional animals will be exposed to whole-body proton irradiation and their relative dose-response curves and time course of mortality will be evaluated. These data will be supplemented with a quantitative evaluation of cellular proliferation changes in the intestinal epithelium as determined by use of tritiated thymidine label.

Pilot experiments have been performed to ensure the adequacy of techniques and procedures for this work. In these experiments, Charles River CD-1 germ-free mice demonstrated an increased radioresistance to ^{60}Co γ rays as expressed by a higher median lethal dose than that for conventional animals. These results indicate a general agreement with earlier studies from other laboratories.

References

1. H Selye, The Physiology and Pathology of Exposure to Stress, Acta Med. Publ. Montreal, 1950.
2. H. E. Newell, Science 131, 385-390 (1960).
3. E. Konecci, J. Aviation Med. 26, 130 (1955).
4. D. J Kimeldorf and B D. Newsom, Federation Proc. 18, 113 (1959).
5. E. Konecci, D. Criscuolo, and M. B. Danford, J Aviation Med. 27, 424 (1956).
6. L O Jacobson, E. K. Marks, E. O. Gaston, E. L. Simmon, and M. H. Block, Science 107, 248 (1948).
7. J. Schack and R. C. MacDuffee, Science 110; 259 (1949).
8. W. W. Smith, S. S Cool, F. Smith, P. D. Altland, Am. J. Physiol. 170, 396 (1952).
9. J. Lane and J. Wilding, Radiation Res. 2, 157 (1955).
10 C. Sullivan and B. Dubois, Radiation Res. 2, 202 (1955).
11. G. Uhlmann and I. Rathgen, Strahlentherapie 35, 174 (1956).
12. R H. Mole, Quart. J. Exptl. Physiol. 38, 69 (1953).
13. H. M. Patt and E. Jackson, Proc. Soc. Exptl. Biol. Med. 78, 774 (1951).
14. S. E. Manoilov and O. A. Bryukhanov, Radiation Sickness Complicated by Injury to the Organism (Leningrad, 1958), p. 97.
15 W A. Creasey and L. A. Stocken, Biochem. J. 72, 519 (1959).
16. T. M. Fliedner, D. S. Sovenson, V. P. Bond, E. P. Cronkite, D. P. Jackson, and E. Adamik, Proc. Soc. Exptl. Biol. Med. 99, 931 (1958).
17. G. V. Dalrymple, I. R. Lindsay, J. J. Ghidoni, J. C. Mitchell, and H. L. Kendel, Some Effects of 138-MeV Protons on Primates, School of Aviation Medicine Report SAM-TR-65-58, Sept. 1965.

18. C. Fortier, Endocrinology 49, 782 (1951)
19. Leo Fox (NASA, Washington), personal communication.
20. C. E Hall, Physiology of Man in Space (Academic Press, New York, 1963), pp. 113-148.
21. C. P. Miller, C. W. Hammond, and M. Tompkin, J. Lab. Clin. Med. 38, 331 (1951).
22. C. P. Miller, C. W. Hammond, and M. Tompkin, Science 111, 540 (1950).
23 G. V Dalrymple, I. R. Lindsay, J. J. Ghidoni, J. C. Mitchell, and I. L Morgan, Some Effects of 400-MeV Protons on Primates, School of Aviation Medicine Report SAM-TR-65-73.
24. J. K. Ashikawa, C. A. Sondhaus, C. A. Tobias, A G. Greenfield, and V Paschkes, Difference in Injury Mode, Dose-Rate Dependence, and RBE of 730-MeV Protons, 100-k$\ddot{V}$p x Rays, and 250-kVp x Rays, UCRL-11014, Sept. 1963.

Page intentionally left blank

Page intentionally left blank

VESTIBULAR ORGANS:

The Structure and Function of the Vestibular Organs As They Relate to the Manned Exploration of Space

Larry W. McDonald and Robert G. Plantz

Linear and angular accelerations and the direction of gravitational fields are sensed in all vertebrate species by the vestibular organs. These are the only sensory organs devoted exclusively to these functions. In manned space flight extremes in accelerations and variations in gravitational fields are encountered. Thus one would expect to find stress of the vestibular organs under space-flight conditions. It is surprising that there have been only minor problems relating to vestibular function in American astronauts. This is probably due to the long training of the American astronaut under conditions that impose a stress on vestibular function.

In all earth-orbital manned space flights to date, radiation exposure has been slight, i.e., less than 1 rad.[1] It is expected, however, that in prolonged space flights beyond the earth's geomagnetic field the radiation exposure may become significant, especially if a solar flare is encountered. What effects whole-body space radiation will have on man is not known and will probably remain unknown until man is exposed to significant amounts of such radiation in space.

By simulating the proton and α-particle radiation of space with the synchrocyclotron, animals may be irradiated and the effects studied. The results of such animal studies help to anticipate and provide for the control of effects of such space radiation on man when it does occur. The purpose of our studies is to evaluate the effect of space radiation on vestibular structure and function in the experimental animal. To do this it is first necessary to define what is known of normal vestibular structure and function.

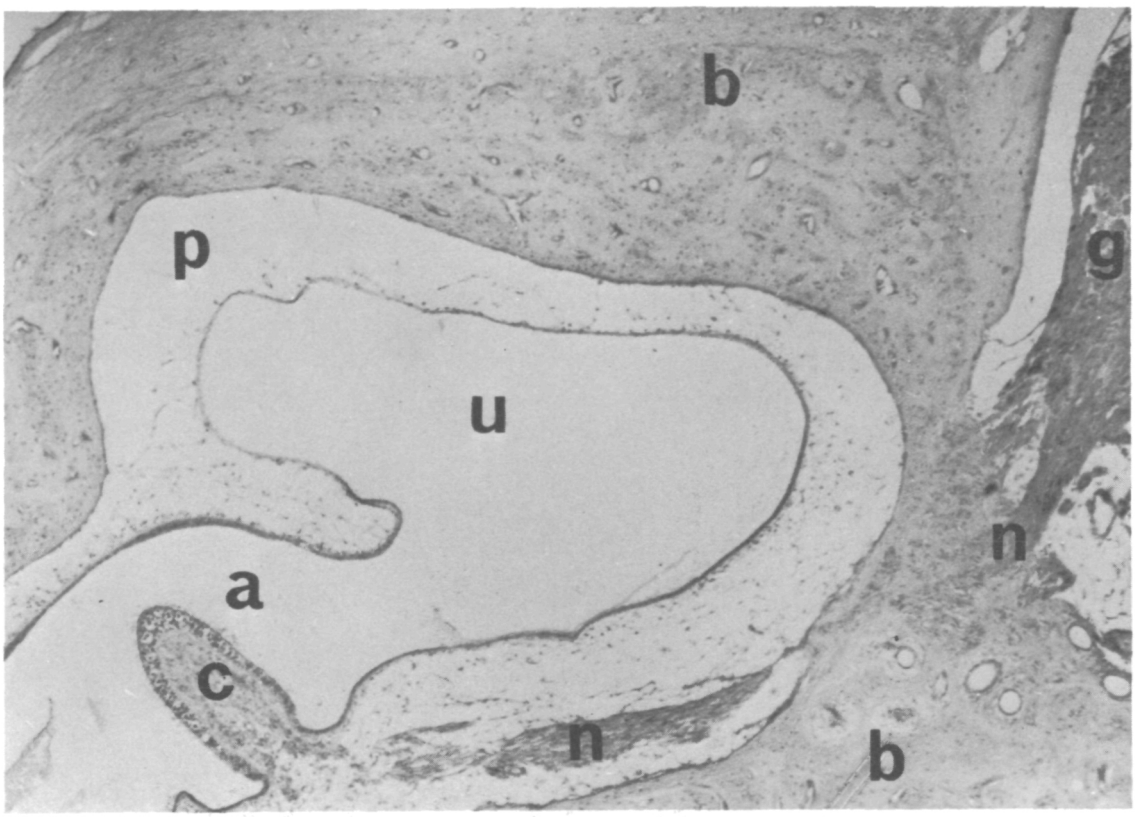
The inner ear is located deep within the petrous portion of the temporal bone. The more anterior part of the inner ear is the cochlea and the more posterior part, which is the subject of our interest, is the vestibular organ. The membranous labyrinth is contained within the bony labyrinth and these together make up the vestibular organ. The fluid within the membranous labyrinth is referred to as the endolymph, and that outside the membranous labyrinth between the petrous temporal bone and the membranous labyrinth is the perilymph. There are three semicircular canals in each of the three planes of space, and these are made up of membranous portions of the labyrinth

contained within the bony labyrinth. Each semicircular canal has one of its ends opening into the utricle. One end of each canal has a dilatation called the ampulla in which projects a crest containing sensory nerve endings. This crest (the crista) has a gelatinous cap, the cupula, into which cilia project from an underlying sensory epithelium. These structural features are shown in Fig. 1. The membranous utricle connects to the membranous saccule. Within areas of the membranous wall of the utricle and the membranous wall of the saccule there are thickenings in which sensory nerves terminate. These thickenings of the wall of the membranous labyrinth are made up of a strong epithelium from which cilia project inward into a gelatinous mass containing calcite crystals. These sensory areas of the utricle and saccule are referred to as the maculae.

The sensory epithelia of the cristae and the maculae have the general structural features diagrammed in Figs. 2 and 3. The structural features are very similar in the two receptors, the only distinct difference being the calcite crystals present in the gelatinous mass of the maculae and not in the gelatinous cupula of the cristae. These structural similarities extend to the ultrastructural level where one finds the sensory receptor cells possessing about 35 stereocilia which increase progressively in length as one progresses from one edge of the cell to the other. These stereocilia have very little internal structure. Where the stereocilia are the longest, there is one edge of the cell with an equally long kinocilium possessing the typical nine-and-two microtubular structure. These general structural features are shown in Figs. 4 through 6. Interestingly the molluscs are found to have similar ultrastructural features of the sensory epithelium of the statocyst which is the gravity-sensing organ of these animals (Fig. 7).

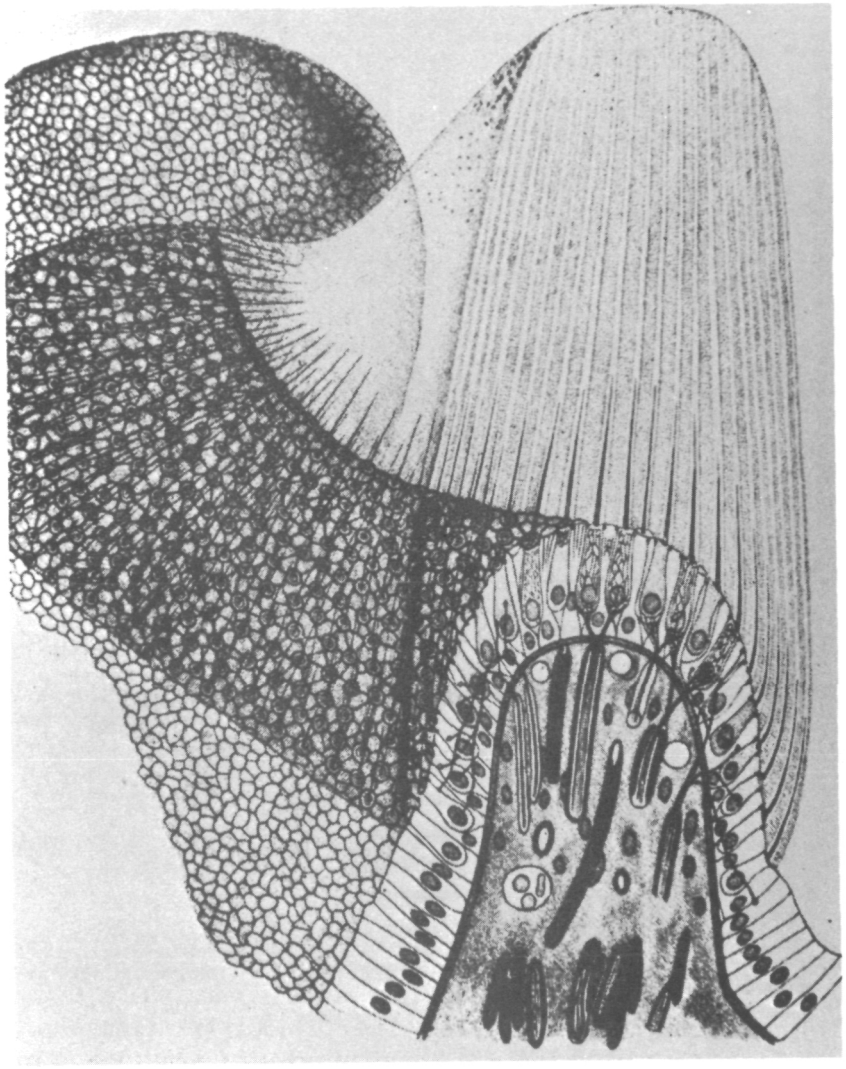
The vessels, mostly capillaries, often lie close to the basement membrane of the sensory epithelia, as shown in Fig. 8. These vessels are lined by a continuous layer of endothelial cells and often shown surrounding perivascular cells. Nerve fibers and supporting cells may be closely applied so that there is little remaining extracellular space, a condition similar to what is found in the central nervous system. These structural features are shown in Fig. 9.

The displacement of the cilia of the sensory cells toward the side of the cell with the long kinocilium causes a stimulation of the receptor cell, i.e., a depolarization. A displacement in the opposite direction away from the kinocilium causes an inhibition of the receptor cell, i.e., a hyperpolarization.[2] In the semicircular canals, this displacement is produced by angular acceleration moving the endolymph and the gelatinous cupula in which the cilia are embedded. In the maculae, the mass of the calcite crystals in the gelatinous covering of the cilia is moved by linear acceleration or change in direction of the gravitational field. This movement of the gelatinous covering of the cilia displaces the cilia and thus produces inhibition or stimulation of the receptor cell.



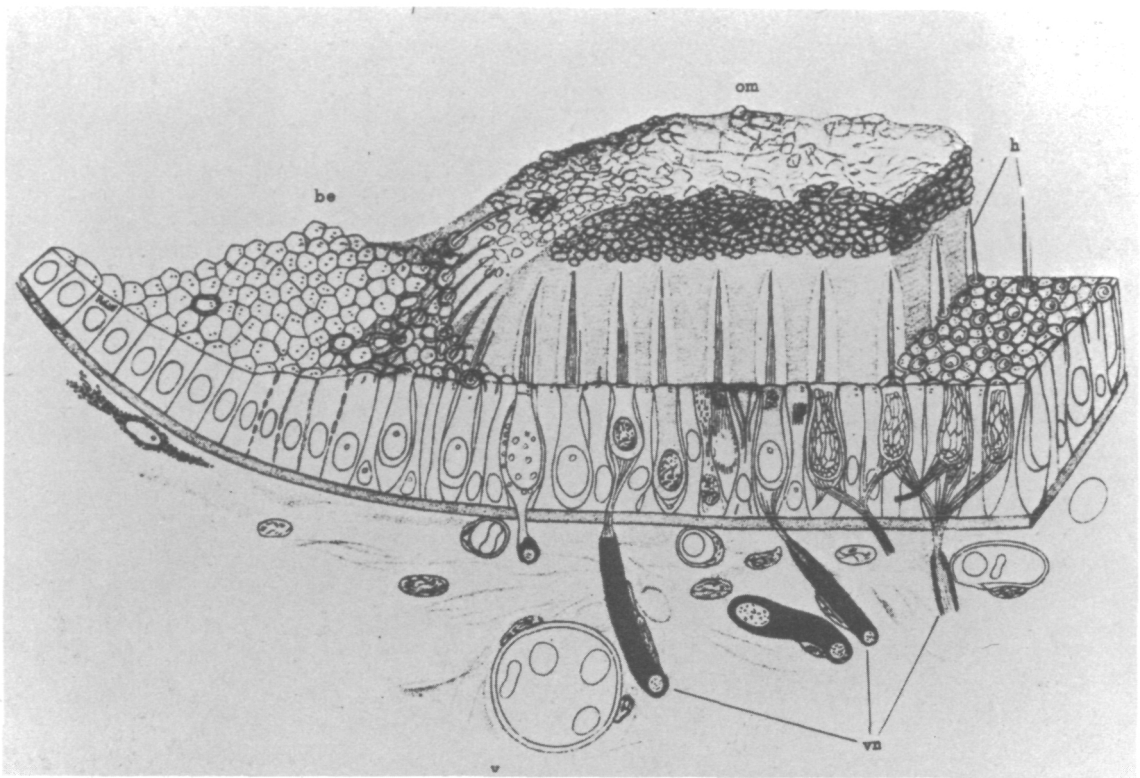
XBB 678-5042

Fig. 1. Section of normal vestibule showing ampulla (a), with crista (c), vestibular ganglion (g), utricle (u) perilymphatic space (p), nerve to ampulla (n), and petrous portion of temporal bone (b). Cupula of crista has been lost in this preparation. Stubs of cilia appear as irregular serrations on crista. Semicircular canal joins ampulla at left margin of photomicrograph. Hematoxylin and eosin stain. ×118.



XBB 678-5043

Fig. 2. Diagram of crista of semicircular canal. The gelatinous cupula projects to the upper right of center and the cilia are seen to project into the cupula to the right of center. Myelin sheaths are seen to terminate at the basement membrane of the sensory epithelium. Blood vessels are shown in the supporting tissue beneath the sensory epithelium.



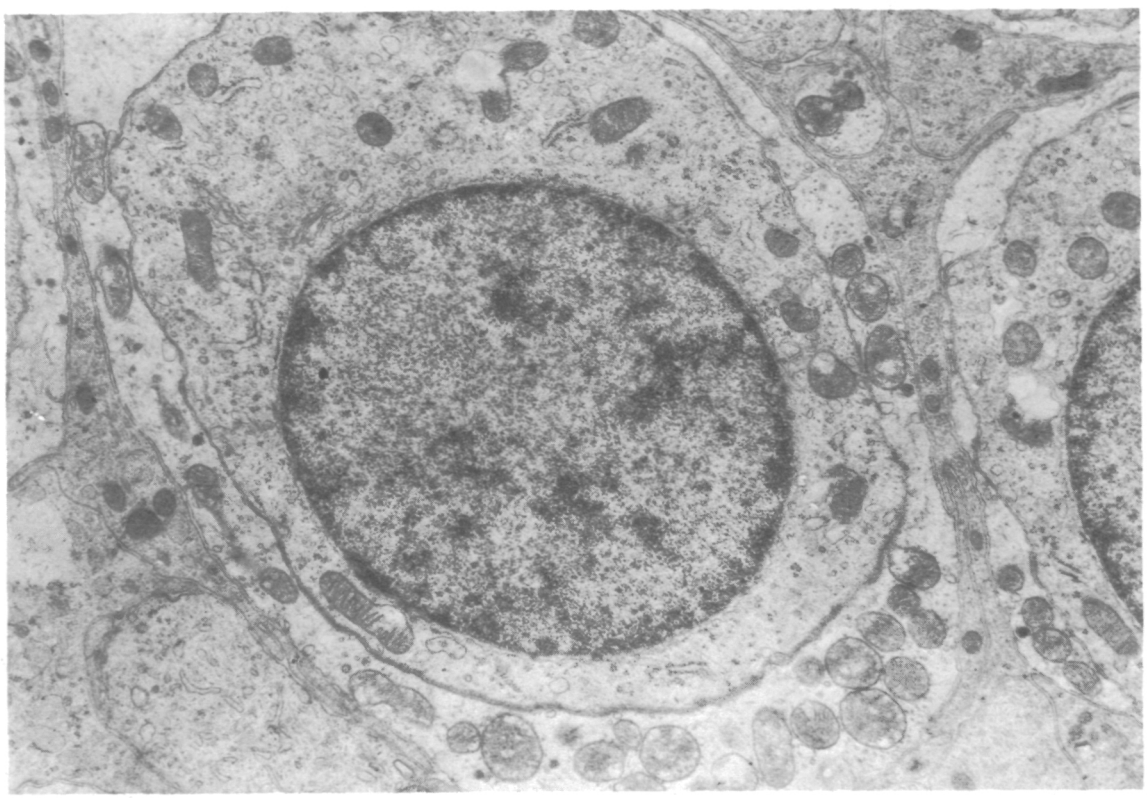
XBB 678-5044

Fig. 3. Diagram of macula. The same general structural features are present as described for Fig. 2 except that otoliths (om) are present in the gelatinous cap into which the cilia (h) project.



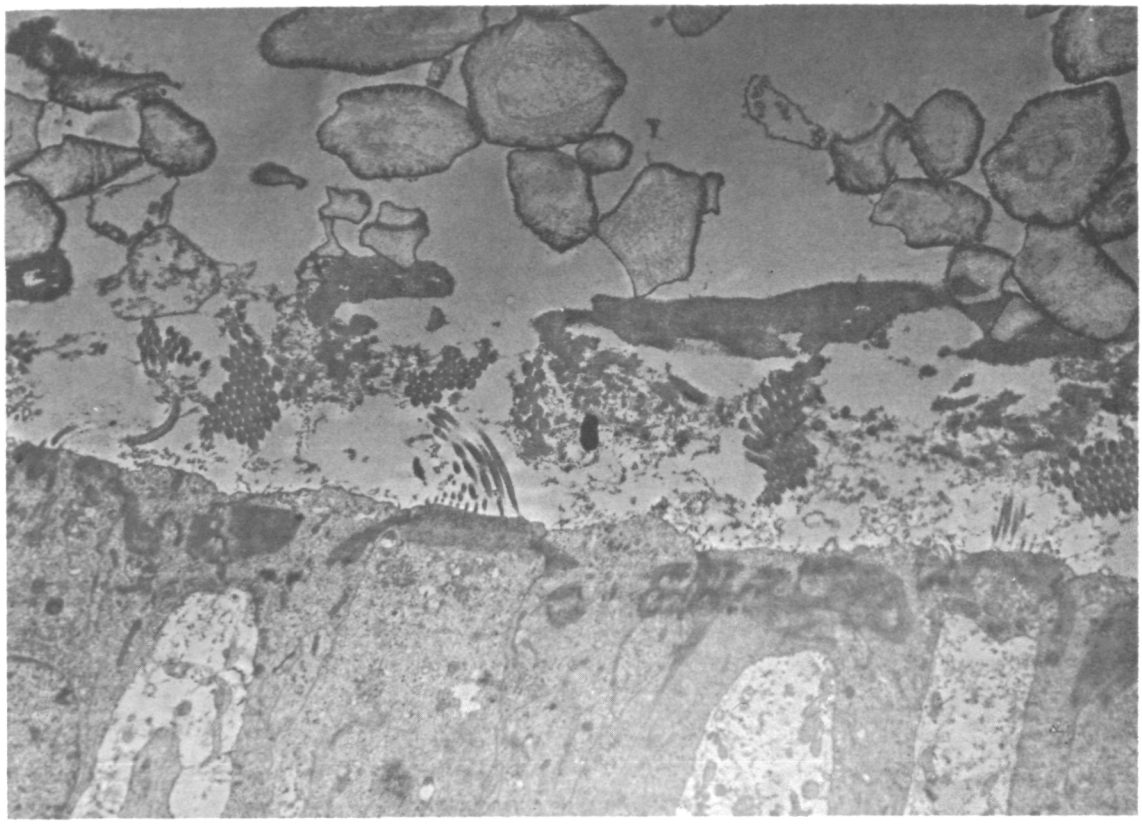
XBB 678-5045

Fig. 4. Electron micrograph showing surface cilia of sensory epithelium of crista. The stereocilia are seen increasing in length from right to left and the kinocilium from the left border of the centrally located cell is shown cut at a point near its base and at another point near the tip. The base plate and mitochondria can also be seen. About ×15 800.



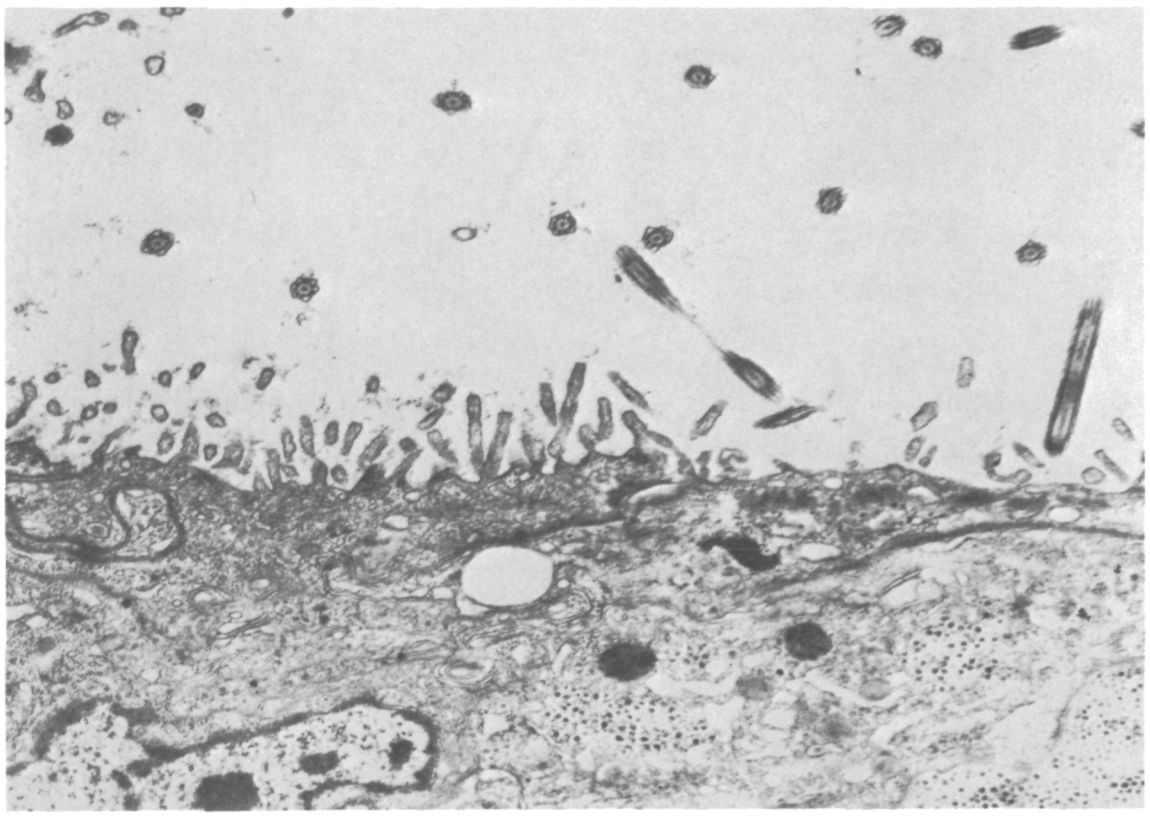
XBB 678-5046

Fig. 5. Electron micrograph of section parallel to surface of macula showing sensory cell surrounded by clear cytoplasm of nerve ending, so-called Type I nerve ending. About × 18 200.



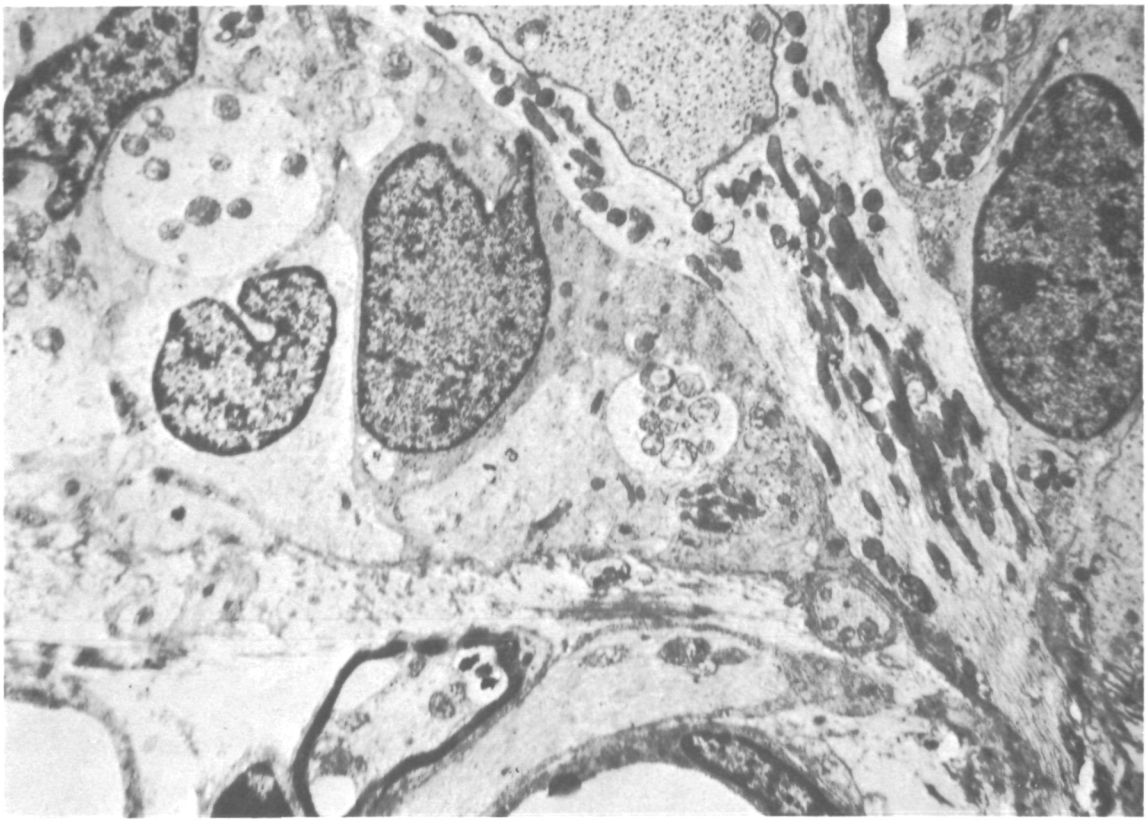
XBB 678-5047

Fig. 6. Electron micrograph of surface of sensory epithelium of macula showing calcite crystals above, and centrally, condensations of the gelatinous material and groups of cilia projecting from the surface of sensory receptor cells. Kinocilia are not readily identified in this micrograph. About ×9250.



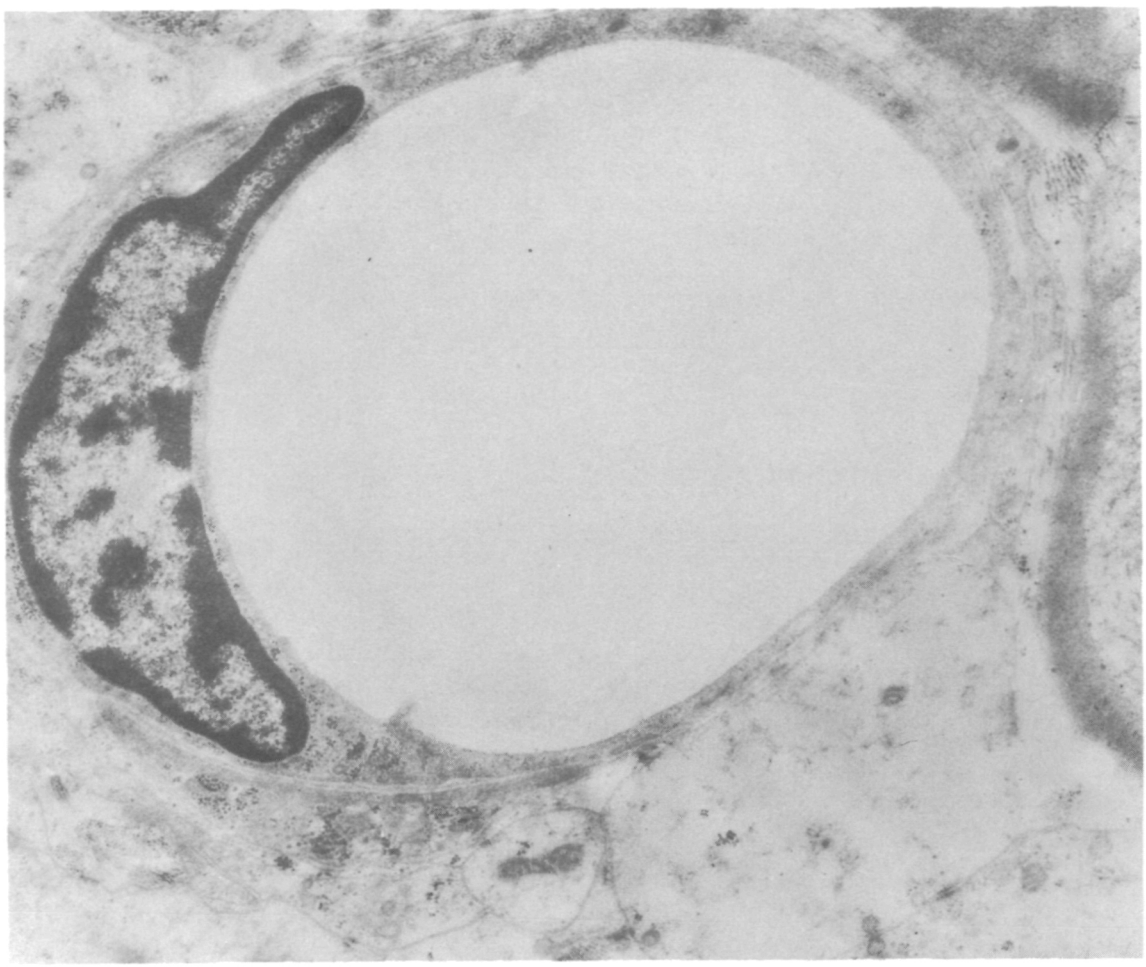
XBB 678-5048

Fig. 7. Electron micrograph of surface of sensory epithelium of statocyst of the mollusc Ariolimax sp. showing both kinocilia with the classical internal structure and the shorter cilia without internal structure. About ×11 100.



XBB 678-5049

Fig. 8. Electron micrograph showing base of sensory epithelium of macula. The basement membrane passes across the micrograph at the level of the upper edge of the lower fourth of the micrograph. At the right a sensory nerve penetrates the basement membrane where it loses its myelin sheath and passes obliquely upward and to the left above center. At the upper center of the nerve endings surround the lower part of a receptor cell. Part of a wall of a capillary is shown at the center of the bottom of the micrograph. About ×13 900.



XBB 678-5050

Fig. 9. Electron micrograph showing capillary beneath sensory epithelium of macula. The endothelial cell cytoplasm completely covers the thin basement membrane. Nerve fibers and other cytoplasmic processes are closely applied about the capillary. Part of the cytoplasm of a perivascular cell can be seen enclosed in a thin layer of basement membrane at the lower and slightly to the left part of the capillary wall. About $\times 9\,900$.

From the receptor cell the nerve impulses pass to the central nervous system via the vestibular nerve. The distribution of the primary afferents is mostly to the vestibular nuclei. The secondary vestibular fibers from the vestibular nuclei have a very wide and complex distribution which exceeds that of any other sensory nerve.[3] In addition to the vestibular afferent nerve fibers there are small efferent fibers which have synaptic relations with the afferent endings in the vestibular sensory epithelia.

References

1. C. A. Berry, Space Medicine in Perspective, J. Am. Med. Assoc. 201, 232-241 (July 24, 1967).
2. Jan Wersall and Per-G. Lundquist, Morphological Polarization of Mechanoreceptors of the Vestibular and Acoustic Systems, in The Role of the Vestibular Organs in Space Exploration, Second Symposium Held Under the Auspices of the National Academy of Sciences–National Research Council Committee on Hearing, Bioacoustics, and Biomechanics, Ames Research Center, Moffett Field, California, January 25-27, 1966, NASA SP-115 (Scientific and Technical Information Division, Office of Technology Utilization, National Aeronautics and Space Adminstration, Washington, D. C., 1966).
3. M. B. Carpenter, Central Connections of the Vestibular Systems, Arch. Otolaryng. 85, 517-520 (May 1967).

VESTIBULAR ORGANS:

Testing the Function of Vestibular Receptors

Robert G. Plantz and Larry W. McDonald

In some physical systems we can write the equations describing the system from a morphological study and a knowledge of how the components work. But many systems, including biological systems, are too complex for such an analysis. Thus we consider the vestibular system as a "black box" and attempt to describe its function from input-output data.

According to Lee,[1] only that part of the system which is both controllable and observable can be identified by using this technique. Roughly, controllability implies that we can find some input that will drive the system to any of its states; observability implies that any change in the state of the system is reflected in the output. These two concepts dictate which quantities may be suitable inputs or outputs.

A morphological study of the vestibular system suggests that the sensors are spring-mass systems with considerable friction. The natural input for such a system is acceleration (angular for the semicircular canals and linear for the otoliths); the system dynamics are described by a second-order differential equation, if it is a linear system. Van Egmond[2] wrote the equation for the horizontal canal with zero input acceleration:

$$\theta \ddot{\xi} + \pi \dot{\xi} + \Delta \xi = 0, \qquad (1)$$

where θ = moment of inertia of endolymph,
π = moment of friction at unit angular velocity,
Δ = directional restoring force at unit angle of the cupula,
ξ = angular deviation of endolymph in relation to the skull,
$\dot{\xi}$ = 1st derivative of ξ with respect to time, i.e., angular velocity of the endolymph, and
$\ddot{\xi}$ = 2nd derivative of ξ with respect to time, i.e., angular acceleration of the endolymph.

In Van Egmond's experiments, the endolymph was given an initial displacement by supplying an impulse of angular acceleration, i.e., time was allowed for the cupula to return to its neutral position during constant angular velocity in the horizontal plane, and the rotation was stopped suddenly. Under such conditions, the angular deviation of the endolymph with respect to the skull is approximately given

by

$$\xi(t) = \gamma \frac{\theta}{\pi} \left(\exp(-\Delta t/\pi) - \exp(-\pi t/\theta) \right), \qquad (2)$$

where γ = initial angular velocity, and it is assumed that $\pi/\Delta \gg \theta/\pi$. The parameters in this equation (θ/π and π/Δ) could be evaluated by repeating the experiment with many different values of γ if we could measure $\xi(t)$. Unfortunately, the physical dimensions of the semicircular canals preclude such a measurement. Thus we must find some indirect measurement of endolymph displacement to use as our output.

The simplest solution is to assume that the frequency of neural discharge of the vestibular afferents is linearly proportional to the endolymph displacement. This assumption seems to be justified in the experiments by Groen et al.[3] on the ray (Raja clavata). They imparted a sinusoidal angular acceleration to the isolated vestibular system in the plane of the horizontal canal. The frequency of neural discharge from some of the fibers was seen to vary sinusoidally at the same frequency as the acceleration.

However, the isolated vestibular system is not very useful in pathology studies, and direct nerve recording is very difficult in the intact vertebrate due to the bony structure encasing the vestibular organ. The existence of nerve fibers running from the vestibular nuclei to the oculomotor nuclei[4, 5] suggests that eye reflexes may be a suitable output. Eye motions can be easily measured by taking advantage of the corneo-retinal potential difference. Small dermal electrodes are placed at each corner of the eye, and the potential difference is amplified electronically and continuously recorded. Unfortunately, the vestibular nuclei also received proprioceptive signals and cerebellar signals, and the oculomotor nuclei receive signals from the eyes and from the cerebrum.[4,5] But it appears that very precise compensatory eye movements depend upon vestibular signals.[6]

It is possible to remove visual cues as an input to the oculomotor nuclei. We have constructed a frosted dome to fit over the animal's head which admits diffuse light but offers no fixation points. (The animal is kept in an illuminated environment to eliminate the change in corneo-retinal potential difference which occurs when it is placed in a dark environment.[7, 8])

The proprioceptive inputs are another story. They are probably reduced by wrapping the animal in a corset. But their elimination would require a spinal preparation, which is not practical in pathology studies over a reasonable length of time. Perhaps moving the axis of rotation to different points along the animal's body would allow the cross-correlation of the results and make it possible to subtract the proprioceptive effects. Presently we are assuming that the effects of proprioceptive inputs are negligible compared with the vestibular inputs.

Nystagmus is the most striking eye reflex resulting from vestibular stimulation. Assuming that nystagmus occurs whenever the endolymph is displaced beyond a threshold position, the slow time constant in Eq. 2 (π/Δ) could be evaluated by noting the duration of nystagmus when stopping the rotation from several initial angular velocities. The problem is that the time between nystagmus sweeps increases as the cupula returns to its neutral position and can actually become of the same order as the time constant we are trying to measure (several seconds). Thus, it is not possible to determine when the endolymph has reached the threshold position with any reasonable accuracy. The minimum time between nystagmus sweeps is about 0.2 second, which is much too long to evaluate the fast time constant in Eq. 2 (θ/π, about 0.1 sec).

Since postrotational nystagmus is not an adequate measurement of vestibular function, we have developed equipment to oscillate the animal sinusoidally in the horizontal plane. This approach was used by Niven et al.;[9] their experiments at peak accelerations of 60 deg per sec^2 and frequencies from 0.02 to 0.20 Hz show nystagmus sweeps superimposed on a general sinusoidal motion of the eyes. But these data are difficult to interpret. First, any measure of amplitude could only be a guess. Secondly, at frequencies approaching 1 Hz the nystagmus sweeps distort the waveform enough to make phase measurements very difficult.

We repeated their experiments using rabbits, and were able to approximately measure the phase difference between the input (angular acceleration) and the output (eye motion). Under these conditions the eyes tend to move horizontally in the direction opposite that of the acceleration direction. This is shown in Fig. 1.

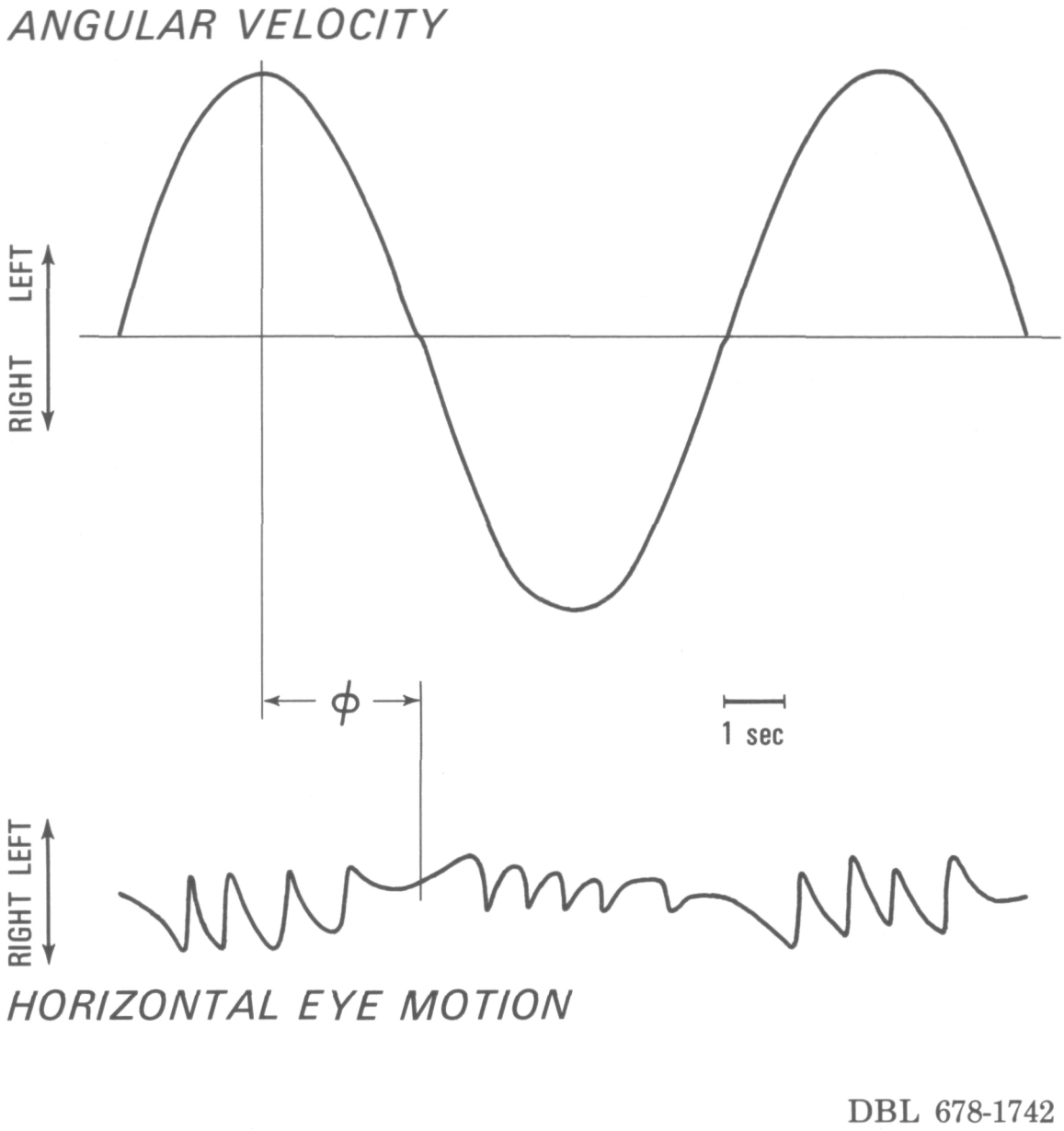
In Fig. 2, we have plotted the phase-shift data from four tests along with the phase shift that would result from a system having the transfer function

$$G(p) = K \frac{e^{-0.1p}}{(p + 1.9)(p + 0.3)}, \qquad (3)$$

where K = undetermined constant depending on amplitude measurements,
and p = the Laplace operator.

This corresponds to a second-order differential equation with a pure time delay of 0.1 sec in series. It is impossbile to distinguish this from a higher-order system with (possibly) no time delay by using only phase-shift data; we must also be able to measure the relative amplitude change as a function of frequency.

The most interesting feature of the recordings is that the eye follows a partial sinusoid between the nystagmus sweeps. By



DBL 678-1742

Fig. 1. Eye motion during sinusoidal oscillation in horizontal plane showing phase difference ϕ at 0.1 Hz. Note that the angular acceleration is zero when the angular velocity is maximum. In this case ϕ = 92 deg. (The curves were traced from an experimental recording.)

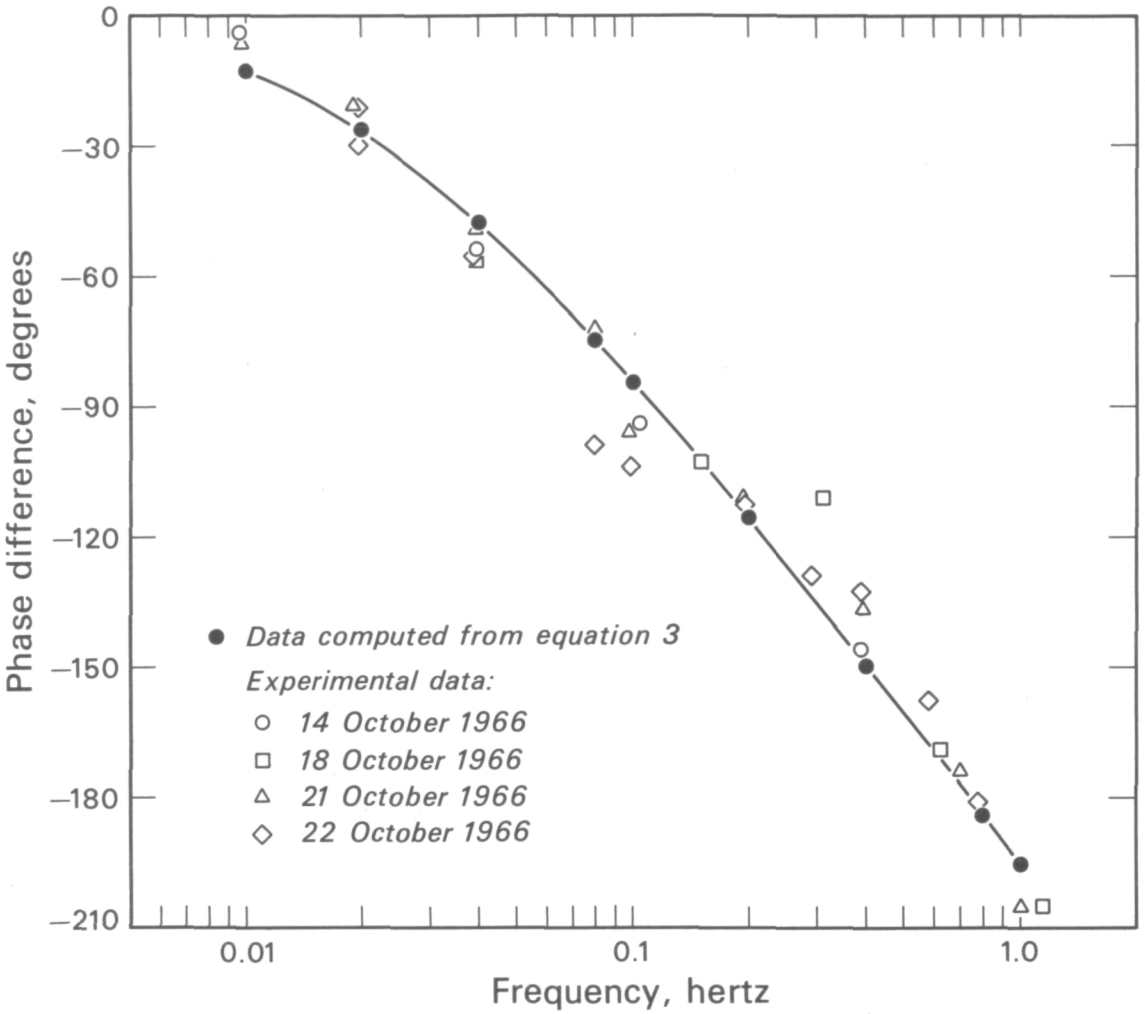
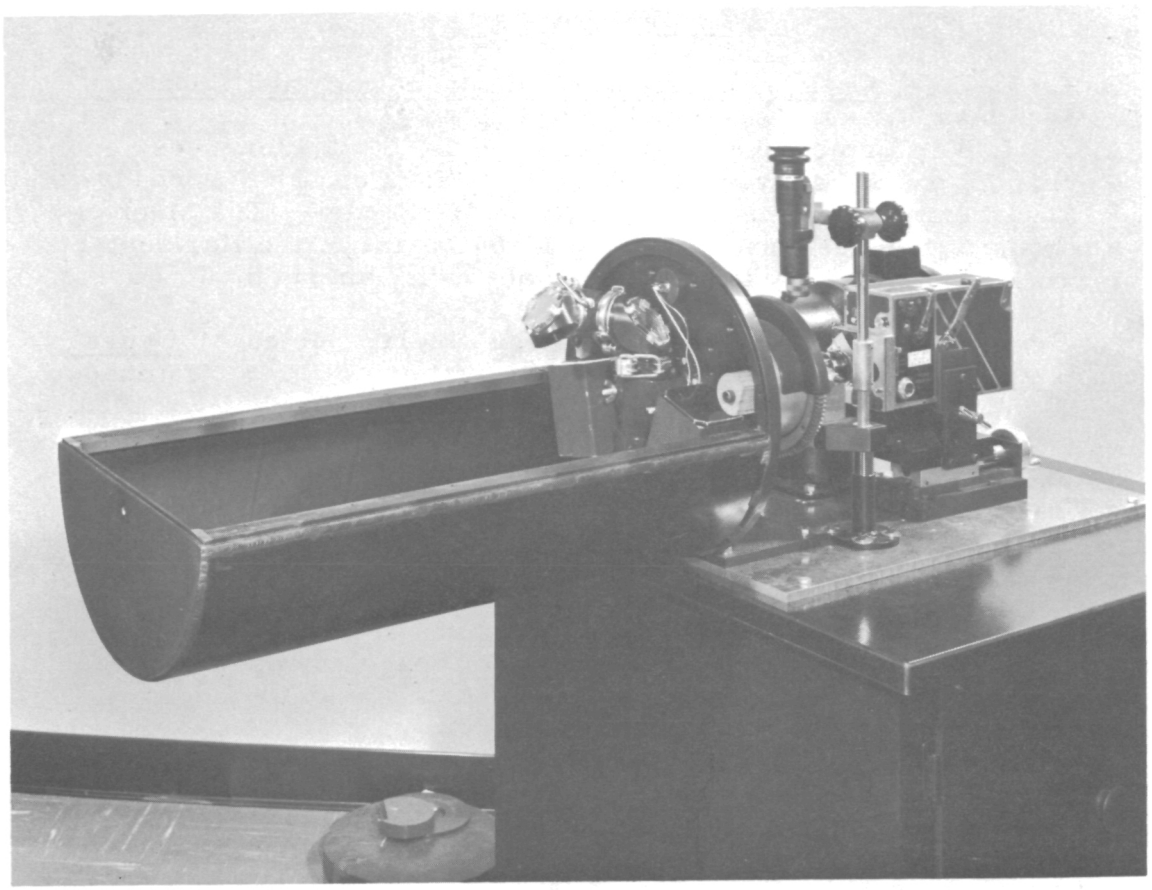


Fig. 2. Phase shift of the vestibular system in the rabbit when subjected to sinusoidal motion in the horizontal plane. Peak angular velocity is 60 deg/sec, which corresponds to 37.6 deg/sec^2 at 0.10 Hz. An ideal linear system with pure time delay is shown for comparison.

decreasing the peak acceleration values to about 10 deg/sec^2 at 0.1 Hz, we have found that the eyes describe a sinusoidal motion of the same frequency as the input without the nystagmus sweeps. Since a linear system with a sinusoidal input can only give a sinusoidal output of the same frequency (with possibly different phase and magnitude), we can now try to fit a linear model to the data without having to resort to trickery in an attempt to measure the sinusoidal component of the eye motion, which is necessary when nystagmus is present.

Using input accelerations below the nystagmus level also paves the way for other experiments. For example, it is possible to digitize the input-output data for an arbitrary input and construct a sampled-data transfer function from it.[1] Then it is a simple matter to convert this to a continuous transfer function.

Until now we have been describing the measurement of semicircular canal function, but equally important to manned space flight is the otolith organ, which senses linear accelerations and the gravity field. The only measurable reflex available for evaluating the function of this receptor is ocular counterrolling. This reflex consists of a rotation of the globe of the eye so as to partially compensate for any rotation of the head about a horizontal axis. Since there is no feasible method of measuring this rotation electrically, photographic methods are being used. We are using a dynamic system with continuous motion pictures similar to the method used by Kellogg[6] on human subjects. The motion picture frames are then analyzed for rotation of the eye with reference to rotation of the head. The apparatus used for this is shown in Fig. 3.



Space Bio 127

Fig. 3. Apparatus for measuring ocular counterrolling. The animal is placed in the cylinder occupying the left and central part of the picture. The top half of the cylinder has been removed. The animal is held in place with suitable holders. Through an optical system the rotation of the animal's eye with reference to the animal's head is recorded by the stationary motion picture camera at the right while the cylinder rotates at 6 rpm.

References

1. R. C. K. Lee, Optimal Estimation, Identification, and Control (M. I. T. Press, Massachusetts, 1964), Ch. 4.
2. A. A. J. Van Egmond, J. J. Groen, and L. B. W. Jongkees, The Mechanics of the Semicircular Canal, J. Physiol. 110, 1-17 (1949).
3. J. J. Groen, O. Lowenstein, and A. J. H. Vendrik, The Mechanical Analysis of the Responses from the End-Organs of the Horizontal Semicircular Canal in the Isolated Elasmobranch Labyrinth, J. Physiol. 117, 3 (1952).
4. A. Brodal, Fiber Connections of the Vestibular Nuclei, in Neural Mechanisms of the Auditory and Vestibular Systems, G. L. Rasmussen and W. F. Windle, Eds. (Charles C. Thomas, Springfield, Ill., 1960), pp. 224-246.
5. M. B. Carpenter, The Ascending Vestibular System and Its Relationship to Conjugate Horizontal Eye Movements, in the Vestibular System and Its Diseases, R. J. Wolfson, Ed. (University of Pennsylvania Press, Philadelphia, 1966), pp. 69-98.
6. R. S. Kellogg, Dynamic Counterrolling of the Eye in Normal Subjects and in Persons with Bilateral Labyrinthine Defects, in The Role of the Vestibular Organs in the Exploration of Space, Symposium Held January 20-22, 1965, U. S. Naval School of Aviation Medicine, Pensacola, Florida, NASA SP-77, pp. 195-202.
7. L. D. Homer and H. Kolder, Mathematical Model of Oscillations in the Human Corneo-Retinal Potential, Pflügers Arch. Ges. Physiol. 287 [3], 197-202 (1966).
8. C. Kris, Corneo-Fundal Potential Variations During Light and Dark Adaptation, Nature 182:4641, 1027-28 (1958).
9. J. I. Niven, W. C. Hixson, and M. J. Correia, An Experimental Approach to the Dynamics of the Vestibular Mechanisms, in The Role of the Vestibular Organs in the Exploration of Space, Symposium Held January 20-22, 1965, U. S. Naval School of Aviation Medicine, Pensacola, Florida, NASA SP-77, pp. 43-56.

VESTIBULAR ORGANS:

Radiation Effects on Structure and Function

Larry W. McDonald and Robert G. Plantz

The function of the semicircular canals depends upon the displacement of the fluid endolymph within the canal and the displacement of the gelatinous mucopolysaccharide cupula of the crista. Fluid shifts and alterations in capillary permeability are among the changes occurring acutely in many tissues following irradiation. Alterations of tissue mucopolysaccharides have been recognized as a late effect of irradiation. Thus we have a receptor organ which we would expect would show both early and late effects of irradiation. Our studies up to the present have shown the late effects, but acute functional alterations, except with very high doses, have been difficult to demonstrate. We believe that, with the slow sinusoidal oscillations described in Part II of this presentation, acute functional changes may be demonstrable. Ultrastructural studies of the acute effects are inconclusive at present.

It is necessary to distinguish between the effects of local irradiation limited primarily to the vestibular organ and whole-body irradiation. Both may affect vestibular reflexes, but local irradiation is acting only on the vestibular receptor organ, whereas whole-body irradiation may be acting at various sites in the vestibular reflex chain or may be producing abscopal (indirect) effects through the alteration in the blood which occurs with whole-body irradiation.

In our studies using postrotational nystagmus, whole-body ^{60}Co gamma irradiation of rabbits was associated with an increase in the variability of the test results as radiation sickness progressed. A group of eight animals was irradiated in this way and those receiving 250 to 500 rad showed definite effects as evidenced by increased statistical variation in the postrotational nystagmus response. Further studies of the effects of whole-body radiation are in progress, utilizing a simulated solar-flare helium-ion beam. The squirrel monkey (Samiri sciurea) is being used in these studies in collaboration with the Naval Aerospace Medical Institute at Pensacola, Florida. Vestibular testing consists of measurement of ataxia shown by an animal trying to balance on a rotating rod, and induction of motion sickness in a slow rotating room, and a caloric test. It is planned to add ocular counter-rolling to the tests being used. All vestibular testing is being done at Pensacola, and irradiations and histological and electron microscopic studies are being done at Berkeley.

In order to localize the cyclotron-produced particle-beam radiation to the vestibule of the rabbit, it has been necessary to make radiographic studies of the animal's head. This was accomplished by serially sectioning a frozen head in a bandsaw and, after thawing and formalin fixation, locating the vestibules in the sections. The sections were then taped together and radiographs taken.

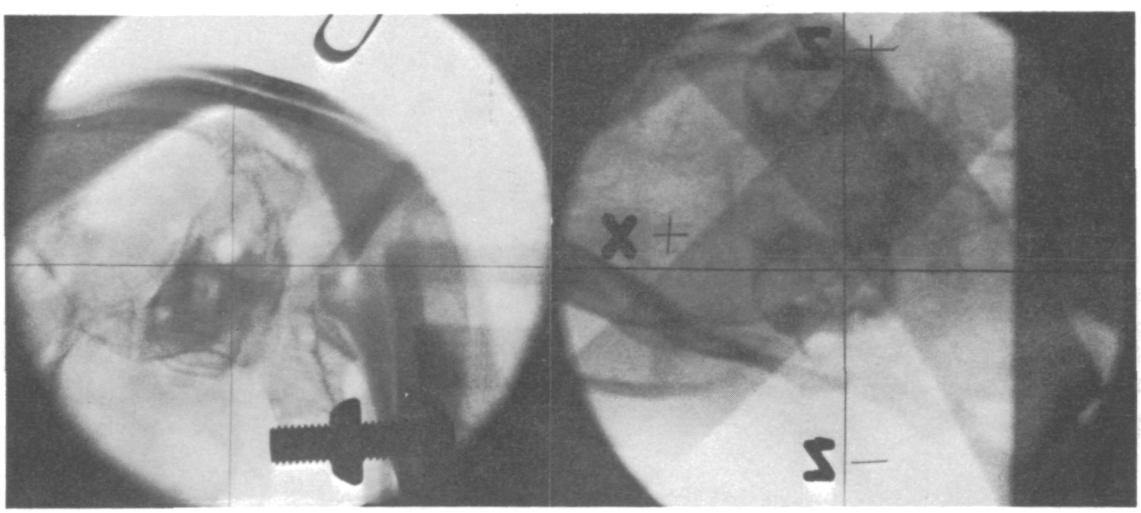
Lateral and dorsal radiographs of an intact living rabbit's head are shown in Fig. 1, with the cross hairs in position for the aiming of the 3/8-in.-diameter beam of the cyclotron.

When either whole-head or localized vestibular irradiation is used in the rabbit, fairly high doses are required to regularly produce alterations in postrotational nystagmus. Control animals often show periods of several days when they have an increased postrotational response. Our results using local irradiation are summarized in Table I. Although some of our early irradiations seemed to alter postrotational nystagmus at doses of 0.5 to 1.5 krad (first row of table), a subsequent larger group of irradiated animals did not confirm this. Radiation doses greater than 4.0 krad are required to produce a reliable alteration in postrotation nystagmus (last row of Table I). This alteration consists of a complete loss of postrotational nystagmus, often preceded by a period of a few days of increased postrotational nystagmus response. With doses of 5 to 8 krad, 3 to 7 days is required before the effects on postrotational nystagmus appear.

Morphological alterations are regularly found within 2 weeks following doses greater than 4 krad to the vestibule. At the light-microscopy level these alterations consist of edema and often hemorrhage in the tissue underlying the sensory epithelia of the maculae and cristae. These changes appear most marked in the maculae. There often appears to be some disarray of the otoliths and clumping of the cilia, but there is a great deal of variation of these features in control tissue sections.

In electron micrographs, no definite abnormalities in cilia have been detected. The most marked finding has been the increase in capillary basement membrane thickness, often more than 150 mμ, and the presence of increased amounts of interstitial space. These features are shown in Fig. 2.

Russian literature reports vestibular effects produced by radiation doses less than 500 rad. [1] These have been both x-ray and particle irradiation of dogs and rabbits with whole-body exposure. Conditioned reflexes involving the vestibular "analyzer" were regularly used, but postrotational nystagmus was also used to detect alteration in vestibular function. Our limited studies with whole-body irradiation suggest an increased variability of vestibular response in the whole-body exposure.



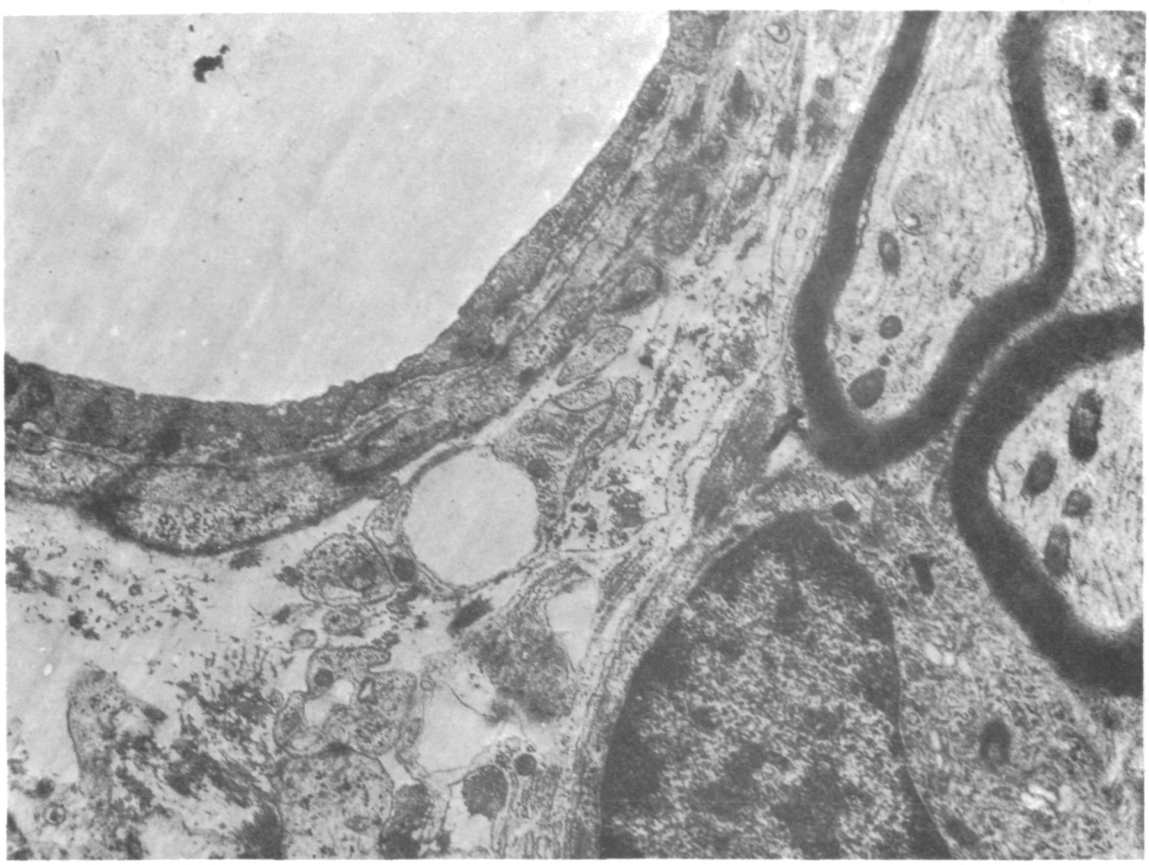
XBB 678-5052

Fig. 1. Radiographs of rabbit's head, showing landmarks used in aiming the cyclotron beam at the vestibule. In the lateral view at the left the radioluscent circular area above and slightly to the left of the intersection of the cross hairs is the recess of the paraflocculer lobe of the cerebellum. The tympanic bulla is in the left lower quadrant of the cross hairs (anterior and ventral). In the dorsal view on the right, the tympanic bulla is to the left of the intersection of the cross hairs. In both views the intersection of the cross hairs is on the vestibule.

Table I. Animals receiving whole-head or vestibular irradiation.

Type of radiation and number of animals	Number of control animals	Dose (krad)	Field	Testing method	Days post-irrad. of 1st test	Postrotational nystagmus following irradiation	Time for functional return
Plateau Alpha's							
2	7	0.50	BL	V	7-12	Equivocal	7-10 wks
3		0.50 to 1.50	UL	V	2	Nystagmus present at 60 days	NC
Plateau Alpha's							
11	5	0.20 to 0.50	BL	E	1	Nystagmus present at 30 days	NC
250-kVp x-ray							
5	4	0.50	WH	E	1	Nystagmus present at 30 days	NC
Plateau Alpha's							
5	2	1.00 to 4.00	BL	E	1	Nystagmus present at 30 days	NC
1		5.00	BL	E	1	Equivocal at 3 days Nystagmus abolished at 23 days	Nystagmus remained abolished at 30 days when animal was sacrificed
1		8.00	BL	E	1	Nystagmus abolished at 7 days	Nystagmus remained abolished at 11 days when animal was sacrificed

BL = bilateral vestibular irradiation
UL = unilateral vestibular irradiation
WH = whole-head irradiation
V = tested for postrotational nystagmus by visual observation
E = tested for postrotational nystagmography
NC = no change, nystagmus is still present



XBB 678-5053

Fig. 2. Electron micrograph of capillary wall underlying the macula of the utricle of an animal receiving 7 krad of α particles to the vestibule. The capillary lumen is at the upper left and myelinated nerves are seen at the right. There are increased amounts of interstitial space about this vessel. The basement membrane is increased to 160 mμ in thickness versus the normal of less than 100 mμ. Compare this micrograph with the figure on page 119. About ×15200.

Our findings at the light-microscopy level have been similar to those reported by several others, including Kelemen.[2] The thickening of capillary basement membrane and increase in interstitial space had not been previously described.

References

1. Yu. G. Grigor'yev, A. V. Sevan'kayev, and A. A. Sveshnikov, Biological Effect of Protons with Energies of 130 MeV, X-Rays with Energies of 180 kV, and Co^{60} Gamma Radiation on the Vestibular Apparatus, in Problems of Radiation Safety in Space Flights, Edited by Yu. G. Nefedov, NASA TT F-353, December 1965, Chapter 7, Pg. 157-184.
2. G. Kelemen, Acta Otolaryngologica Suppl. 184, 1963.

THE RIGHTING REFLEX OF THE FROG AS INFLUENCED BY IRRADIATION

Cornelius T. Gaffey and Victor J. Montoya

The primary gravireceptor in the frog is the otoliths in the utricle. A frog placed on its dorsal surface will orient itself in an upright position in about 0.8 sec. This stereotropism is initiated by the otoliths' change in position upon the hair cells of the sensory epithelium of the utricle. Stressed hair cells initiate neural impulses that are transmitted by the vestibular nerve to the vestibular nucleus in the hindbrain. Removal of the otoliths or destruction of the utricle abolishes the frog's righting reflex. The otolith organ also responds to tilting and linear acceleration. In the frog the semicircular canals are concerned with equilibrium disrupted by angular acceleration. It was our purpose to test the utricle's stereotropic sensitivity to irradiation. Alpha particles (910-MeV) and deuterons (455-MeV) generated by the Lawrence Radiation Laboratory (LRL) 184-inch cyclotron were used in whole-body irradiations. Protons (48-MeV) accelerated by the LRL 88-inch cyclotron were employed in localized hindbrain irradiations.

Previous studies on frogs' isolated sciatic nerve demonstrated that 300 krad of 910-MeV α particles immediately block conduction of the nerve impulse. This same species of frog (Rana pipiens) had its righting reflex activity inhibited by irradiation at doses only 1/15 of the nerve-block dose. Specifically, it was found that 18 to 22 krad (whole body) of 910-MeV α particles immediately removed the frog's righting reflex response. A desensitization and gradual loss of reflex ability followed 15 to 18 krad of high-energy irradiation. With 10 to 15 krads of α particles there was a reduced level of reflex activity indicated by a protracted latency period. However, these lower doses did not eliminate the righting reflex. The effect of whole-body irradiation with 455-MeV deuterons gave changes comparable to those induced by 910-MeV α particles.

Local head irradiations with a 3/8-in. circular beam of 48-MeV protons are being performed. The field of irradiation is restricted to the hindbrain of the frog and is aligned to irradiate the prootic bones of the skull, which house the inner ear. High-energy protons seem to produce a loss of the righting reflex at 20 krad, but unlike whole-body irradiation, this discrete head irradiation requires a postirradiation interval to manifest its destructive effect. Clear effects of hindbrain irradiation on the frog's righting reflex remain to be determined.

Page intentionally left blank

Page intentionally left blank

THE VESTIBULAR APPARATUS AS INFLUENCED BY LOCALIZED HIGH-ENERGY IRRADIATION

Cornelius T. Gaffey and Victor J. Montoya

The vestibular apparatus of adult male cats was locally irradiated by 910-MeV α particles generated by the Lawrence Radiation Laboratory's 184-inch cyclotron. Irradiation was restricted to a 1/4-in.-diameter alpha beam. The α-particle beam was used to irradiate one and then the other vestibular apparatus. Three reflexes were tested to evaluate the radiosensitivity of the vestibular apparatus: (a) the labyrinthine righting reflex (an otolith function), (b) the static head reflex (an otolith function), and (c) vestibular placing reflex (semicircular canal linear acceleration function).

The labyrinthine righting reflex is described as the ability to assume a reference position in a gravitational field. In this project the righting reflex was evaluated as the capacity of an inverted animal to change to the upright position during free fall. A blindfolded cat was dropped with its legs pointed upward. Normal cats turn with amazing speed and deftly land on all fours. The head initiates the turn, and this rotation is referred to as the labyrinthine righting reflex. After the head became aligned during free fall, the upper body followed (neck righting reflex), and then the lower body completed the turn. Bilateral irradiation of the vestibular apparatus caused the loss of this righting reflex provided the animal was tested without visual cues.

A blindfolded cat demonstrated head orientation irrespective of the space position of the remainder of the cat's body. This reaction disappeared if the otoliths were surgically destroyed. This static head reflex stems primarily from gravitational stimuli, and is independent of movement or acceleration. Irradiation can influence this postural reflex.

If a blindfolded cat is suddenly tilted or lowered through the air with its head down, its forelegs become extended and its toes spread (vestibular placing reflex). This is the normal feline response to linear acceleration and is controlled by the semicircular canals. The vestibular placing reflex can be inhibited immediately by 50 000 rads of 910-MeV α particles. A dose of 8000 can produce the same destructive effect but requires 8 days.

Page intentionally left blank

Page intentionally left blank

BRAIN IMPEDANCE STUDIES AND THEIR RELATION TO RADIATION EFFECTS IN SPACE FLIGHT

Richard L. Schoenbrun

The critical demands of the manned space mission have challenged the neurophysiologist to develop precise and sensitive measures of radiobiological effects in neural tissue. Development of a novel technique for measurement of electrical impedance changes in small volumes of cerebral tissue by use of implanted electrodes has permitted study of a new parameter of brain function.[1,2] This technique has been used in our Laboratory to study the effects of high-energy particle irradiation on the functional integrity of the central nervous system in the cat.

Historical Review

The theoretical basis for electrical impedance measurements in tissue can be traced back to Maxwell,[3] but the first experimental measurements were made by Fricke[4,5] using red blood cell suspensions, and by Cole[6,7] on sea urchin eggs in sea water. An important conclusion of these studies was that the impedance of a tissue is mainly a function of the extracellular electrolytes. The first physiological experiments using impedance measurement of cerebral tissue were those of Leão and Ferreira,[8] who observed with a bridge method an increase in resistance of rabbit cortex during asphyxiation and other conditions. Asphyxial changes have been extensively studied by Van Harreveld and others.[9-11] Cerebral impedance measured between electrodes placed on the cortical surface was seen to increase sharply (30-50%) within a few minutes after circulatory embarrassment. It was suggested that the mechanism underlying the impedance increase involved the movement of extracellular electrolytes (Na and Cl) and fluid into the intracellular compartment, with a consequent decrease in extracellular conductance. This was substantiated by histochemical studies which showed the movement of Cl^- into swollen dendrites during asphyxiation.[12]

It was assumed that most of the current flow during impedance measurement occurred through extracellular compartments, since resistance was low compared with that of the neuronal membranes.

Adey and his co-workers have extensively studied localized impedance changes in the brain during changing physiological states of consciousness, and in response to somatic, olfactory, visual, and auditory stimuli.[13-15] Impedance was seen to rise during states of decreased consciousness, such as with sleep or barbiturate anesthesia.

By contrast, impedance decreased during states of emotional arousal and goal-directed discriminative performance.

Adey theorozes that the significant pathway for the impedance-measuring current may involve both neuroglial elements and an intercellular substance containing large quantities of mucoproteins and mucopolysaccharides. He also suggests that modulation of conductivity in this substance by adjacent neuronal and neuroglial elements may be involved in information transaction and storage. These studies serve to illustrate the point that electrical impedance is a sensitive measure of physiologic and pathologic processes in the central nervous system.

Measurement of specific impedance has been used to estimate the size of the extracellular space in brain.[16,17] If experience with cell suspensions is applicable to tissues, an appreciable extracellular space (more than 20% of the tissue volume) would have to be present in the cortex to account for the low specific resistance values found in these experiments. However, electron microscopy studies, using conventional fixation methods, have generally indicated a very small (less than 5%) extracellular space. Harreveld, on the other hand, using an ultrarapid cryogenic technique, has clearly demonstrated a considerably larger extracellular space of about 20% of the tissue volume.[18,19]

An excellent study by Nevis and Collins has demonstrated that tissue dehydration during fixation may account for the minimal extracellular space seen in electron micrographs of perfusion-fixed material.[20] They tested a variety of fixatives and buffers and various combinations of their constituents for effect on brain impedance ultrastructural appearance. The results showed marked changes in impedance during fixation which correlated generally with the size of extracellular space as determined by electron microscopy.

Current Research

The purpose of our study is to correlate changes in brain impedance with structural damage consequent to high-energy particulate irradiation. The major sources of potentially hazardous radiation to man in space appear to be heavy primary cosmic particles, geomagnetically trapped corpuscular radiations, and solar-flare protons and α particles. Analysis of the Apollo radiation environment shows that the solar-flare particle events are the primary hazard.[21] The 184-inch cyclotron has been modified by means of variable ridge filtration to produce a defocused beam simulating the LET spectrum of a typical solar flare event. Experimentation is under way with simulated solar flare irradiation of primates.

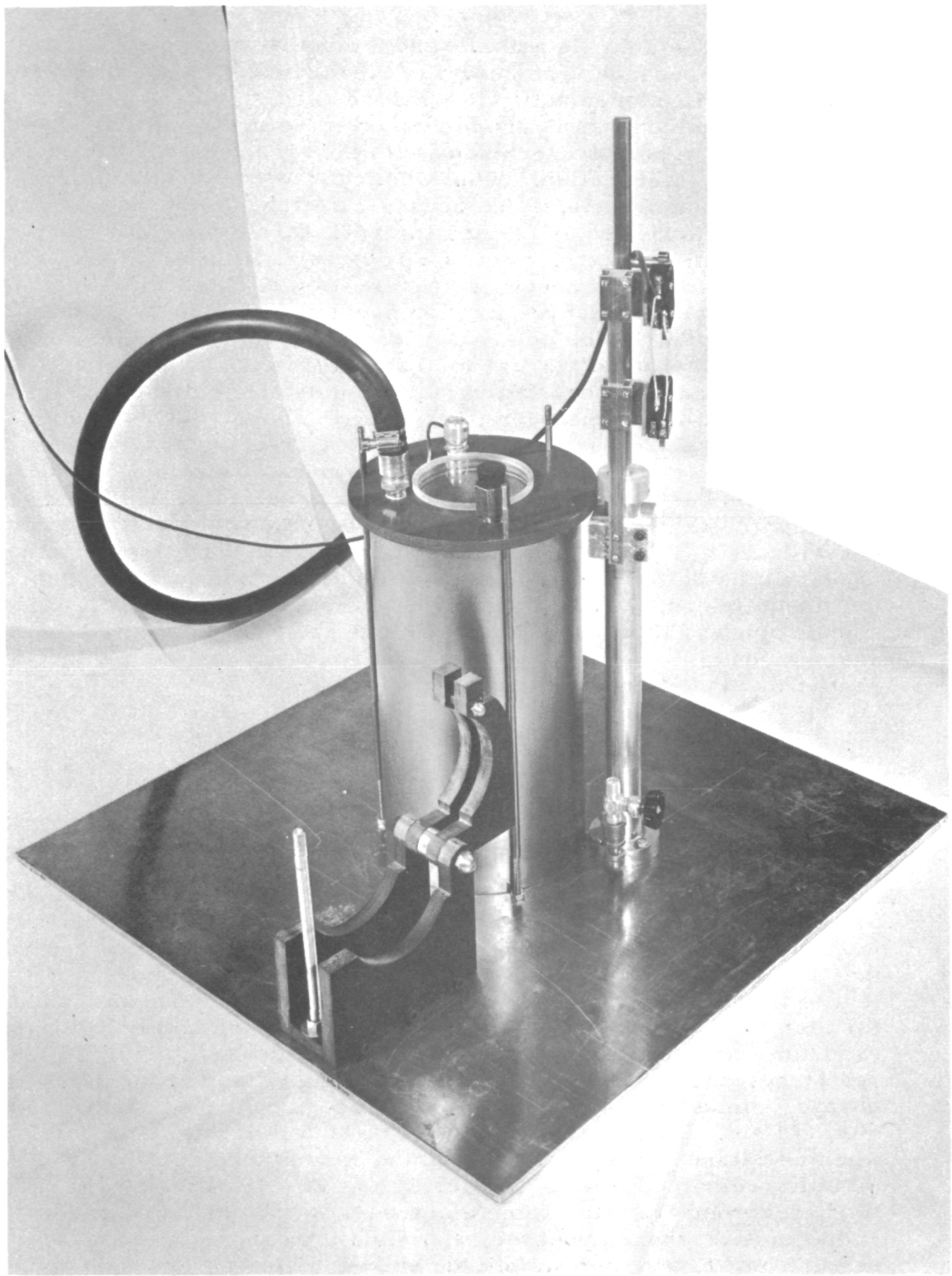
In our study, cats and monkeys are stereotaxically implanted with stainless steel concentric electrodes placed in deep brain

structures. The animals are allowed 2 months' recovery, during which time impedance is monitored several times daily. Sham irradiations are performed until all measures are stable. Focal irradiation at the electrode tip is accomplished by using a multiple-exposure narrow-beam cross-fire technique with the electrode positioned at the point of beam intersection. Whole-body exposures can be performed with the beam appropriately defocused. Following irradiation the animals are sacrificed at varying intervals up to 30 days. The brains are prepared for electron microscopy by two methods, both of which are designed to insure adequate preservation of extracellular spaces. One involves glutaraldehyde fixation perfusion with postfixation osmication. The other technique is ultrarapid freeze-substitution fixation. With the latter method the tissue is rapidly frozen by bringing it into contact with a heavy copper plug, electrolytically polished, that has been cooled to liquid nitrogen temperature (about -207 C, under reduced pressure. Figure 1 shows the rapid-freezing apparatus, which consists of a Dewar flask placed inside a protective steel cylinder with vacuum hose attached to the lid, and tissue holder with controlling microswitches and pneumatic piston. Figure 2 shows the inner cylinder with the heavy copper base plug unscrewed. This inner cylinder is placed inside the Dewar flask and immersed in liquid nitrogen, and the tissue is dropped at a controlled rate onto the surface of the cold copper plug. The tissue is next subjected to substitution fixation in acetone containing 2% OsO_4 at -85°C for 2 days, and then embedded, sectioned, and stained for electron microscopy.

Results

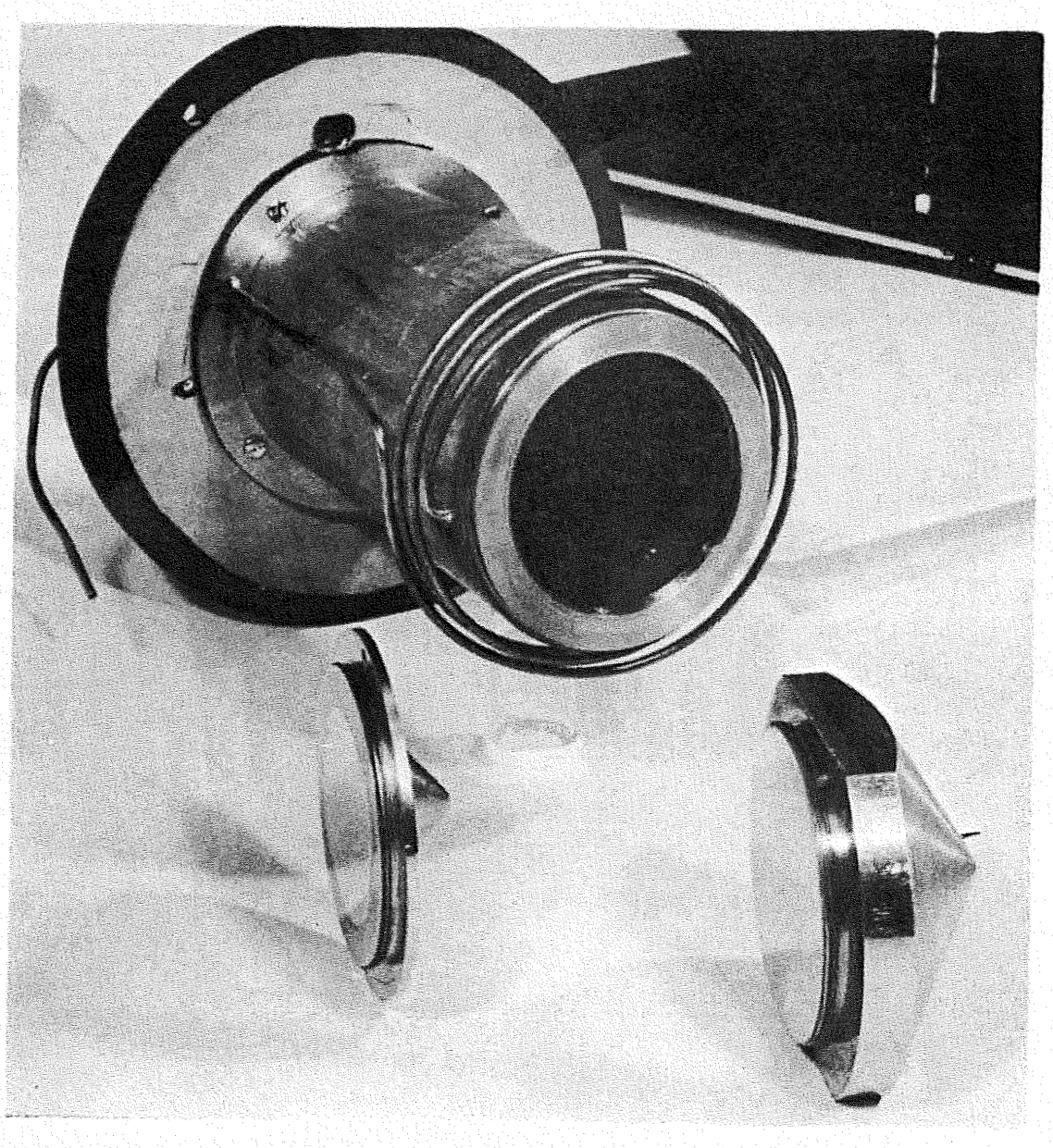
Results to date have revealed tissue conductance changes in response to focal brain irradiation with 910-MeV helium nuclei at dose levels in excess of 10 kilorad. Work is in progress to investigate lower dose levels. Impedance changes following a typical exposure are presented in Fig. 3, where resistance and capacitance recorded from the same electrode are graphed over the 5 days preceding and the 10 days following a 20-kilorad irradiation. Resistance is equivalent to the total impedance, since the capacitive component accounts for less than 1/1000 of the total impedance. Immediately following exposure, as soon as recordings could be made (within 30 min), the resistance decreased and the capacitance increased at the site of exposure. Impedance was unchanged at recording sites outside the radiation field. Values returned to the base-line levels until Day 4, when resistance sharply increased and capacitance decreased. This situation remained to time of sacrifice at Day 10. Brain-wave activity recorded from the same electrodes was highly abnormal at the radiation site; there appeared, shortly after exposure, epileptiform seizure bursts and high-amplitude spikes. Electron microscopy is incomplete at present.

To explain these results we envisage a compartment model for neural tissue, with intraneuronal, intraglial, extracellular, and



XBB 672-1036

Fig. 1. Rapid-freezing apparatus.



XBB 672-1038

Fig. 2. Inner cylinder with base plug removed.

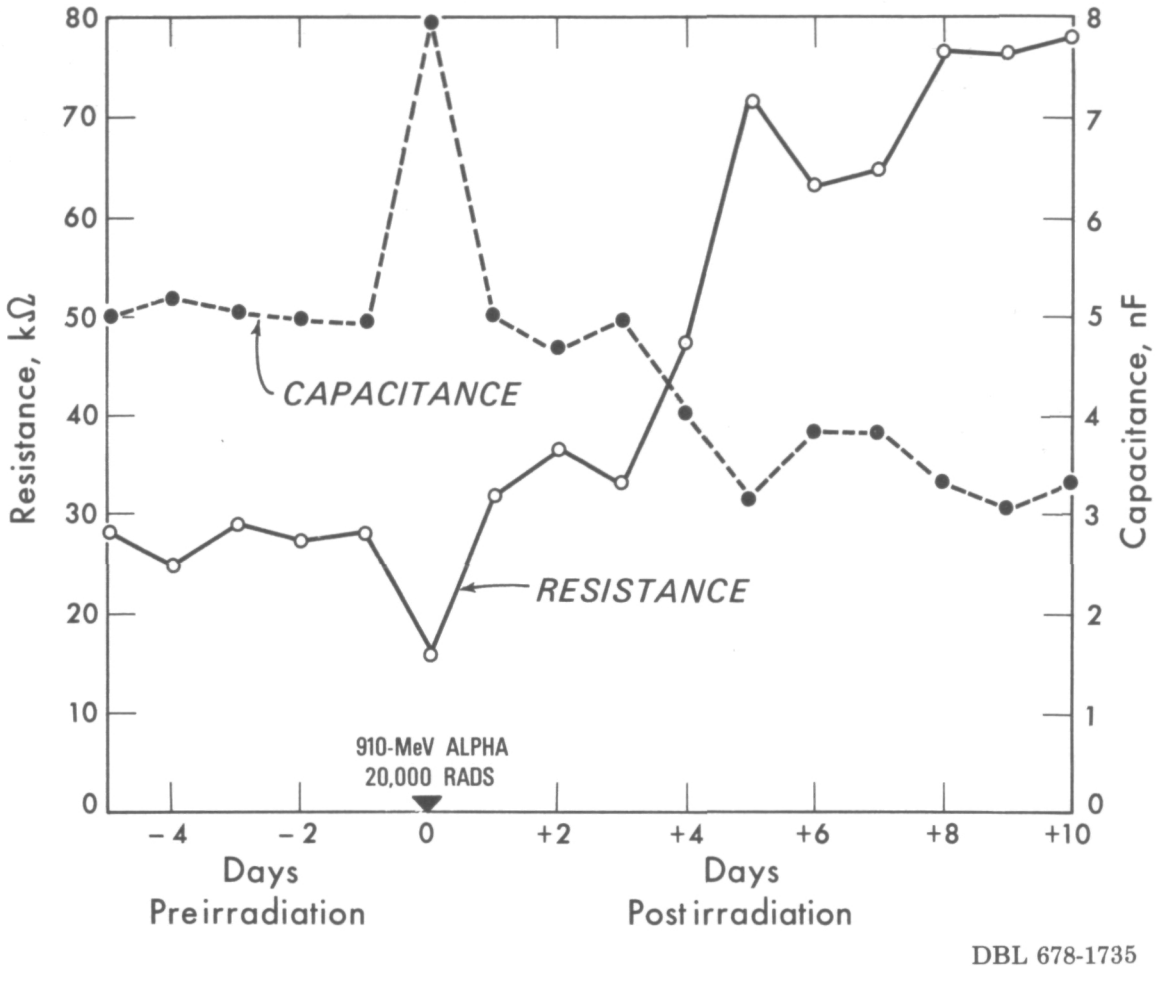


Fig. 3. Impedance changes following a typical exposure.

intravascular compartments. It is reasonable to expect the measuring currents to follow paths of greatest conductivity. It seems well established that under physiologic conditions impedance measures reflect primarily the conductivity of the extracellular spaces. The contribution of the intravascular channels is considered minimal (less than 5% of the total current flow). The glial components may contribute significantly, but a quantitative estimate must await accurate determination of the glial membrane resistance in situ. The contribution of the intraneuronal compartment is probably small, since the membrane resistance of neurons is relatively high compared with the resistance of the extracellular space. Thus, the great bulk of the measuring current is thought to be carried by extracellular electrolytes.

Increases in impedance reflect decreased conductivity of the extracellular spaces produced by a loss of electrolyte and fluid. Electrolytes, principally Na and Cl, appear to move into the neuronal compartment. This movement can under certain conditions be visualized by special stains for chloride and by the ultrarapid cryogenic methods for electron microscopy. Conversely, decreased impedance probably reflects increased conductivity of the extracellular spaces. Electrolytes may move into this compartment from several sources, including the intraneuronal and, under certain conditions, the intravascular compartments.

At present the ionic hypothesis of Bernstein[22] modified by Hodgkin and Huxley[23] offers the best explanation of the ionic shifts underlying changes in cerebral impedance. Briefly stated, this hypothesis assumes that the resting membrane is readily permeable to potassium and chloride ions, which are distributed according to a Donnan equilibrium. This membrane is only slightly permeable to sodium ions, and an energy-requiring "pump" removes them from inside the cell. The distribution of ions across membranes, and hence in the various compartments, depends upon certain "passive" and "active" permeability characteristics of those membranes. Other hypotheses are available but are less well substantiated.

The effects of ionizing radiation on cerebral impedance may be explained on the basis of permeability changes in membranes. The initial, immediate drop seen in impedance may signal a permeability increase in the blood brain barrier with an outpouring of fluid and electrolytes from the intravascular compartment into the extracellular compartment. Such an effect after brain irradiation has been demonstrated histologically in several studies.[24-26] The subsequent increase in cerebral impedance occurring around Day 4 may correlate with movement of electrolyte into compartments enclosed by high-resistance membranes, such as the intraneuronal compartment.

Dose levels of solar flare radiations expected on the Apollo mission are potentially hazardous to brain function, as judged by studies on experimental animals. Recently published maximum

permissible emergency doses for the Apollo mission are 700 rem for the skin of the whole body, 200 rem for the eyes and blood-forming organs, and 980 rem for the feet, ankles, and hands.[27] The probability of receiving doses like these is 1 in 1000 in the command module and 1 in 100 on the lunar surface. By use of data from a recent large solar flare event, total doses (both protons and α particles) in the command module are estimated at 20 to 50 rem for the skin of the chest, 15 to 30 rem for the eye, and 3 to 9 rem for the blood-forming organs.[28] In the lunar excursion module doses are expected to be considerably higher, with 350 to 800 rem at the chest, 100 to 180 rem at the eye, and 3 to 12 rem at the blood-forming organs. The expected dose for the brain is unspecified, and our assumption is that it will approximate the dose for the eye.

There is ample evidence to show that doses in the range of from 50 to 500 rad are capable of grossly altering central nervous function and behavioral performance.[29-31] The Russians claim changes in conditioned reflexes with doses as low as 0.5 to 20 rads, and changes in brain wave activity at only 0.05 to 1.3 rads.[32] Nervous activity in animals is certainly altered by dose levels likely to be encountered during space flight.

The practical significance of the impedance studies is the conclusion that ionizing radiation similar to that encountered in space can produce alterations in fluid and electrolyte distribution in the central nervous system and abnormalities in brain electrical activity. The rigors of space flight produce a variety of physiological stresses which may act synergistically with radiation by virtue of disturbances in the homeostatic control of the bodily fluids. For example, data from the Gemini mission reveal cardiovascular and renal compensatory changes resulting in significant diuresis, and other changes in fluid and electrolyte distributions in the various body compartments.[33,34] Cerebral impedance serves as a sensitive parameter with which to monitor subtle fluctuations in brain-tissue electrolytes and fluids.

References

1. R. L. Schoenbrun, Studies on Brain Activity and Learning Behavior Using Heavy-Particle Irradiation, in Biomedical Studies with Heavy Ion Beams, Lawrence Radiation Laboratory Report UCRL-17357, March, 1967, pp. 164-174.
2. R. L. Schoenbrun, E. Campeau, and W. R. Adey, Electroencephalographic and Behavioral Effects from x Irradiation of the Hippocampal System, in Response of the Nervous System to Ionizing Radiation, Eds. T. J. Haley and R. S. Nider (Little, Brown and Co., Boston, 1964), pp. 591-620.
3. J. C. Maxwell, A Treatise on Electricity and Magnetism, Vol. 1, 3rd Ed. (Academic Reprints, Stanford, 1953).
4. H. Fricke, The Electric Conductivity of Disperse Systems, J. Gen. Physiol. 6, 741 (1924).

5. H. Fricke, The Electric Impedance of Suspensions of Biological Cells, Cold Spring Harbor Symp. Quant. Biol. 1, 117 (1933).
6. K. S. Cole and J. M. Spencer, Electric Impedance of Fertilized Arbacia Egg Suspensions, J. Gen. Physiol. 21, 583 (1938).
7. K. S. Cole and H. J. Curtis, Electric Impedance of Nerve and Muscle, Cold Spring. Harb. Symp. Quant. Biol. 4: 73 (1936).
8. H. A. Leão and H. M. Ferreira, Altracao da Impedancia Electrica no Decurso de Depressao Alastranto de Atividade do "cortex cerebral," Anais Acad. Brasil. Cienc. 25, 259 (1953).
9. A. Van Harreveld and S. Ochs, Cerebral Impedance Changes After Circulatory Arrest, Am. J. Physiol. 187, 180 (1956).
10. A Van Harreveld, On Distribution and Movement of Water and Electrolytes in the Cerebral Cortex, in Structure and Function of the Cerebral Cortex, Eds. D. B. Tower and J. P. Schade (Elsevier, Amsterdam, 1960).
11. H. Collewijn, Ionic Movements in the Cerebral Cortex (Thesis), University of Amsterdam, 1963.
12. A. Van Harreveld, Asphyxial Changes in the Cerebellar Cortex J. Cell. Comp. Physiol. 57, 101 (1963).
13. W. R. Adey, R. T. Kado, and J. Didio, Impedance Measurement in Brain Tissues of Animals Using Microvolt Signals, Exptl. Neurol. 5, 47-66 (1962).
14. W. R. Adey, R. T. Kado, J. Didio, and W. J. Schindler, Impedance Changes in Cerebral Tissue Accompanying a Learned Discriminative Performance in the Cat, Exptl. Neurol. 7, 259-281 (1963).
15. W. R. Adey, R. T. Kado, J. T. McIlwain, and D. O. Walter, The Role of Neuronal Elements in Regional Cerebral Impedance Changes in Alerting, Orienting, and Discriminative Responses, Exptl. Neurol. 15, 490-510 (1966).
16. J. B. Ranck, Analysis of Specific Impedance of Rabbit Cerebral Cortex, Exptl. Neurol. 7, 144 (1963).
17. P. W. Nicholson, Specific Impedance of Cerebral White Matter, Exptl. Neurol. 13, 386 (1965).
18. A. Van Harreveld, H. Collewijn, and S. K. Malhortha, Water, Electrolytes, and Extracellular Space in Hydrated and Dehydrated Central Nervous Tissue, Am. J. Physiol. 210, 251 (1966).
19. A. Van Harreveld, T. Crowell, and S. K. Malhortha, A Study of Extracellular Space in Central Nervous Tissue by Freeze-Substitution, J. Cell. Biol. 25, 117 (1965).
20. A. H. Nevins and G. H. Collins, Electrical Impedance and Volume Changes in Brain During Preparation for Electron Microscopy, Brain Res. 5, 57-85 (1967).
21. J. L. Modisette, Apollo Radiation Environment Analysis, in Second Symposium on Protection Against Radiation in Space, NASA-SP-71, 1965, pp. 147-150.
22. J. Bernstein, Untersuchungen zur Thermodynamik der bioelektrischen Strome, Pflügers Arch. Ges. Physiol. 92: 521-562 (1902).

23. A. L. Hodgkin and A. F. Huxley, A Quantitative Description of Membrane Current and Its Application to Conduction and Excitation in Nerve, J. Physiol. 117, 500-544 (1952).
24. C. D. Clemente and H. E. Richardson, Some Observations on Radiation Effects on the Blood-Brain Barrier and Cerebral Blood Vessels, in Response of the Nervous System to Ionizing Radiation, Ed. T. J. Haley and K. S. Snider (Academic Press, New York, 1962), pp. 411-428.
25. I. Klatzo, J. Miguel, C. A. Tobias, and W. Haymaker, Effects of Alpha-Particle Radiation on Rat Brain, Including Vascular Permeability and Glycogen Studies. J. Hemopath. Exptl. Neurol. 20, 459-483 (1961).
26. A. V. Lebedinsky and Z. N. Nakhil'nitskaya, Effects of Ionizing Radiation on the Nervous System (Elsevier, Amsterdam, 1963), pp. 135-136.
27. J. Billingham, Second Symposium on Protection Against Radiation, in Space, NASA-SP-71, 1965, p. 139.
28. S. B. Curtis, Radiation Doses on Manned Space Missions, in Biology and Medicine Semiannual Report, Lawrence Radiation Laboratory Report UCRL-16613, Jan. 1966, pp. 1-5.
29. H. G. Gangloff and T. J. Haley, Effects of x Irradiation on Spontaneous and Evoked Brain Electrical Activity in Cats, Radiation Res. 12, 694-704 (1960).
30. M. Monnier and P. Krupp, Action of Gamma Radiation on Electrical Brain Activity, in Response of the Nervous System to Ionizing Radiation, Eds. T. J. Haley and R. S. Snider (Academic Press, New York, 1962), pp. 607-619.
31. J. Garcia and N. A. Buchwald, Perception of Ionizing Radiation: A Study of Behavioral and Electrical Responses to Very Low Doses of x Ray, Bol. Inst. Estud. Med. Biol. (Mex.) 21, 391-405 (1963).
32. N. I. Grashchenkov, Morphologic and Pathophysiologic Signs of the Response of the Nervous System to Ionizing Radiation, in Response of the Nervous System to Ionizing Radiation, Eds. T. J. Haley and R. S. Snider (Academic Press, New York, 1962), pp. 297-314.
33. C. A. Berry, D. O. Coons, A. D. Catterson, and G. F. Kelly, Man's Response to Long-Duration Flight in the Gemini Spacecraft, in Gemini Midprogram Conference, NASA-SP-121, 1966, pp. 235-261.
34. L. F. Dietleir and E. Harris, Bioassays of Body Fluids, in Gemini Midprogram Conference, NASA-SP-121, 1966, pp. 403-406.

MATHEMATICAL MODELING OF SPACE RADIATION HAZARDS

Palmer G. Steward and Cornelius A. Tobias

The ability of an astronaut to effectively perform tasks while in space is a function of his response to the physiological and psychological stresses posed by his unnatural environment. Since one may assume that the adaptability of homeostatic responses is a function of the aging process, it is important to consider the acceleration of the aging process due to radiation in space as well as due to other unusual aspects of the astronaut's space environment.

It is realized that the complexities of man's responses are such that complete understanding of the aging process cannot be hoped for at this time. Nevertheless, it may be possible, through mathematical modeling of the injury due to radiation and other environmental stresses, to arrive at estimates of changes in mortality rate due to various stresses. Such a model, when incorporated into a computer program, can be of aid in planning crucial experiments, and in addition may furnish valuable estimates of the magnitude of injury sustained due to space radiation and other environmental factors.

At this time we are not aiming at a refined model to account for minute details of experimental results (as was done, for example, by Sacher and Grahn). The aim is instead to have a simplified model, responding to constants measurable in radiobiological experiments, that could state overall results from animals to man, and eventually yield an index for the magnitude of injury following a known dose schedule.

A fundamental relationship of the aging process, proposed by Gompertz over a hundred years ago, relates to the rate of death $\frac{dN}{dt}$ of a population of N living individuals of age t,

$$R = \frac{dN}{dt} / N = A e^{\beta t} = \text{Age-specific death rate,} \qquad (1)$$

where A and β are constant, representative of the particular population considered, and of the hazards of the environment. This relationship applies surprisingly well to animal and human populations. In humans, the relationship holds for adults. In various countries and subpopulations, the "doubling time" of age-specific death rate, $\log 2/\beta$, is 8.5 years. According to Jones[1] the magnitude of A reflects mortality due to diseases of early childhood and that of early disease experiences. In Jones's

model a single stressful episode may shift expression (1) toward larger A, but the slope β remains constant. A chronic environmental hazard (e.g., continuous radiation) may also alter the slope β toward decreasing doubling time of R.

A useful model proposed by Strehler and Mildvan[2] gives plausibility to Eq. (1) and relates physiological and environmental conditions to aging. Strehler makes two postulates. First, he assumes that death occurs when the maximum response of the organism as directed by its homeostatic system is less than that required to overcome a given environmental challenge. The second postulate is that the magnitudes of environmental challenges are distributed as a Maxwell-Boltzmann energy distribution. Strehler replaces the Boltzmann ratio that usually occurs in potential barrier problems of physics, E/RT, by the hypothetical ratio $V/\epsilon D$. Here E is the energy, RT the most probable energy; V is a quantity that represents the potential of an organism to overcome challenges of the environment and is called "vitality," D is called "deleteriousness" of an environment, and ϵ is a constant chosen so that the ratio $V/\epsilon D$ is unitless. With these postulates and definitions, Strehler derives a mortality rate of

$$R = k\,(V/\epsilon D)^{1/2}\; e^{-V/\epsilon D}. \qquad (2)$$

For the case of $V >> \epsilon D$ we have the expression

$$R = K e^{-V/\epsilon D}. \qquad (3)$$

If now we equate $V/\epsilon D$ to relative aging injury, Eq. (3) is the familiar Gompertz transformation (1) between injury and mortality rate as described by Sacher.[3] The mortality is great when the vitality is small, or when the deleteriousness is large.

Strehler assumes that the vitality is a function of age: it is greatest at the beginning of the period of validity of the equation (young adults), then monotonically decreases with age, thus causing an increase in mortality. Strehler proposes use of an "attrition coefficient" B, defined as the fractional loss of original vitality per unit time. Thus

$$V = V_0\,(1 - Bt),$$

where t represents age or time and V_0 is the vitality of the individual at t = 0. Strehler views the attrition coefficient as the sum of a constant term b representing the attrition coefficient due to normal aging and a term f(D) which is the attrition coefficient due to the environmental factors. Since several other factors may affect vitality, we represent the ratio $V/\epsilon D$ by

$$\frac{V}{\epsilon D} = \frac{V_0}{\epsilon D} \{1 - [b + f(D)]t - \alpha_1 I_1 - \sum_i \alpha_{i+1} I_{i+1}\}, \quad (4)$$

where I_1 is irreversible radiation injury weighted so as to be proportional to the aging injury, α_1 is the relative contribution of this injury towards the total aging injury, and the I_i's and α_i's similarly are various other injuries and their relative importances respectively. Included in the summation may be such factors as permanent physiological injury caused by environmental temperature, atmospheric composition, gravitational forces, state of physical exhaustion, nutritional state, and psychological stress. Many of these factors will clearly be functions of time, e.g., irreversible radiation injury and reversible radiation injury following a solar flare, which is represented by one of the terms of the summation. Of course, at this time we do not actually know how to quantitate injury from a given environmental stress; neither is it known whether or not the injuries produced can be subtracted from vitality in the manner suggested above. However, it is possible to construct an injury function, at least for chronic radiation exposure at low and intermediate radiation levels. The simplest assumption one can make for various injuries is that they are additive. Finally, this formulation allows us to make theoretical predictions for mortality rate, which can then be verified by experiment, at least in certain strains of animals.

In the first phase of this effort we assumed that only normal attrition and radiation stress are present. We also assume that all individuals are exposed to the same basic environment. Thus we have, instead of Eq. (4),

$$\frac{V}{\epsilon D} = \frac{V_0}{\epsilon D} (1 - \beta t - \alpha_1 I_1). \quad (5)$$

The irreversible injury due to radiation which is effective in producing aging is represented by I_1 in Eq. (5). It is commonly assumed that radiation injury per unit mass is proportional to the dose deposited in that mass. Assuming a constant density for biological material, we may write $I_1 = Adf$, where d is dose and A is the proportionality constant between dose and injury per unit volume, and f is that fraction of the radiation injury which is irreversible. If the radiation is delivered at a constant rate d* in time, $d = d^*t$.

If irreversible radiation injury is delivered at a constant time rate d*, so that $d = d^*t$, then radiation exposure causes a linear decrease in vitality with time and correspondingly a higher-than-normal mortality rate, an accelerated physiological aging, and less resistance to a milieu of normal deleteriousness.

Under certain conditions it has been claimed that survival of a mammal may be determined by the extent of cellular radiation injury. For example, mice sometimes survive acute radiation injury when about 1% or more of their stem cells survive.

The Strehler model can be related to cellular lethality, or injury, in the following way: Assume that the critical "stem" cells have an exponential survival curve,

$$S = e^{-kd},$$

where S is the fraction of stem cells remaining alive following dose d:

$$\log S = -kd.$$

The logarithm of stem cell survival is proportional to the attrition of vitality caused by dose d. Thus, attrition of vitality may be linked to cellular survival.

Blair[4] has found that in mice and rats the threshold of radiation injury for lethality is independent of the volume fraction irradiated and also of the position in the body of this volume fraction. It is assumed that this volume fraction is of sufficient size that its injury can be considered a general injury and not an injury to a particularly vital or non-vital location.

In dogs, however, Blair finds that the injury threshold for lethality is not a constant but inversely proportional to the volume fraction exposed to a uniform dose. If we assume that the threshold for any given aging effect varies similarly, we have

$$I_1 = Bf\, d\, V_f^2, \tag{6}$$

where I_1 is the effective irreversible aging injury, B is the proportionality between whole-body dose and aging radiation injury, and V_f is the volume fraction of the dog which is uniformly exposed to the single dose d.

Now let us consider the problem of radiation injury to an astronaut in space. We assume that Eq. (6) is valid for man. In the case of galactic radiation, V_f is unity and d is probably a fairly uniform dose over the body. The fraction f of total radiation damage which is irreparable is a strong function of LET, which varies for acute doses from probably less than 0.1 to 1.0 as the LET, represented by ϵ, varies from about 3 to 200 keV/μ. There is some indication that f is also a function of dose rate. Thus $f(\epsilon)$ may be different for protracted doses received from galactic radiation and the relatively acute doses received from a solar flare event. In solar flare radiation there is the further complication that the dose is not uniform over the body, since the energy

spectrum of the solar flare particles is soft (i.e., mostly low-energy). When the radiation injury is a step function of position in the body it is not clear how to weight this injury with respect to volume fraction in order to obtain the effective aging injury. If we assume that the aging effect of radiation injury is proportional to the volume fraction in which it is confined, regardless of its distribution of magnitude, then we can write Eq. (6) in a more detailed form as

$$I_1(t,\ V_f) = B\,V_f \sum_i \int dE \int \frac{d\vec{r}}{V_0} \int_0^t dt'\ f(R_i\ (t',\ \vec{r}),\ \epsilon_i(E)\ )\ \epsilon_i(E)\ \phi_i\ (E,\vec{r},\ t'), \quad (7)$$

where

$$R_i\ (t,\vec{r}) = \int \epsilon_i(E)\ \phi_i\ (E,\ \vec{r},\ t)\ dE$$

is the dose rate at position $\vec{r}$ and time t, $\phi_i(E,\ \vec{r},\ t)dE$ is the flux of particles of the ith type in the energy interval between E and E + dE, and V_0 is the total volume of the animal. The integration over the volume elements $d\vec{r}$ is carried out over the region of the animal where the injury is considered significant.

Further work is in progress to determine the function $f(R, \epsilon)$ and also how to weight the local injury in order to obtain the effective aging injury.

References

1. H. B. Jones, A Special Consideration of the Aging Process, Disease, and Life Expectancy, Advan. Biol. Med. Phys. 4, 281-337 (1956).
2. B. L. Strehler and A. S. Mildvan, General Theory of Mortality and Aging, Science 132, 14 (1960).
3. G. A. Sacher, The Gompertz Transformation in the Study of the Injury-Mortality Relation: Application to Late Radiation Effects and Aging, in Radiation and Aging, Proceedings of a Colloquium held in Semmering, Austria, June 23-24, 1966, Edited by P. J. Lindop and G. A. Sacher (Taylor and Francis, Ltd., London, 1966).
4. H. A. Blair, On Addition of Modes of Radiation Injury in Producing Lethality in Dogs and Rodents, University of Rochester Report UR-654, 1964.

Page intentionally left blank

Page intentionally left blank

AUTHOR INDEX

Aceto, H.	83
Amer, N. M.	25
Buckhold, B. M.	43
Feola, J. M.	29
Gaffey, C. T.	123-125
Gunter, T. E.	3
Jones, W. B. G.	9
Lyman, J. T.	63
Maccabee, H. D.	59
Martins, B. I.	37
McDonald, L. W.	97-109-117
Montoya, V. J.	123-125
Plantz, R. G.	97-109-117
Raju, M. R.	55
Schoenbrun, R. L.	127
Schooley, J. C.	29
Shetlar, M. D.	19
Slater, J. V.	43
Steward, P. G.	137
Tobias, C. A.	137
Welch, G. P.	77

This report was prepared as an account of Government sponsored work. Neither the United States, nor the Commission, nor any person acting on behalf of the Commission:

A. Makes any warranty or representation, expressed or implied, with respect to the accuracy, completeness, or usefulness of the information contained in this report, or that the use of any information, apparatus, method, or process disclosed in this report may not infringe privately owned rights; or

B. Assumes any liabilities with respect to the use of, or for damages resulting from the use of any information, apparatus, method, or process disclosed in this report.

As used in the above, "person acting on behalf of the Commission" includes any employee or contractor of the Commission, or employee of such contractor, to the extent that such employee or contractor of the Commission, or employee of such contractor prepares, disseminates, or provides access to, any information pursuant to his employment or contract with the Commission, or his employment with such contractor.